Mussel-inspired chemistry and its applications

Juan Yang

Thesis committee

Promotor

Emeritus Prof. Dr. M. A. Cohen Stuart

Professor of Physical Chemistry and Colloid Science

Wageningen University

Co-promotor

Dr M.M.G. Kamperman

Assistant professor, Physical Chemistry and Soft Matter

Wageningen University

Other members

Prof. Dr W.J.H. van Berkel, Wageningen Unversity

Prof. Dr C. Detrembleur, University of Liège, Belgium

Prof. Dr F. Picchioni, University of Groningen, The Netherlands

Prof. Dr H. Birkedal, Aarhus University, Denmark

This research was conducted under the auspices of the Graduate School VLAG (Advanced studies in Food Technology, Agrobiotechnology, Nutrition and Health Sciences).

Mussel-inspired chemistry and its applications

Juan Yang

Thesis

submitted in fulfillment of the requirements for the degree of doctor

at Wageningen University

by the authority of the Rector Magnificus

Prof. Dr A. P. J. Mol,

in the presence of the

Thesis Committee appointed by the Academic Board

to be defended in public

on Tuesday 12 January 2016

at 4 p.m. in the Aula.

Juan Yang
Mussel-inspired chemistry and its application
214 pages.

PhD thesis, Wageningen University, Wageningen, NL (2015)
with references, with summaries in English.

ISBN:978-94-6257-625-4

Table of contents

Chapter 1

General Introduction

1.1 Water-borne coatings

Coating, by definition, is a layer of substance applied to the surface of an object for decoration or protection purposes[1]. Coatings can be applied to almost any substrate, such as wood, ceramics, masonry, metals, alloys, plastics and glass. Therefore, coatings are used almost everywhere for a myriad of applications, such as architectural industry, automotive, wood finishes, aerospace, etc. Given the wide range of applications, the use of coatings has experienced an enormous growth in the past few years, and the growth is expected to continue. It has been reported that the current market value of the global coating resins market is about €24,000 million by 2013, and is estimated to reach €35,000 million by 2019, with a compound annual growth rate (CAGR) of 6.25% between 2014 and 2019[2].

A typical coating formulation consists of four components: binders/resins, pigments, solvents and additives. The roles of the four components are as follows.

- Binders/resins: the essential ingredients that form a transparent, adherent and enduring film.
- Pigments: finely dispersed insoluble particles in coatings that can provide the color and opacity.
- Solvents: reduce the viscosity and provide a suitable consistency to the pigment/resin mixture so that it can be applied uniformly as a thin layer.
- Additives: specialty chemical compounds that are added in small amounts to improve or modify the property profile of the coating,
- such as viscosity, drying time, storage stability, opacity and ease of application.

The earliest use of coatings dates back to the prehistoric era during the Greek and Roman civilization, when human beings used natural gums, starches, beeswax for decorative paints.[3] Gradually, humans learned to use linseed oil and natural resins (amber) as binders for the coatings. The first volatile solvent, namely, turpentine was introduced early in the 15th century. The industrial revolution brought a dramatic increase in the demand for coatings, which resulted in the massive use of solvent-based coatings. The solvents used are mostly volatile organic compounds (VOCs), which yield coatings with satisfactory properties such as flow, leveling, drying time, gloss etc. However, considering that a significant proportion of coatings are used indoors for decoration and protection reasons, the increased usage of these volatile solvents has created serious problems in indoor air quality. These problems have led to a broad range of health problems, and some of them may even be fatal. Nine substances, as addressed by World Health Organization, contribute to indoor air pollution.[4] Among these substances, five compounds are emitted during coating application, namely, benzene, formaldehyde, naphthalene, tetrachloroethylene and trichloroethylene.

To improve the indoor air quality in buildings, waterborne coatings have proven to be a promising alternative to conventional solvent-borne coatings since the 1980s. Generally, instead of using volatile organic solvents, water is used to disperse the resins into small particles (typically in the range of 10-1000 nm), making the coatings more eco-friendly. A typical waterborne coating contains up to 50% water, with small quantities of other co-solvents (e.g. glycol ether).

Although water-borne coatings have proven to be environmentally friendly, to achieve a comparable performance as the solvent-based coatings, there are significant technical challenges. For waterborne dispersion coatings, the

suspension usually disperses in small clusters of insoluble resin particles by mechanical agitations. Compared to the solvent-based counterparts, in which the resins are fully dissolved, the water-borne coatings exhibit very different rheological properties. These properties have a profound effect on the properties of coating formulations during storage and application. Some common problems in current water-borne coatings are sedimentation (related with storage stability), sagging, bad leveling and open time (during application).

In view of the challenges discussed above, to fundamentally improve the properties of the coating, we need to move away from the current approach of using dispersed polymers in aqueous conditions. Instead, it is desirable to have a polymer that is completely soluble in water. This similarity to the solvent-based counterparts with respect to its full dissolution in the solvent would ensure proper rheological properties. After application, the polymers require crosslinking to result in mechanically robust and water-resistant coatings. To date, no chemistry in current coating systems fulfills these requirements. Therefore, one promising direction is to learn from natural organisms that produce high-performance coatings in aqueous conditions from soluble precursors. These will be discussed in the next section.

1.2 Bio-inspiration materials

Natural organisms are experts in producing high-performance coatings to protect themselves against corrosive factors in the environment. Examples include mussel byssal threads[5], squid beak[6,7], and protective cuticles on plants[8]. The natural coatings are mostly produced by a similar processing strategy as used in water-borne coatings: i) secretion of fluidic and pliable proteins in aqueous media (formulation and application of aqueous coatings), and ii) fast curing to form hard and tough solids (dry film

formation). For instance, in mussels (e.g. *M. californianus* (Fig. 1.1)), they produce viscous liquid mussel foot proteins (mfps) at pH < 5 inside granules. Upon being secreted into the seawater, at pH 8, the mfps solidify in a few minutes to form tough and hard cuticle[9]. The cuticle, a 2-5 μm thick layer, covers all parts of the mussel byssus thread exposed to seawater and insulates the collagenous core against microbial attack[10]. The stiffness and hardness of the cuticle, as assessed by indentation, are 2.5 and 0.5 GPa, respectively[11,12]. This high hardness is comparable to that of the hardest known epoxies (average hardness is 0.5 GPa). More interestingly, despite the high stiffness of the cuticle, the thread has a high extensibility of 70-100%. Another example is the beak of cephalopods such as squid. In the beak of *Dosidicus*, polyphenolic compounds form a dense crosslinked network in 30 s, providing an efficient hydrophobic coating around the soft and hydrophilic chitin nanofibers, preventing the chitin from softening by water adsorption[6]. Although no minerals are present, the stiffness of the beak is as high as 5 GPa at the distal tip that decreases to 50 MPa in the proximal wing[13].

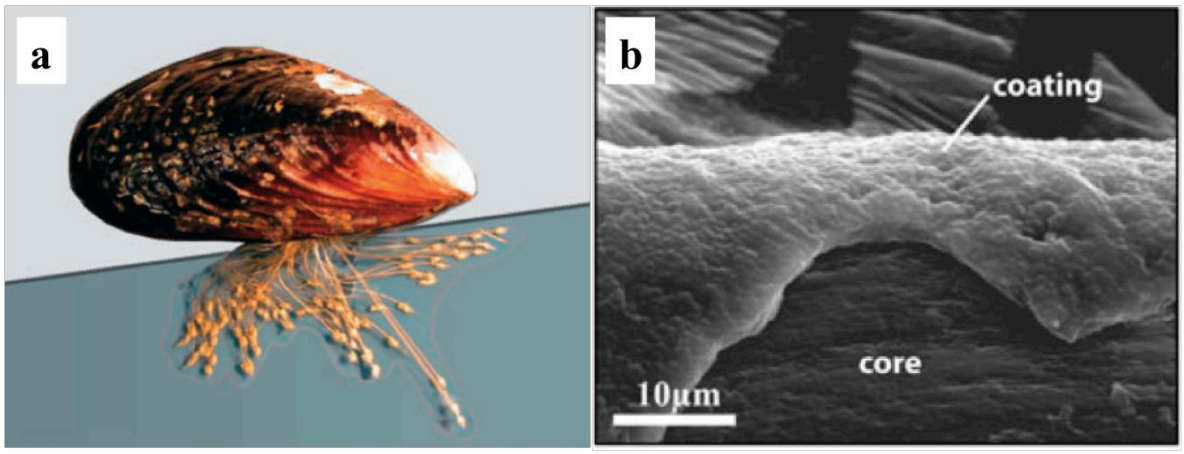

Figure 1.1. (a) A mussel attached to a mica surface and (b) SEM of *mussel* distal thread with partial delamination of cuticle, exposing the underlying

collagenous core. Reprinted with permission: Holten-Andersen, N and Waite, J. H.[10]

For both mussels and squids, the production of high-performance natural coatings relies on the composition of the natural proteinous resin/binder. It has been identified that, for both species, there is significant amount of catecholic amino acid 3,4-dihydroxyphenylalanine (DOPA) present in the coating[6,14]. The curing of these proteins takes only a few minutes, which is related to the efficient and versatile crosslinking chemistry of catechol groups in DOPA. Generally, the *o*-dihydroxylphenyl/catechol moiety in DOPA forms crosslinks along a variety of pathways. A detailed description of all the reaction possibilities will be discussed in Chapter 2. Here, the mechanism will be only briefly mentioned. Upon exposure to oxygen, catechols are easily oxidized to form reactive *o*-quinones. The *o*-quinones can then either i) react with catechols via dismutation reactions, or ii) with amines via Michael type addition or Schiff base reactions, or iii) with thiols via Michael addition to form crosslinks[15]. In addition, catechols can interact with transition metals (e.g. Fe^{3+}) by forming strong coordination bonds to give catechol-metal complexes.

Inspired by the excellent performance of natural coatings, researchers have been devoting significant efforts to mimic their properties using synthetic polymers. One possible route is to incorporate catechol functionalities into synthetic polymers either in the main chain, or at the ends of the polymer chains. Different synthetic approaches are possible, such as radical polymerization, post modification, and so on. A comprehensive overview of the synthesis approaches of catechol-functionalized polymer was reported by Faure et al.[16] In the present thesis, we aim at incorporating catechol functionality into synthetic polymers using free radical polymerization. The

polymer is designed to fulfill two requirements so that it can be used as binder for water-borne coatings: 1) during storage and application, the catechol-containing polymer should be water-soluble; 2) during drying and curing, by triggering the catechol crosslinking chemistry, a solid adherent film should be formed on the substrate.

1.3 Free radical polymerization

In general, the characteristics of a binder determine the nature of the coating and have a major influence on the method of application and conditions of film formation. For this reason, instead of using a homopolymer, it is desirable to have a copolymer, in which it is possible to tune the properties such as water solubility and glass transition temperature by tuning the monomer compositions. Free radical polymerization allows for easy incorporation of several monomers, and thus allows for easy incorporation of monomers of different properties into the polymer. Besides, free radical polymerization has some practical advantages over other polymerization techniques such as anionic polymerization. For instance, free radical polymerization can be carried out under relatively un-demanding conditions. Without the necessity to remove the stabilizers in commercial monomers, high molecular weight polymers can be produced. This technique also shows relatively high tolerance of trace impurities, e.g. no necessity to remove traces of oxygen in the solvent, and no necessity to dry or purify commercial solvents. In fact, one remarkable point of free radical polymerization is that it can be carried out in aqueous media. These virtues have made free radical polymerization a popular technique for both industrial and laboratory scale polymer synthesis. Therefore, in this thesis, we choose free radical polymerization as the technique to synthesize all the catechol-containing copolymers. The detailed synthetic protocols are given

in Chapter 4 and 5. Here we will discuss the mechanisms that were used to obtain the copolymer used in this thesis.

The concept of a chain polymerization was first proposed by Staudinger and his colleagues in 1920s.[17] Generally, chain radical polymerization is a chain reaction consisting of a sequence of three steps- radical initiation, chain propagation, and chain termination (Scheme 1.1). To be more specific, after the reactive radical center is generated by initiation, a polymer forms by successive addition of (co)monomer units.

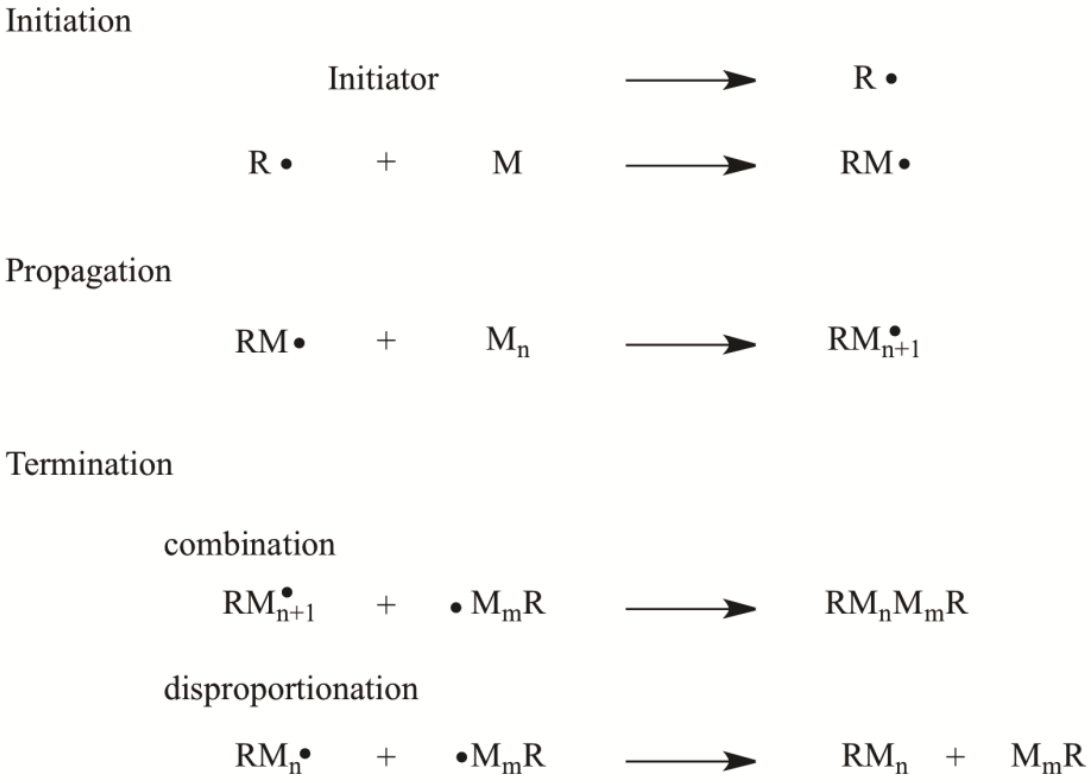

Scheme 1.1. Schematic illustration of three-step free radical polymerization

The mechanism of free radical polymerizations is different from some other polymerization techniques. For instance, in free radical polymerization, once a radical reactive center is generated, it adds many monomers units in a chain reaction, and grows rapidly to a large size polymer. In other words, high molecular weight polymer is formed almost immediately. At any instant of the polymerization, the reaction mixture consists of monomer,

propagating chains, and high molecular weight polymer. The molecular weight of the polymer remains unchanged during polymerization. Throughout the course of the reaction, the amount of high molecular weight polymer increases at the cost of the monomers. In contrast, for step polymerization, any two monomer species can react to form a dimer, trimer, and so on. The molecular weight increases throughout the course of the reaction, and high-molecular-weight polymer is not obtained until the end of the polymerization. To achieve high molecular weight and high conversion, long reaction times are needed.

In addition, free radical polymerization is also different from cationic/anionic polymerization in which ionic initiators are used. In radical polymerization, most monomers are found to undergo polymerization with a radical initiator. However, in ionic polymerization, monomers show high selectivity toward ionic initiators. In other words, some monomers do not polymerize with a cationic initiator, while others do not polymerize when an anionic initiator is used. Therefore, radical polymerization is more versatile with regards to the possible choices of monomers.

The characteristics of radical polymerization, together with our industrial-orientated aim of developing catechol-containing polymers, have led us to employ free radical polymerization as the technique throughout this thesis. The chemical structures of several catechol-containing monomers and co-monomers are shown in Scheme 1.2 and 1.3.

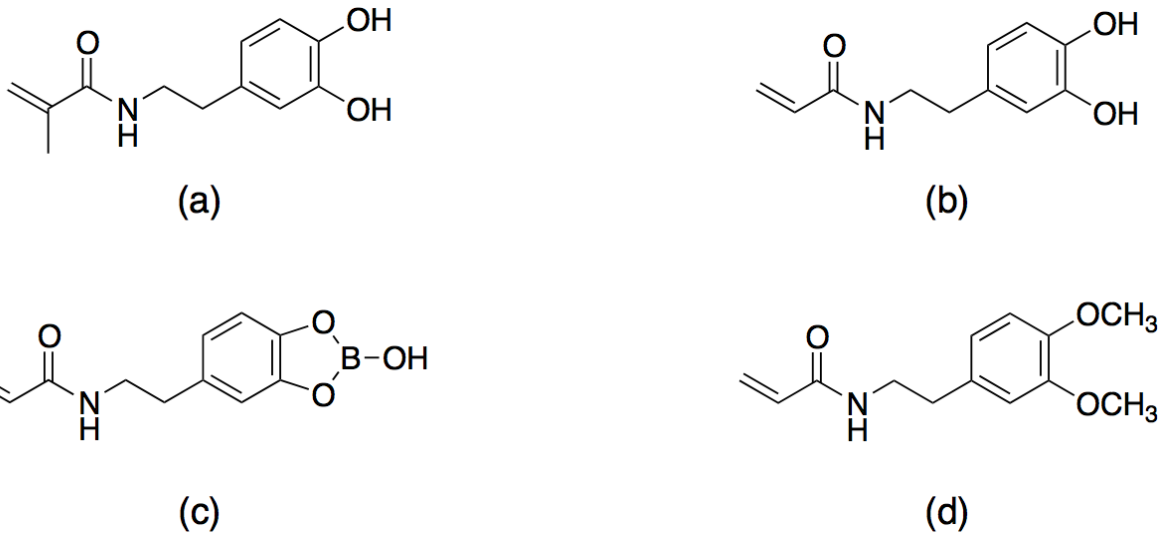

Scheme 1.2. Catechol-containing monomers used for free radical polymerization in this thesis: a) *N*-(3,4-dihydroxyphenethyl)methacrylamide, b) *N*-(3,4-dihydroxyphenethyl)acrylamide, c) borax-protected *N*-(3,4-dihydroxyphenethyl)acrylamide, d) *N*-(3,4-dimethoxyphenethyl)acrylamide

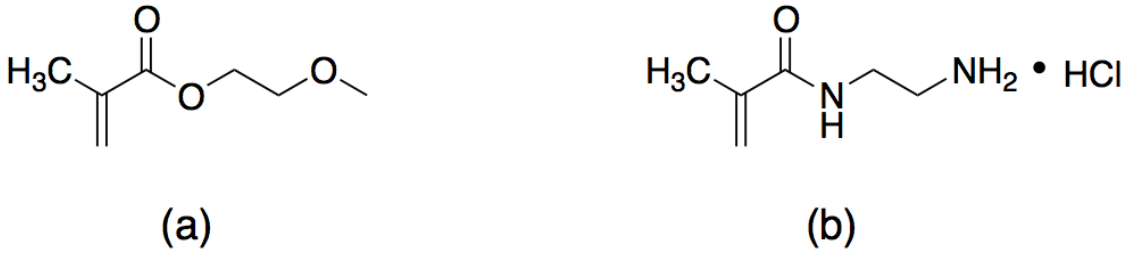

Scheme 1.3. Co-monomers used for free radical polymerization in this thesis: a) 2-methoxyethyl methacrylate, b) N-(2-aminoethyl) methacrylamide hydrochloride

1.4 Outline of the Thesis

This thesis is divided into two parts. Part I is about the crosslinking chemistry of catechol-derivatives, and part II is on the design and synthesis of catechol-functionalized polymers.

In part I, we focus on investigating the crosslinking chemistry of catechols. In Chapter 2, we will give a comprehensive overview of the possible

crosslinking mechanisms of catechols that have been proposed in the last few decades in both natural and synthetic systems. We rationalize the parameters that may affect the crosslinking pathways and kinetics such as pH, temperature, types of oxidant and so on. This rational understanding facilitates better control of the crosslinking chemistry through regulating these parameters. Motivated by the open questions as discussed in Chapter 2, we investigate, in Chapter 3, the crosslinking mechanism of catechols with amines using model compounds 4-methyl catechol (4MC) and propylamine (PA) in aqueous media. From the spectroscopic and chromatographic studies, we find that the reaction between 4MC and PA is very fast and complicated. In the first five minutes, more than 60 products have already been formed. These products are mainly formed via three pathways, i.e., Michael-type addition, Schiff-base reaction, and phenol-phenol coupling. Among these products, the majority are amine-catechol adducts formed by Michael-type addition.

In part II, we focus on designing and developing catechol-containing polymers for applications such as water-borne coatings. In Chapter 4, we design a bio-inspired polymer containing both functionalities-amines and catechols: poly(dopamine acrylamide-*co*-2-aminoethyl methacrylamide hydrochloride). We synthesize the copolymer in aqueous medium using free radical polymerization. The polymer is pH-responsive and meets two important requirements for a binder that can be used in water-borne coatings: (1) it is water-soluble at acidic pH during storage; (2) during drying and curing at basic pH, it becomes water-insoluble. The aqueous solubility switch is ascribed to the crosslinking reactions between catechols and amines at basic pH. Besides fulfilling the requirement of solubility switch, the coatings should also have proper adhesion properties to work

effectively. Therefore, in Chapter 5, we investigate the effect of catechol on the adhesion properties of catechol-containing polymers under both dry and wet conditions. We synthesize five copolymers from free radical polymerization of *N*-(3,4-dihydroxyphenethyl)methacrylamide (DMA) and 2-methoxyethyl methacrylate (MEA) with different compositions. We find that, under dry and wet conditions, an optimal composition for the best adhesion is achieved at 5 mol% of DMA. Polymers with a higher concentration of DMA show little adhesion, which is attributed to the high stiffness of the material, resulting in poor contact with the probe.

Chapter 6 is the final chapter of this thesis. In this chapter, we reflect on the previous chapters, and ask ourselves two questions: Did we acquire a better understanding of the crosslinking chemistry of catechols? Is it possible to develop a binder for water-borne coatings using catechols? We will further discuss the questions we formulated during our investigations, and point to potentially interesting but unexplored research paths. We will touch upon some remaining questions that can be interesting for a continuation of this research line.

References

(1) Wikipedia *Keywords: coating*.

(2) *Coating Resins Market by Type (Acrylic, Alkyd, Vinyl, PU, Epoxy, Amino, UPR, SPR & Others), by Technology (Waterborne, Powder, High Solvents, High Solids, UV Cure), by Application (Architectural, Automotive, Wood, & Others) - Global Forecast to 2019*, 2014.

(3)http://www.europeancoatings.com/var/StorageVincentz/VNLink/599_SampleChapter.pdf.

(4) *World Health Organization; WHO guidelines for indoor air quality: selected pollutants* Geneva, 2010.

(5) Waite, J. H. *Comparative Biochemistry and Physiology Part B: Comparative Biochemistry* **1990**, *97*, 19.

(6)Miserez, A.; Rubin, D.; Waite, J. H. *Journal of Biological Chemistry* **2010**, *285*, 38115.

(7) Miserez, A.; Schneberk, T.; Sun, C.; Zok, F. W.; Waite, J. H. *Science* **2008**, *319*, 1816.

(8) Bargel, H.; Koch, K.; Cerman, Z.; Neinhuis, C. *Funct*. *Plant Biol*. **2006**, *33*, 893.

(9) Holten-Andersen, N.; Harrington, M. J.; Birkedal, H.; Lee, B. P.; Messersmith, P. B.; Lee, K. Y. C.; Waite, J. H. *Proc*. *Natl*. *Acad*. *Sci*. *U*. *S*. *A*. **2011**, *108*, 2651.

(10) Holten-Andersen, N.; Waite, J. H. *J*. *Dent*. *Res*. **2008**, *87*, 701.

(11) Holten-Andersen, N.; Zhao, H.; Waite, J. H. *Biochemstry* **2009**, *48*, 2752.

(12) Holten-Andersen, N.; Fantner, G. E.; Hohlbauch, S.; Waite, J. H.; Zok, F. W. *Nat*. *Mater*. **2007**, *6*, 669.

(13) Uyeno, T. A.; Kier, W. M. *J*. *Morphol*. **2005**, *264*, 211.

(14) Waite, J. H.; Tanzer, M. L. *Science* **1981**, *212*, 1038.

(15) Yang, J.; Cohen Stuart, M. A.; Kamperman, M. *Chem*. *Soc*. *Rev*. **2014**, *43*, 8271.

(16) Emilie, F.; Celine, F. D.; Christine, J.; Joel, L.; David, F.; Patrice, W.; Christophe, D. *Prog*. *Polym*. *Sci*. **2013**, *38*, 236.

(17) Moad, G.; Solomon, D. H. *The Chemistry of Radical Polymerization*; Elsevier, 2006.

Chapter 2

Jack of all trades: Versatile Catechol Crosslinking Mechanisms

Abstract

Catechols play an important role in many natural systems. They are known to readily interact with both organic (e.g., amino acids) and inorganic (e.g., metal ions, metal oxide) compounds, thereby providing a powerful system for protein curing. Catechol cross-linked protein networks, such as sclerotized cuticle and byssal threads of the mussel, have been shown to exhibit excellent mechanical properties. A lot of effort has been devoted to mimic the natural proteins using synthetic catechol-functionalized polymers. Despite the success in developing catechol-functionalized materials, the crosslinking chemistry of catechols is still a subject of debate. To develop materials with controlled and superior properties, a clear understanding of the crosslinking mechanism of catechols is of vital importance. This review describes the crosslinking pathways of catechol and derivatives in both natural and synthetic systems. We discuss existing pathways of catechol crosslinking and parameters that affect the catechol chemistry in detail. This overview will point towards a rational direction for further investigation of the complicated catechol chemistry.

This chapter is based on publication as:
Juan Yang, Martien A.Cohen Stuart, Marleen Kamperman, *Chemical Society Reviews*, 2014, 43(24), 8271-8298.

1 Introduction

Catechols are prevalent in many natural systems; playing an essential role in living organisms such as mussels, sandcastle worms and squids,[1-4] and in food processing such as cocoa fermentation and tea preparation[5-8]. A famous example is the mussel that secrets water-resistant adhesive proteins containing significant amounts of the catechol-containing amino acid 3,4-dihydroxyphenylalanine (dopa).[9] In 1981, Waite and Tanzer identified dopa as a key element for the enduring fixation of mussels to various types of surfaces under harsh marine conditions.[9] Since then, a lot of research has been performed, trying to unveil the exact roles of catechols in mussel adhesion. Six mussel foot proteins (mfps) containing dopa have been identified.[10] Though a complete understanding of the roles of catechol in mussel adhesion is still missing, significant progress has been made and many possible mechanisms have been proposed. Two aspects of the function of catechol in mfps are partly understood: adhesion and cohesion. For adhesion, mfps containing relatively high concentrations of dopa (e.g., 20 and 25 mol% dopa for mfp-3 and mfp-5, respectively[11]) are present at the interface. The high concentration of dopa may enable strong interactions between catechol and organic or inorganic substrates, thereby ensuring water-resistant adhesion to various surfaces.[12,13] Several modes of interaction between catechol and different surfaces have been described in excellent reviews.[12,14] The cohesive properties of the mfps are related to the formation of load-bearing joints during the curing of the freshly secreted mfps, which are secreted as viscous fluids. The curing process of mfps relies on the versatile chemistry of catechols.[15-17]

Chemists have been inspired by the unique properties of the glues secreted by marine organisms, and the incorporation of catechol functionality into synthetic materials and subsequent crosslinking has aroused much interest.[18-20] Some synthetic materials have shown excellent properties. For instance, del Campo et al. developed nitrodopamine-ended four-arm poly(ethyleneglycol) (PEG-ND_4). By mixing the material with Fe^{3+} (molar ratio Fe^{3+}/PEG-ND_4 = 3: 1), a gel was formed through the complexation between Fe^{3+} and catechols in PEG-ND_4. The crosslinked material showed self-healing behavior and could be easily degraded by exposure to UV light. These two properties make this dopa-inspired material promising for cell biology and medical applications.[19] Another well-known example inspired by mussels is polydopamine. Lee et al. reported a method to form multifunctional polymer coatings through simple dip-coating of objects in a Tris buffer (pH = 8.5) of dopamine. Using this method, a thin but robust film having a thickness ranging from a few nm to > 100 nm was deposited on virtually any material surface.[20] The versatility of this method with respect to the material of the substrate has opened up new possibilities for extraordinary applications, such as surface coating, biotechnology and biomedicine.[21-23] A comprehensive summary of all the catechol-based biomimetic functional materials has been given elsewhere.[24,25]

Despite the success in fabricating catechol-based functional materials, the versatile chemistry of catechols, including the structure of polydopamine, is still a subject of debate. To advance the subject, and to provide a basis for the creation of superior materials, a clear understanding of the catechol reaction mechanisms is mandatory. An overview of the existing pathways of catechol crosslinking in natural protein systems and in synthetic mimics will, on one hand, help in gaining a full picture of the current status in this

field; and on the other hand, point towards a rational direction for further investigation of the complicated catechol chemistry. Fig. 2.1 presents a brief scheme of the crosslinking chemistry of catechols. Catechols are easily oxidized to form reactive *o*-quinones[26], which then can undergo secondary reactions to form covalent crosslinks.[27,28] In addition, catechols can interact with transition metals by forming strong coordination bonds to give catechol-metal complexes.[12]

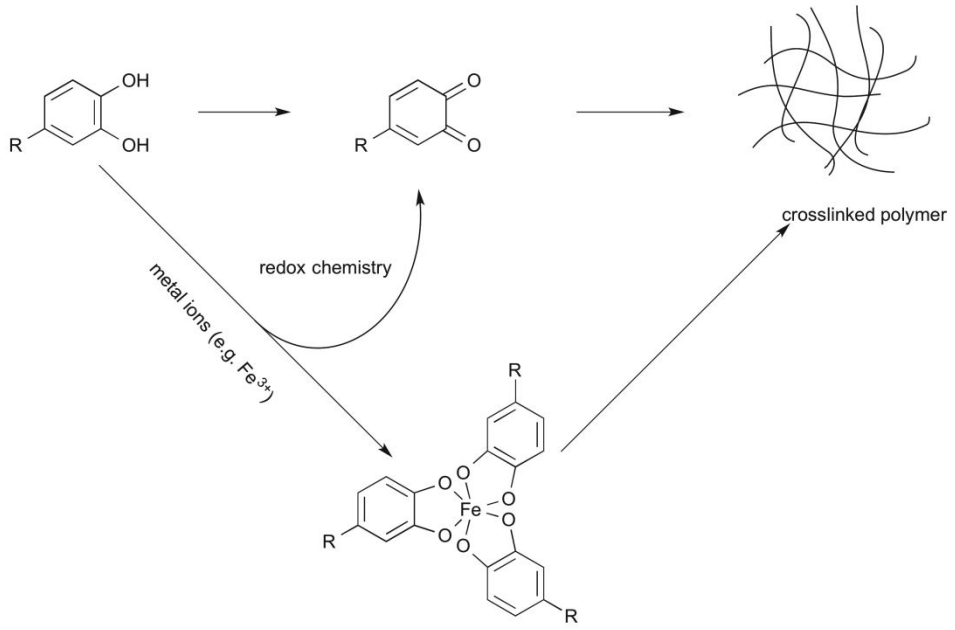

Figure 2.1. General crosslinking pathways of catechols

The details of the various crosslinking mechanisms are the topic of this review. As similar remarkable crosslinking chemistries of catechol have been observed in other living organisms, such as sandcastle worms,[2] and squid beaks,[1] studies based on these organisms will be discussed, too. Moreover, catechols, or more generally, phenols are also prevalent in natural food products, such as tea, wine, tobacco.[5-8] The oxidized phenols can also react with free amino acids, peptides, proteins or quinonic

compounds, resulting in a phenomenon called “enzymatic browning”. The browning of the food adversely affects the quality of food, e.g., color, aroma and flavor. A detailed overview of the browning of natural products has been reviewed in other work.[29] The chemistry of this effect, i.e., possible reactions between quinone and amino acids will be discussed in this review.

This review will be structured according to the possible crosslinking mechanisms of catechol that have been proposed so far, regardless whether the described system is natural or synthetic. Section 2 will focus on the catecholic covalent crosslinking mechanism in the absence of transition metals (e.g. Fe^{3+}), unless otherwise mentioned. This section will be divided into three sub-sections. In section 2.1, we will discuss the one or two-electron enzymatic or non-enzymatic oxidation of catechols to form *o*-quinone. The effect of pH, redox potential, and substitution on the catecholic benzene ring, etc., on the oxidation will be reviewed. In section 2.2, we will present the current knowledge on the subsequent secondary reactions of *o*-quinone with nucleophilic groups. This section comprises three sub-sections: i) Section 2.2.1 will focus on the reaction of *o*-quinone with amines; ii) Section 2.2.2 will focus on the reaction of thiol groups; and iii) Section 2.2.3 will focus on the reverse dismutation of *o*-quinone with catechols to form aryl radicals, which can further couple to form crosslinks. The proposed formation mechanism of polydopamine and its possible structures will be reviewed in section 2.3. In section 3, the affinity of catechol to transition metals, mainly focusing on Fe^{3+}, will be reviewed. Finally, section 4 will conclude with an overview of all possible reactions identified so far.

2 Curing of catechol-based materials by covalent crosslinking

2.1 Catechol oxidation

Catechols have been known for more than 70 years to be susceptible to oxidation upon exposure to air.[30] This spontaneous oxidation of catechol in the presence of oxygen is referred to as "auto-oxidation". In the auto-oxidation step, catechols undergo sequential abstraction of two electrons with the concomitant loss of two hydrogen atoms (Fig. 2.2). The first step is the one-electron oxidation of catechol to the *o*-semiquinone radical, during which O_2^- is formed. The formed O_2^- then reacts with catechol to form an *o*-semiquinone radical and H_2O_2. The formation of *o*-semiquinone has been identified[31,32] and detected by electron paramagnetic resonance (ESR) using continuous flow methods.[33] The formed *o*-semiquinone radicals are transient, and they decay rapidly through disproportionation to form *o*-quinone and catechol.

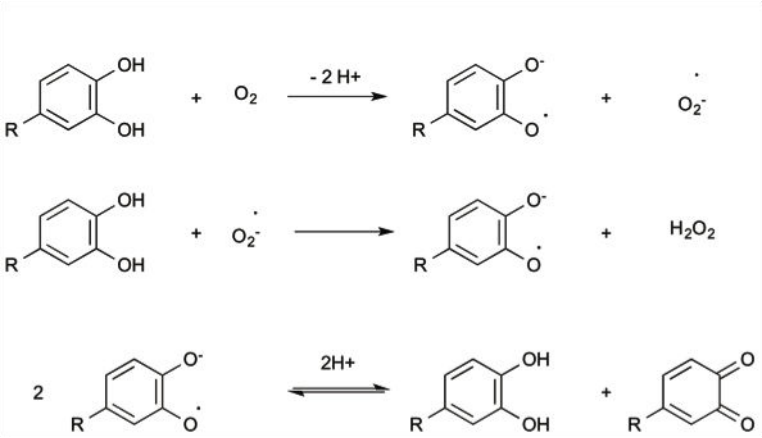

Figure 2.2. Reaction scheme of auto-oxidation of catechol to *o*-quinone[152]

The redox reaction between catechol and oxygen under biological conditions (i.e. air-saturated solution, around pH 7 and less than 10^{-2} M catecholic material) is thermodynamically unfavorable. For step 1 of the auto-oxidation of catechol, at pH 7, the redox potential of the pair catechol/*o*-semiquinone is 530 mV,[34] while the redox potential of O_2/O_2^- is -

155 mV.[35,36] Therefore, the equilibrium in step 1 is biased to the left, i.e., the oxidation of catechol is all but complete.

2.1.1 Enzymatic oxidation

In natural systems, the obstacle of catechol auto-oxidation, i.e., the high activation energy barrier is overcome by the presence of enzymes (e.g. tyrosinase, horseradish peroxidase/H_2O_2) or metal ions (e.g. Fe^{3+}). The mechanism of the reaction catalyzed by tyrosinase is a two-electron oxidation process, while for horseradish peroxidase/H_2O_2 it is a one-electron oxidation process. The catechol oxidation by transition metal ions will be discussed in section 3.

Tyrosinase is widely present in living organisms.[37] Tyrosinase belongs to a larger class of copper-containing proteins; these proteins are able to bind oxygen (Fig. 2.3). A common feature is the presence of a binuclear copper site coordinated by six histidines.[38-40]

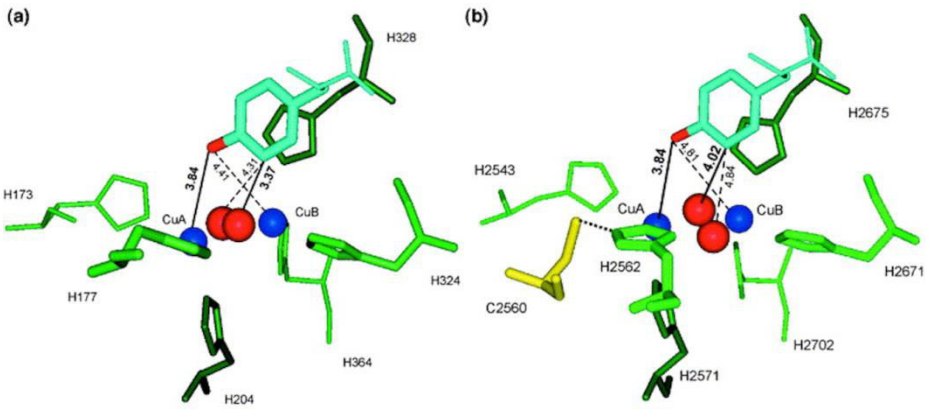

Figure 2.3. View of the structure of tyrosinase around the oxygen-binding site of Limulus polyphemus hemocyanin, as based on the X-ray structure.[153] Reprinted from ref. 153, Copyright 2000, with permission from Elsevier.

2.1.1.1 Oxidation mechanism using tyrosinase

A lot of research has been performed to study the effect of tyrosinase on phenol (including catechol) oxidation. The detailed function of tyrosinase on phenol oxidation has been reviewed by Riley et al.[41] Here, we briefly discuss the mechanism of tyrosinase-catalyzed oxidation of catechol based on the study of the electronic structures of active sites of tyrosinase.[42] The electronic structures of the copper site were studied by spectroscopic methods (e.g. Raman, electron paramagnetic resonance) and quantum mechanics calculations. Catechol oxidation catalyzed by tyrosinase involves two steps: (i) the activation of tyrosinase (Fig. 2.4) and (ii) the catecholic oxidation cycle by the activated tyrosinase (Fig. 2.5). The initial tyrosinase is in its inactive *met*-tyrosinase form, in which the binuclear copper site is in the wrong oxidation state to bind oxygen.[42] In the presence of catechols, *met*-tyrosinase is converted to *deoxy*-tyrosinase. Meanwhile, the catechols are oxidized by the two-electron transfer process, in which an *o*-semiquinone radical is formed in a secondary reaction between *o*-quinone and catechol, as described in Fig. 2.5. The *deoxy*-tyrosinase readily binds oxygen to give *oxy*-tyrosinase, which can oxidize catechol to form *o*-semiquinone and quinone.

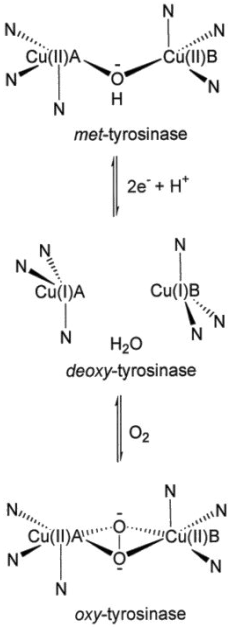

Figure 2.4. Activation of tyrosinase for catechol oxidation[41]

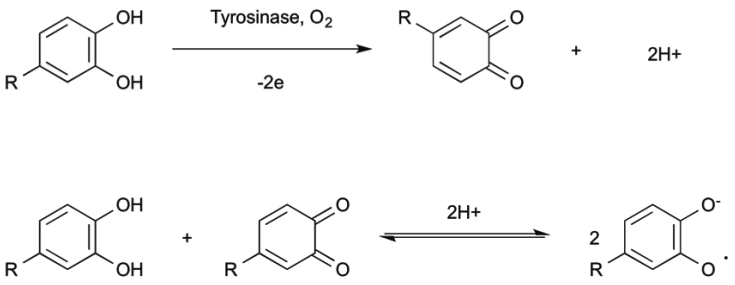

Figure 2.5. Oxidation mechanism of catechol catalyzed by tyrosinase.[41] Step 2 is identical to step 3 in Fig. 2.2.

As shown in Fig. 2.6, by oxidizing catechol to *o*-quinone, *oxy*-tyrosinase is reduced to *met*-tyrosinase, which cannot bind oxygen to regenerate *oxy*-tyrosinase. Only in the presence of a second catechol the *met*-tyrosinase is activated again. The inactivation of tyrosinase during catechol oxidation has

also been proposed by Dawson and co-workers, who studied the catechol oxidation in a buffered tyrosinase-catechol system using polarimetry.[43,44]

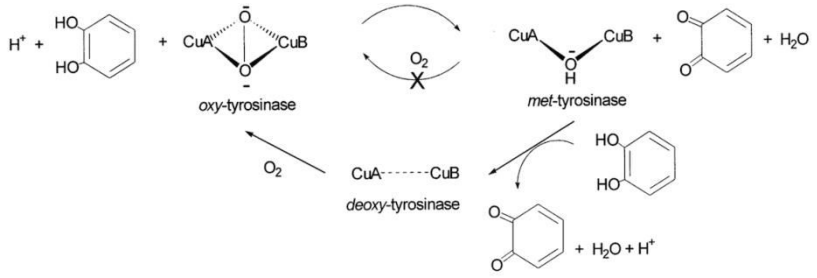

Figure 2.6. Catecholic oxidation cycle mediated by tyrosinase[41]

The extent of oxygen consumption during the enzymatic oxidation of catechol has been studied and appears controversial. Several investigations reported that for complete oxidation of catechols, two oxygen atoms are needed per catechol molecule.[45-47] Wright and Mason reported, however, that the consumption of oxygen depends on the enzyme and catechol concentration.[48] When the enzyme concentration was less than 3.3 catecholase units per ml of reaction volume, the oxygen atom consumption increased to 2.5 oxygen atom per catechol molecule. A further increase in enzyme concentration did not lead to an increase in oxygen consumption. Wright and Mason also showed that a higher concentration of catechol results in a lower oxygen consumption.

2.1.1.2 Influence of pH and ring substituents

The oxidation kinetics of catechols by tyrosinase can be affected by several parameters, such as pH and the nature of ring substituents of catechol. The effect of pH on the catechol oxidation can be described in relation to reduction potentials. As mentioned before, the one-electron reduction potential of catechol/semiquinone is 530 mV at pH 7.[34] At pH 11, one of the catecholic hydroxyl groups is deprotonated, leading to a lower one-electron

reduction potential of 98 mV.[34] Therefore, deprotonation shifts the reaction equilibrium in Fig. 2.2 towards the right side. This effect of alkaline conditions on catechol oxidation has been extensively reported.[49-51] Wright and Mason studied the catechol oxidation in presence of tyrosinase at pH 3, 4, 5 and 7. It was found that when the pH was increased, the initial rate of oxidation was increased.[48]

The nature of ring substituents of catechol also affects the oxidation kinetics through its steric, hydrophobic and electronic properties. According to Riley, the oxidation of catechol by tyrosinase can be described as depicted in Fig. 2.7, in which k_1 is the oxidation rate and k_2 is the rate of inactivation of tyrosinase.[43]

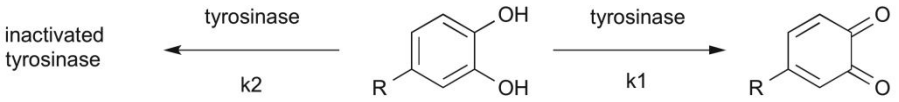

Figure 2.7. Competing oxidase (k_1) and inactivation (k_2) reactions of tyrosinase[43]

The oxidase activity (log k_1) can be approximated using the following empirical relationship (1), in which π describes the hydrophobility of the substituent and L describes its length, i.e., whether the substituent is long or short.

$$\log k_1 = 0.364(\pm 0.097)\pi - 0.297(\pm 0.077)L + 2.369 \qquad (1)$$

By investigating the oxidation kinetics of catechols with different substituents on the 4- position, Ramsden and Riley demonstrated that shorter substituents (smaller L) or more hydrophobicity (larger π) gave faster oxidation rates; and larger substituents (larger L) or more hydrophilic substituents (smaller π) resulted in slower oxidation. [43]

The electronic properties of the substituents also affect the oxidation rates. For substituents that are more electron-withdrawing (such as NO_2, CN, CF_3), catechols become difficult to oxidize.[43,52] In contrast, substituents that are more electron-donating (such as -OMe, -Me) stabilize the radicals, resulting in the opposite effect. [53] These effects of the substituents may also be applicable for other oxidants with different oxidation mechanisms. However, more in-depth studies are needed to clarify this. In addition, it should be noted that these effects were found for 4-substituted catechols. Whether these effects are applicable to substituents at other positions is still an open question.

2.1.2 Chemical oxidation of catechols

Catechols are also readily oxidized in the presence of chemical oxidants. The most commonly used oxidants are sodium periodate[15,54] and silver oxide[55]. The periodate-mediated oxidation proceeds via a two-electron oxidation, and that for silver oxide proceeds via a one-electron oxidation reaction.[56,57] A clear understanding of the reaction mechanism of periodate-oxidation of catechol is lacking. Nevertheless, Kaiser et al. have proposed three reaction pathways, based on investigations on the oxidation of catechol by sodium periodate with a stopped flow apparatus at different pH, ranging from 0 to 10.[58-60] They detected an intermediate during the oxidation without identifying the nature of the product. It was proposed that the intermediate was a cyclic diester of periodic acid. Two possible structures were suggested, as indicated in Fig. 2.8 (a) and (b).

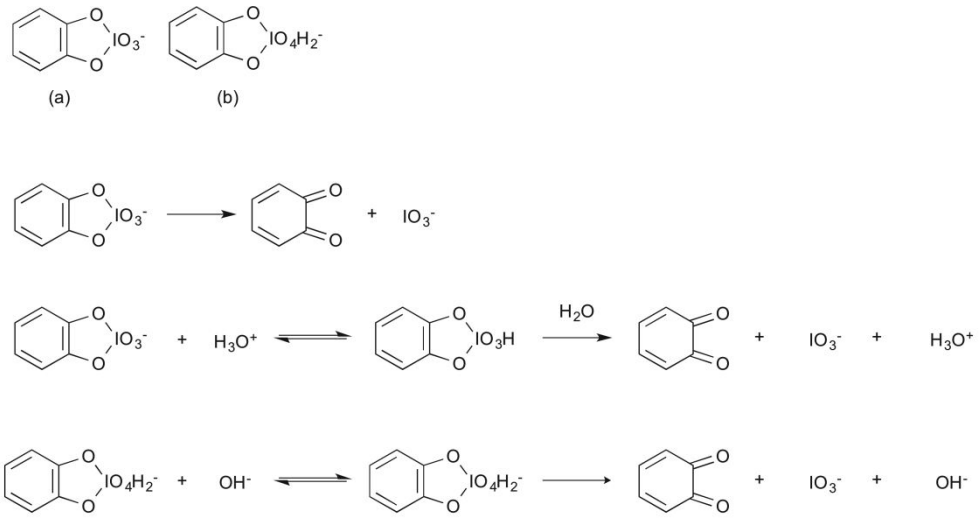

Figure 2.8. Proposed pathways of decomposition of the intermediate to form *o*-quinone.[58]

The intermediates were proposed to be able to decompose to *o*-quinone via three pathways (Fig. 2.8).

To summarize, catechols in both synthetic mimics and natural systems are susceptible to aerobic oxidation. The oxidation process is influenced by pH and aromatic ring substituents on catechols. In general, a higher pH leads to a higher oxidation rate. Catechols with aromatic ring substituents that have electron-withdrawing properties (NO_2, CN, CF_3) are more difficult to oxidize; while those with substituents that have electron-donating properties (-OMe, -Me) are easier to oxidize. For enzymatic oxidation of catechols, the mechanism has been well studied. The inactive tyrosinase is first activated to its reactive state *deoxy*-tyrosinase, which then catalyzes catechol to undergo a two-electron oxidation process. For the oxidation of catechols in the presence of chemical oxidants, such as sodium periodate, the mechanism is not well understood. It is proposed that catechols and sodium

periodate form a cyclic diester of periodic acid as an intermediate, which ultimately forms *o*-quinone.

2.2 Secondary reaction of *o*-quinone with nucleophilic groups

The *o*-quinone groups are unstable intermediates and highly reactive electrophilic molecules that can further undergo several secondary reactions to form reddish brown or black pigments. These secondary reactions comprise: a) reactions with amine groups, b) reactions with thiol groups; c) aryloxy radical coupling. In the following sections, we will elaborate on the three reaction ways one by one.

2.2.1 The interaction of *o*-quinone with amines

O-quinones can react with amines through three pathways: i) Michael-type addition; ii) Schiff base reaction and iii) Strecker degradation. In this review, the first two will be discussed in detail, and Strecker degradation will be discussed briefly in section 2.2.1.3. The factor that mainly determines which of these three reaction types will predominate is the type of amine.[61] For example, Manthey et al. identified the oxidation products of catechol in the presence of two aliphatic (aniline and *p*-anisidine) and aromatic amines (2-phenylethylamine and butylamine) using ^{1}H and ^{13}C NMR. They found that aromatic amines favor Michael-type addition (i.e., 4,5-disubstituted *o*-quinone adducts), and aliphatic amines favor Schiff base reaction (i.e., 2,4,5-trisubstituted or 2,4-disubstituted *o*-quinone adducts).[61]

2.2.1.1 Michael-type addition

Quinones undergo a nucleophilic attack by amines to form quinone-amine adducts. The complete reaction mechanism between *o*-quinone with primary amines has not been experimentally verified. However, it has been

proposed that the mechanism between *o*-quinone and amine resemble that of *p*-quinone and amine.[62] Therefore, in the following, we first show the reaction mechanism of *p*-quinone and amine, as indicated in Fig. 2.9.

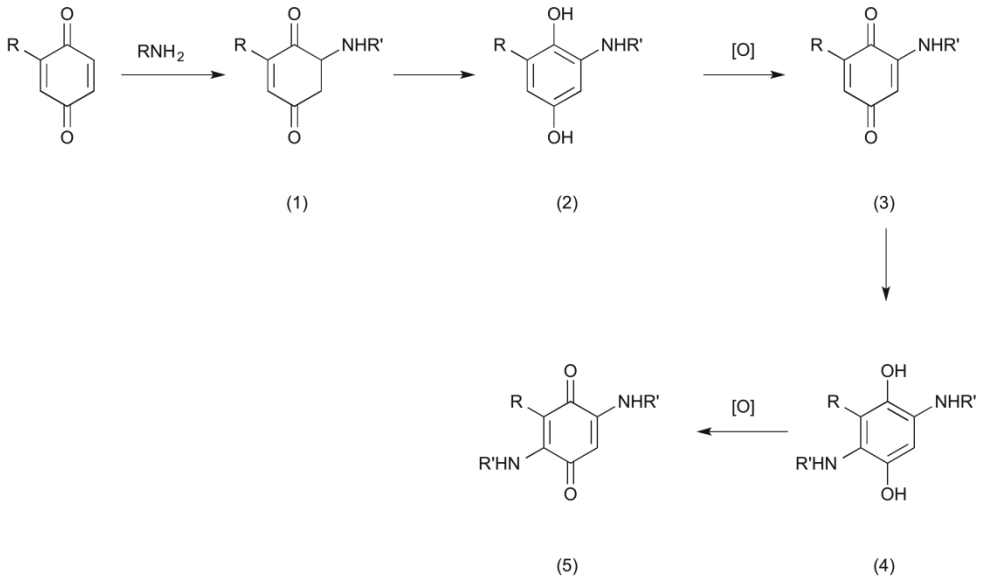

Figure 2.9. Reaction mechanism of *p*-quinone with primary amines through Michael-type addition[62]

The reaction is initiated by the addition of an amine to a carbon-carbon double bond, forming an intermediate (1). The intermediate is then isomerized to form aminohydroquinone (2), which is subsequently oxidized to form monoaminoquinone (3). The monoaminoquinone (3) reacts further with amine to produce diaminoquinone (5) via an intermediate (4).

Despite of the unclear mechanism, in natural living organisms and food processing, the formation of *o*-quinone-amino adducts have been identified. In many of these natural systems it involves a reaction between dopa and histidine. For instance, Waite et al. found dopa and several crosslink derivatives from the beak cutouts of squid *Dosidicus gigas*. They isolated

protein fragments by phenylboronate chromatography followed by reverse-phase HPLC, and the fragments were measured by UV-Vis spectroscopy, ^{1}H NMR, electrospray ionization mass spectrometry, and tandem mass spectrometry. They identified that the hydrolyzed compounds obtained from the insoluble black pigments from squid beaks are multimers (dimer, trimer and tetramer) of catechol-histidine adducts.[1,63] The structures of the multimers are shown in Fig. 2.10. The imidazole nitrogens either attach to the 2- or the 6-position (or both) on the aromatic ring of catechol in these adducts.

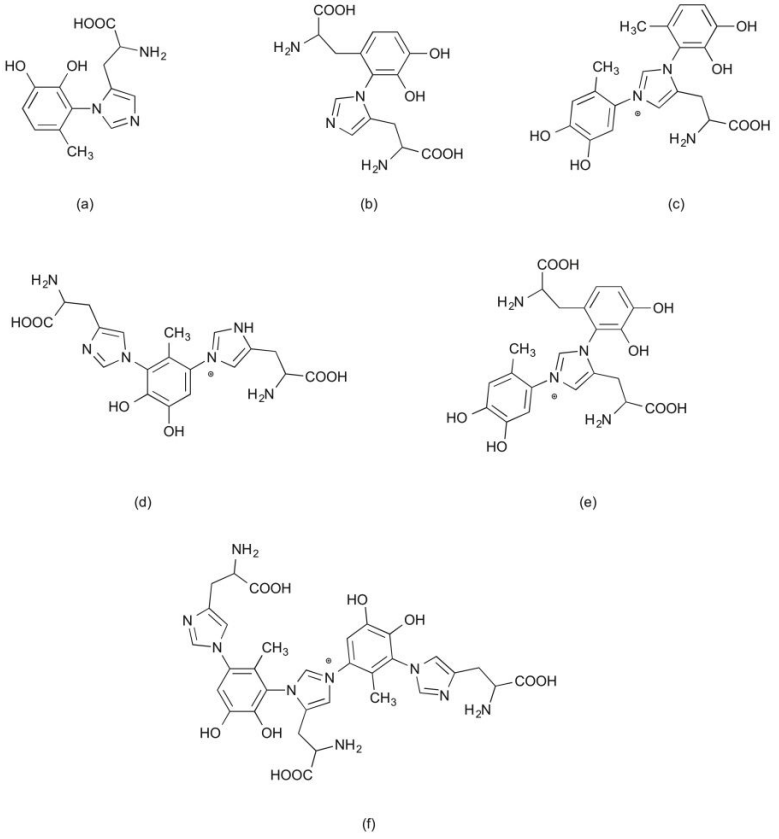

Figure 2.10. Crosslinks identified in *D. gigas* squid beak by MS/MS, the structures are (a) 4-methylcatechol-histine (4MC-His); (b) dopa-histidine;

(c) 4MC-his-4MC; (d) His-4MC-His; (e) 4MC-His-dopa; (f) His-4MC-His-4MC[63]

In addition, Turecek et al. characterized the catechol-amino acid adducts in acid hydrolysates of sclerotized cuticles by mass spectroscopy and HPLC.[64] They identified the presence of C-N bonds, which had been formed between the nucleophilic imidazole N of histidine in cuticular protein and both the ring and side chain C of three sclerotization precursors, i.e. N-acetyldopamine, N-beta-alanyldopamine and 3,4-dihydroxyphenylethanol. The authors proposed a pathway for protein crosslinking by C-N bond formation during sclerotization, as shown in Fig. 2.11.[64] The substitution pattern (4-substituted) is different from the observations in Fig. 2.9. Up till now, it is not clarified at which position on the aromatic ring of *o*-quinone the amine is most likely to attach.

The presence of dopa-histidine crosslinks has also been reported in other work.[65-67] The proposed structure of the crosslink structure is shown in Fig. 2.12.

In tobacco processing, the formation of *o*-quinone-amine adducts has also been identified. During the drying process of tobacco, *o*-quinone reacts with nornicotine, resulting in a red color absorbing at 570 nm.[68,69] A model reaction of nornicotine with *o*-quinone is indicated in Fig. 2.13.[29] Products from both Michael addition and Schiff base reactions (which will be discussed in the next section) were formed.

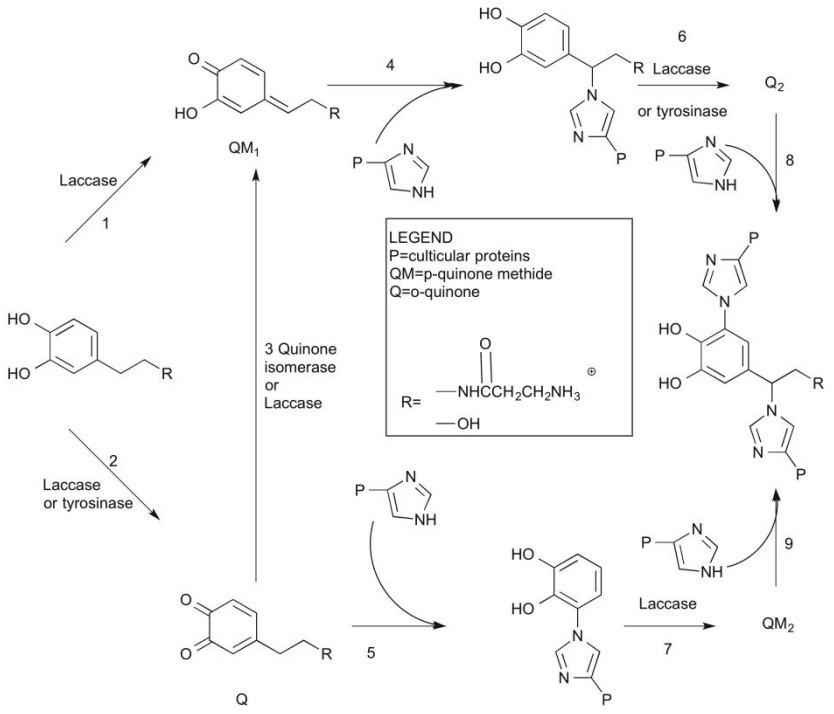

Figure 2.11. Proposed crosslinking pathway for sclerotization.[64] Reprinted from ref. 64, Copyright 2001, with permission from Elsevier.

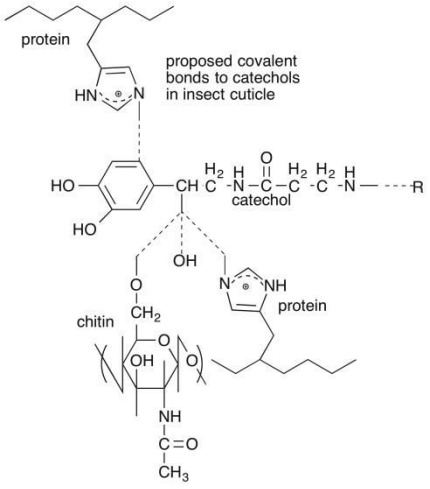

Figure 2.12. Proposed crosslink structure for sclerotized insect cuticle involving N-β-alanyldopamine.[65]

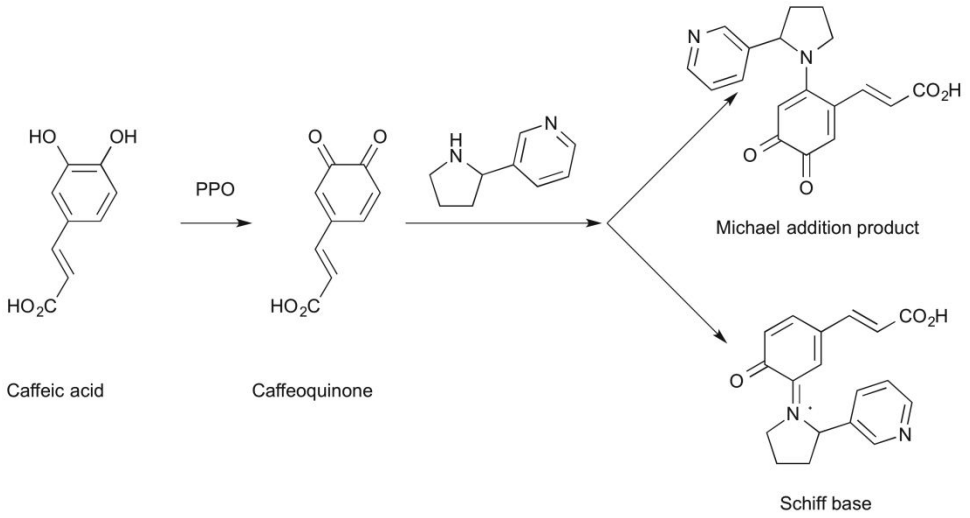

Figure 2.13. Reaction of *o*-quinone with nornicotine.[29] Reprinted from ref. 29, Copyright 2004, with permission from Springer.

Similar amino-catechol adducts from Michael addition were studied by Rafiee and co-workers. They employed cyclic voltammetry and controlled potential-coulometry to study the electrochemical oxidation of catechol (1) in the presence of sulfanilic acid (2) resulting in the formation of an amino-*o*-quinone derivative (3a) (Fig. 2.14).[70]

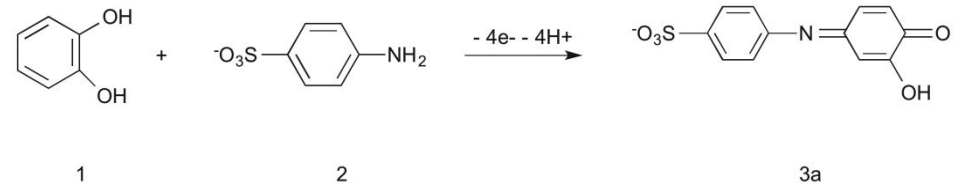

Figure 2.14. Reaction scheme of catechol with sulfanilic acid.[70] Reprinted from ref. 70, Copyright 2006, with permission from Springer.

Messersmith et al. identified quinone-amine adducts indirectly using atomic force microscopy measurements on the interaction of a single *N*-Boc-protected dopa residue in contact with an amine-containing Si surface.[71] They found that the pull-off force is initially 2.2 nN at pH 9.7, after which, an additional contact/pull-off measurement showed no adhesion force. This result indicated that the formation of a covalent, irreversible dopa-N bond is possibly formed via Michael addition. Similar reactions between dopa and amines may also occur in mussel-secreted proteins; however, no direct evidence of this exists up till now.

Parameters influencing Michael-type addition

Three parameters that affect the Michael addition of catechol and amine groups are pH, the type of catechol groups and the basicity of the nucleophile amines. For instance, Truscott et al. investigated the oxidation of catechol by tyrosinase in the presence of aniline at pH 7 and 11.7, respectively.[61] By analyzing the aromatic and olefinic resonance in the ^{1}H and ^{13}C NMR spectrum of the final products, they found that at pH 7, the majority of the products is 4,5-diarylamino-1,2-dihydrobenzene formed by Michael addition (Fig. 2.15 (a)) with small amounts (4%) of a compound formed by Schiff base reaction (Fig. 2.15 (d)) (as will be discussed in the next section). In comparison, at pH 11.7, only tautomers of 4,5-diarylamino-1,2-dihydrobenzene (Fig. 2.15 (a), (b) and (c)) were formed. pH also affects the reaction rate of Michael addition through the protonation state of the amines. For instance, Shirmohammadi et al. studied the reaction of electrochemically generated *o*-quinones and nucleophilic N-methylaniline by cyclic voltammetry.[72] They found that the rate constant for Michael addition increases with increasing pH, up to pH 6. This trend is

related to the deprotonation of the amine group. By increasing the pH to a value higher than 6, the rate constant slightly decreases. This decrease may be explained by the fact that the conversion of *o*–quinone to catechol needs proton exchange. An increase in reaction rate of *o*-quinone with amine groups with increasing pH was also reported for catechol oxidation in the presence of sulfanilic acid: At pH 3 the rate constant is 0.35 $M^{-1}s^{-}$, while at[1]pH 6.5, the calculated rate constant is 0.45 $M^{-1}s^{-1}$. At low pH, sulfanilic acid is protonated, yielding deactivated amine groups towards the Michael addition reaction with *o*-benzoquinone.[70] Therefore, the reaction rate is decreased. Similar observations have also been reported for the reaction between 3-substituted catechols with dibenzylamine.[73]

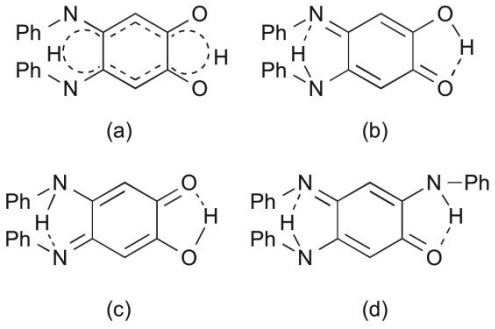

Figure 2.15. Michael addition reaction products from reaction of aniline and o-quinone; (a) 4,5-diarylamino-1,2-dihydrobenzene (b) and (c) tautomers of 4,5-diarylamino-1,2-dihydrobenzene. d) Product from Schiff base reaction.[79]

The second parameter that affects Michael addition is the type of catechols. Shirmohammadi et al. studied the effect of catechol type on the kinetics of catechol oxidation in the presence of N-methylaniline.[72] The reaction mechanism is shown in Fig. 2.16. They reported that the reactivity of

catechol is higher than that of 4-methylcatechol. The lower reactivity of 4-methylcatechol is related to the steric effect of the methyl group. The occupation of methyl group reduces the probability of reaction by a factor of two. This reduced reactivity is also reflected in the difference in half-wave potential ($\Delta E_{1/2}$) of reactants (catechol/ 4-methylcatechol) and products (diphenylamine). $\Delta E_{1/2}$ for the catechol and 4-methylcatechol are 210 mV and 95 mV, respectively. By simulation, they also reported that the rate constants for the catechol and 4-methylcatechol are 1.23 and 0.42 $M^{-1}s^{-1}$, respectively. Besides the steric effect, the substitution group on the catechol ring also plays a role via its electronic properties. For substitution groups that are electronic-donating, they lead to a lower homogeneous rate constant in the Michael addition. For instance, the homogeneous rate constant in the case of catechol is 0.068 $M^{-1}s^{-1}$, while for 3-methylcatechol and 3-methoxycatechol these are 0.045 and 0.023 $M^{-1}s^{-1}$, respectively. [73]

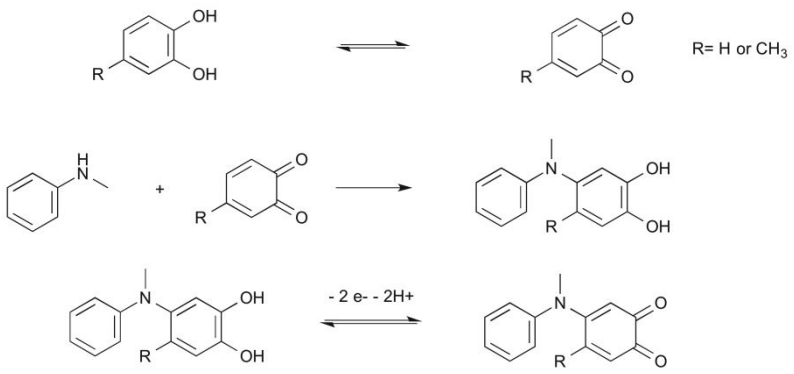

Figure 2.16. Reaction mechanism of catechol/4-methyl catechol with N-methylaniline[72]

The Michael addition is also affected by the basicity of the nucleophilic amines. Kazemi and coworkers reported the oxidation of catechol in the

presence of three secondary amines morpholine, dimethylamine and diethylamine.[73] The basicity trend of the three amines is decreasing in the order of diethylamine (basicity constant $k=1.05*10^{-3}$), dimethylamine ($k=4.79*10^{-4}$) and morpholine ($k=2.14*10^{-6}$). At a fixed pH, the concentration of free amines that are active for Michael addition showed an increasing trend in the series of diethylamine, dimethylamine and morpholine. A higher concentration of nucleophile causes a higher reaction rate. Therefore, morpholine showed the highest reaction rate. In the presence of aromatic amines, when the pKa of aromatic amine is low (pKa ~ 5.0), the quinone-aromatic amine adducts even formed at acidic pH.[74,75]

2. 2. 1. 2 Schiff base reaction

O-quinone can also react with amines by Schiff base reaction. The reaction mechanism is unclear. However, the quinone-imines from Schiff base reaction have been detected using ^{1}H NMR. Horak and co-workers characterized the product (Fig 2.17 (3)) from the reaction between cyclohexylamine (Fig. 2.17 (2)) with 3,4-di-tert-butyl-1,2-benzoquinone (Fig. 2.17 (1)) using ^{1}H NMR.[76]

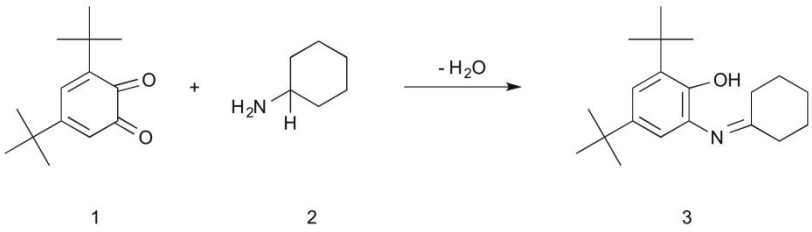

Figure 2.17. Reaction scheme of 3,4-di-tert-butyl-1,2-benzoquinone with cyclohexylamine[76]

The structures of the amine-catechol adducts have also been confirmed by characterization with FTIR. Feng et al. reported the reaction of poly(dopamine) with polyetherimide (PEI), and detected an absorption at 1623 cm^{-1} by FTIR. This absorption was attributed to the C=N stretch, which originates from a Schiff base formation.[77] The Schiff base reaction has also been identified for the reaction between lysine or polylysine with *o*-quinone.[78,79] Burzio and Waite reported the coupling of a model catechol-containing decapeptide compound with the amino acid lysine or glycine.[15] They analyzed the material by MALDI-TOF mass spectrometry, and found that the molar mass decreased by 18 after adding the amino acid to the oxidized decapeptide. This mass loss corresponds to a loss of one water molecule, which should be due to the Schiff base reaction between amine and *o*-quinone. Faure et al. have also indirectly observed the Schiff base product.[80] They reported that a nanogel formed from the reaction between a homopolymer of methacrylamide bearing 3,4-dihydroxy-L-phenylalanine (P(mdopa)) and poly(allylamine) at pH 10. They performed solid state ^{13}C NMR and found that the peak at a chemical shift of 160 ppm increased. They assigned this peak to the imine bond formed by the Schiff base reaction between oxidized *o*-quinone in P(mdopa) and the amines in poly(allyamine). When the oxidized *o*-quinones were occupied by metal ions, e.g. Ag^+, the product showed increased peak intensity at a chemical shift of 140 ppm in solid state ^{13}C NMR, indicating the formation of an amine-catechol adduct formed by Michael addition.[80]

Parameters influencing Schiff base reaction

The Schiff base reaction is strongly affected by pH. As proposed by Manthey et al., the reaction between catechol and 2-phenylethylamine at

neutral pH first forms a phenylethyl product (Fig. 2.18a) as the intermediate, which further transforms to imine-quinone adduct through Schiff base reaction (Fig. 2.18a).[79] At higher pH (11.7), as shown in Fig. 2.18b, the product is catalyzed to give an intermediate, which undergoes further Schiff base formation at the carbonyl of the vinylogous amide moiety rather than that of the less reactive vinylogous carboxylate anion.[79]

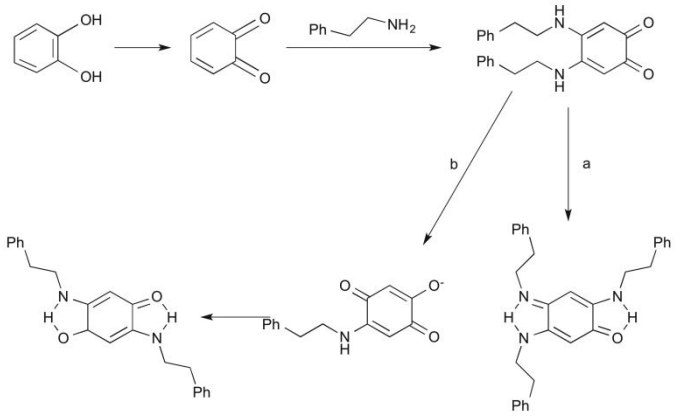

Figure 2.18. Reaction mechanism of catechol with 2-phenylethylamine under a) neutral pH; b) high pH (11.7)[79]

Another parameter that strongly affects Schiff base reaction is the chain length of the compound containing the primary aliphatic amine. A longer chain length leads to a decrease in the basicity of the α-NH_2, which enables the formation of catechol-NH_2 at a lower pH. As reported by Sealy, the ease of forming catechol-amine adducts is GlyGlyGly > GlyGly > Gly.[74]

2.2.1.3 Strecker degradation

O-quinone can also react with amines by Strecker degradation.[29] This reaction is an oxidative degradation at high temperature of α-amino acids

by *o*-quinone (Fig. 2.19). During the reaction, critical intermediates, i.e. related aldehydes (Strecker aldehydes) and 2-aminocarbonyl compounds, are produced. Such compounds contribute to aromas in processed food. Though the reaction is important, it is beyond the scope of our review, since our focus is on the crosslinking reactions of catechols in living organisms and natural products, without involving the reaction under heating conditions. Yaylayan et al. has written an excellent review about this research field. [81]

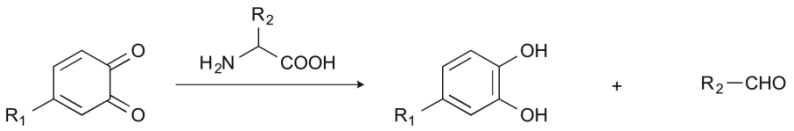

Figure 2.19. Strecker degradation reaction

To summarize, the reactive *o*-quinones react with nucleophilic amines, as indicated in Fig. 2.20, through three reaction pathways, i) Michael type addition, ii) Schiff base reaction and iii) Strecker degradation. In a Michael type addition an amine is attached to the catechol ring at the 4- or 5-position, and in a Schiff base reaction the amine attacks the 2- position at the catechol ring and an imine is created.

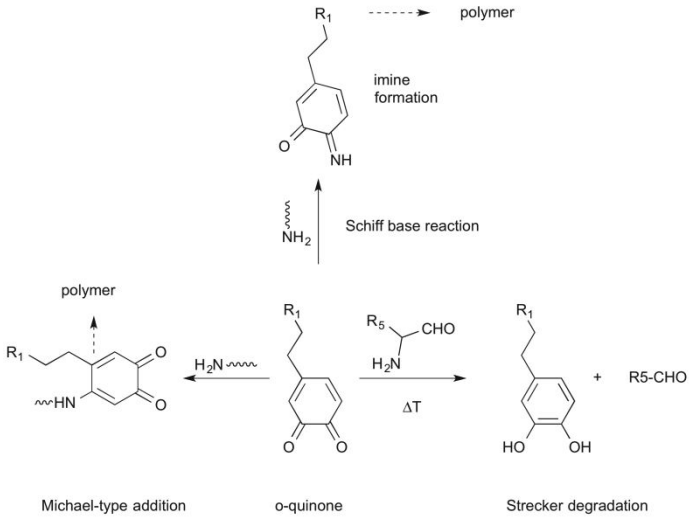

Figure 2.20. *o*-quinone reaction with amines

The reaction pathway between *o*-quinone and amine depends on the type of amine. Generally, aromatic amines favor Michael-type addition, whereas aliphatic amines favor Schiff base reaction. The quinone-amine adducts formed from these three mechanisms have been detected in both natural and synthetic mimics systems, such as cuticle sclerotization and natural food products. Three parameters can affect Michael type addition, i.e., pH, type of catechol groups and the basicity of nucleophile amines. In general, an increase in pH results in a higher reaction rate. Catechols with a substitute on its ring such as 4-methylcatechol reduce the reactivity when compared to catechols, mostly due to the steric effect of the methyl group. In addition, substituents that are electron donating also lead to a lower reaction rate. A third factor is the basicity of the nucleophilic amines. Generally, a more basic amine resulted in a higher reaction rate.

Schiff base reactions are affected by the pH and the chain length of the compound containing the primary amine The pH for the formation of

catechol-amine adducts can be tuned by the chain length of the primary aliphatic amine. A longer chain length leads to a decrease in the basicity of the primary amine, which allows the reaction to proceed at lower pH.

2.2.2 Reaction between catechols with thiols

The electrophilic *o*-quinone is highly reactive, and can react through Michael-type addition with nucleophilic thiol groups to form catechol-thiol adducts. The conjugation of the nucleophilic thiols to *o*-quinones was proposed to proceed as shown in Fig. 2.21.[82] The catechol and its derivatives are readily oxidized to form *o*-quinone. The quinones spontaneously undergo an attack by the nucleophilic thiol group at the 2-position of the ring, which leads to the regeneration of a catechol. The 2-substituted catechol moiety can be re-oxidized to form quinones. Thereafter, the resultant 2-substituted *o*-quinones undergo a second nucleophilic attack at the 5-position of the ring.

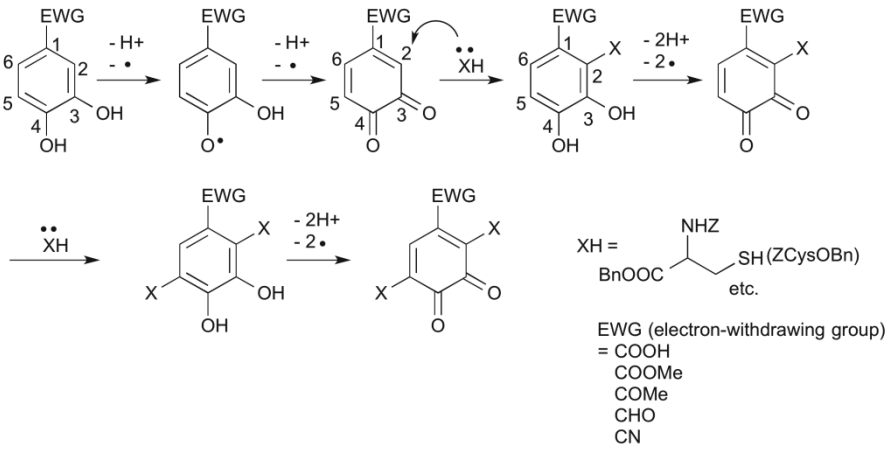

Figure 2.21. Proposed mechanism for the conjugation of catechol to a nucleophilic thiol group in aprotic solvent[82]

The presence of catechol-thiol adducts have been detected in many different systems.[83, 84] For instance, Waite and co-workers analyzed the components in cured glues secreted by the polychaete *Phragmatopoma californica*.[2] They found that the proteins contained 5-*S*-cysteinyl-dopa crosslinks that had been formed from dopa and cysteine during the setting process. The 5-*S*-cysteinyl-dopa has a molecular weight of 316.1 Da and the crosslink density was estimated to be one per 100 amino acids.[2] The same adduct has also been detected in the plaque footprints of California mussels *Mytilus californianus*. The crosslinked proteins could be isolated by acid hydrolysis due to the stability of catechol-thiol adducts in acid.[2,15,85] The obtained compounds were characterized by UV-Vis spectrophotometry, electrospray ionization mass spectrometry and tandem mass spectrometry. In another type of mussel: the green shell mussel *perna canaliculus*, both 5-*S*-Cysteinyl-dopa and 2-*S*-Cysteinyl-dopa crosslinks were detected. 5-*S*-cysteinyl-dopa crosslinks were 10 times more abundant than 2-*S*-Cysteinyl-dopa, reaching more than 1 mol% in the threads. These two crosslinks could also be formed in vitro by incubating the protein (*perna canaliculus* foot protein pcfp-1) solution with tyrosinase at pH 7.5.[2] Mfp-6 is known to have high concentrations of cysteine (more than 11 mol%).[3,86] The cysteine has a low pKa, which enables the formation of thiolate at pH 5.5 inside the mussel.[87] Since thiolates are more reductive than thiols, in mussel foot proteins, the thiolates are the operative antioxidant group.[88] The mechanism of dopaquinone reduction to catechol by thiolate is proposed to consist of two steps: i) nucleophilic attack of quinone by the first thiolate anion to form *S*-cysteinyl-dopa adducts; ii) the thiolether adducts are attacked by a second thiolate anion to form disulfide and dopa, as depicted in Fig. 2.22.[3]

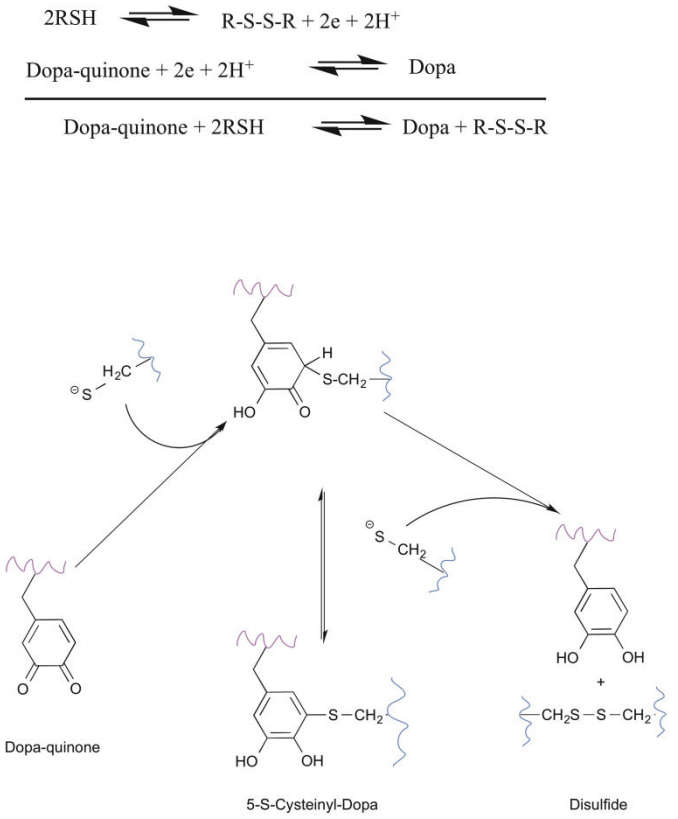

Figure 2.22. Proposed reaction mechanism of quinone reduction by thiolates.[154] Reprinted from ref. 154, Copyright 2011, by permission from Macmillan Publishers Ltd.

Thiol-catechol adducts have also been identified in synthetic polymers. Yoo and co-workers prepared electrospun nanofibrous meshes from catechol-conjugated 8-arm poly(ethylene glycol) (8cPEGa) and thiolated poly(lactic-co-glycolic acid) (PLGA-SH). They identified the conjugation of thiol and catechol by comparing the Raman spectra differences between nanofibers before (NF) and after crosslinking (XNF) using sodium periodate solutions.[89] They identified peaks at 640-820 cm^{-1} and 2180-2290 cm^{-1},

which were ascribed to C-S or C-S-C and sulfur-hydrogen bonds, respectively. The peak intensity of C-S or C-S-C in XNF increased 40-fold compared to NF, while the peak intensity of sulfur-hydrogen bond signals decreased significantly. These observations indicated the conjugation of the sulfur atom of PLGA-SH to the carbon atom of 8cPEGa.[89] Messersmith et al. designed a bio-inspired composite hydrogel with excellent tissue-adhesion properties using the thiol-catechol reaction. The composite was prepared by mixing hyaluronic acid conjugated with dopamine (HA-DA) with a thiol end-capped Pluronic F127 (Plu-SH) in PBS buffer at pH 7.4. By using UV-Vis spectroscopy, oxidation of catechol in HA-DA resulted in quinones (absorbance peak at 375 nm), which subsequently reacted with Plu-SH via thiol-catechol linkage at pH 7.4 (absorbance at 293 nm and 615 nm).[90]

Parameters influencing reaction between catechol and thiol

The addition efficiency of catechol to thiols depends on the oxidation rate of the catechols and on the nucleophilic strength of the thiols. In general, a higher oxidation rate of the catechols leads to a more efficient thiol-catechol conjugation. As reported by Darriet and co-workers, the type of catechol derivative affects the efficiency of catechol-thiol conjugation.[91] By analyzing the addition products upon reaction of 3-sulfanyhexan-1-ol (3SH) with *o*-quinones derived from (+)-catechin, (-)-epicatechin and caftaric acid, it was found that the production of adducts decreases in the order of catechin, epicatechin and caftaric acid. Another parameter that affects the addition efficiency is the nucleophilic strength of the thiols, which was modulated by the steric hindrance of the thiol groups. Primary thiols are more reactive than tertiary thiols.[92] Nikolantonaki et al. reported the

reactions between the thiols 3-sulfanyhexanl-ol (3SH), 2-furanmethanethiol (2FMT) and 4-methyl-4-sulfanylpentan-2-one (4MSP) and the catechol derivatives (+)-catechin and (-)-epicatechin. They demonstrated that 4MSP was relatively less reactive towards *o*-quinones than 2FMT and 3SH. 2FMT, is a primary thiol and is expected to have the least sterically hindered sulfhydryl group of the three thiols. Therefore, 2FMT showed the highest reactivity with the quinones. In contrast, 3SH and 4MSP are secondary and tertiary thiols, respectively. The stronger steric hindrance resulted in lower reactivity.[93]

To summarize, *o*-quinone undergoes a nucleophilic attack by thiols at the 2- and 5- position of the aromatic catechol ring, and thiol-catechol adducts are formed (Fig. 2.23). The addition efficiency of the reaction is increased by a higher oxidation rate of catechols. Moreover, primary thiols with less steric hindrance exhibit higher reactivity than secondary and tertiary thiols.

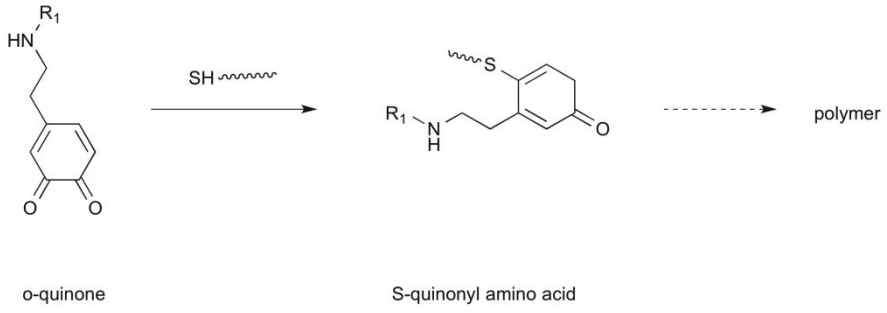

Figure 2.23. Michael type addition of catechols with thiols

2.2.3 Aryloxy radical coupling

The *o*-quinone groups can also go through reverse dismutation to an unoxidized catechol, yielding two highly reactive semi-quinone

radicals.[15,37] The formed radicals can couple to form di-dopa crosslinks (Fig. 2.24).

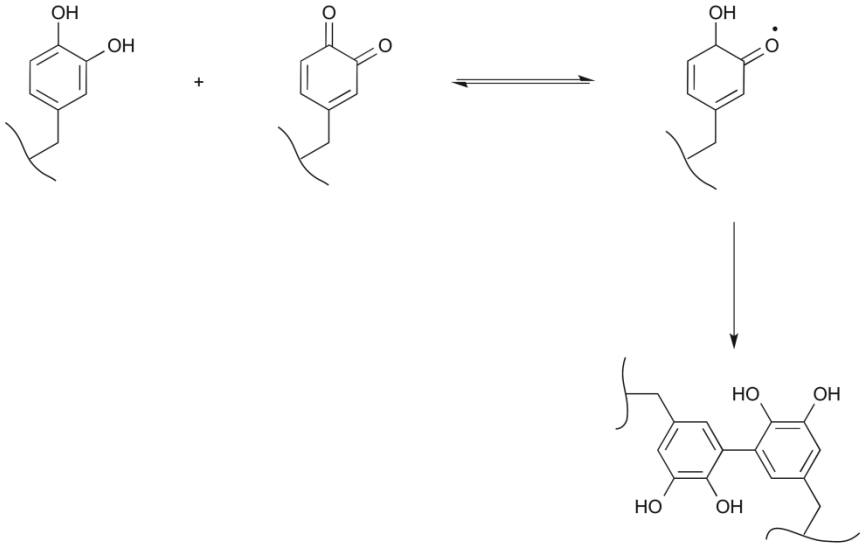

Figure 2.24. Crosslinking pathways by aryloxyl coupling

Haemers and co-workers studied the oxidation and aggregation of mfp-1 under different conditions by using photo correlation spectroscopy and proposed a kinetic model for the crosslinking pathway.[94] The crosslinking kinetics are related to the rate of dopa oxidation and the rate of *o*-quinone dismutation to form semiquinone radicals. They studied the crosslinking and aggregation of mfp-1 with and without the presence of a strong oxidizing reagent (iodate). In the presence of iodate, the dismutation of *o*-quinone with catechols is the rate-determining step, but the oxidation of catechol to *o*-quinone is very fast. Crosslinking stops when all dopa has been oxidized to *o*-quinone, resulting in limited crosslinking. Therefore, addition of an oxidizing reagent limits semiquinone radical formation, resulting in few crosslinks and small aggregates of mfp-1.

In the absence of a strong oxidizing reagent at high pH, Haemers and co-workers observed small particles at the beginning and large aggregates at the end of the reaction.[94] This observation indicates that the oxidation of catechol is the rate-determining step. This limitation causes dopa to remain available for the dismutation of *o*-quinone to form semiquinone radicals, so as to form more crosslinks and large aggregates. Increasing the pH in the absence of a strong oxidizing agent leads to faster catechol oxidation. In this way, more *o*-quinone can react with the remaining dopa to form more semiquinone radicals that can crosslinks. Therefore, a high pH yields a mfp-1 sample with more aggregates.

The presence of di-dopa crosslinks has also been identified in other natural systems.[15] For instance, Waite et al. has identified the 5, 5'-di-dihydroxyphenylalanine crosslinks in the protein of *Mytilus edulis* by NMR spectroscopy studies.[37] In a different study the reactivity of peptidyl-dopa in two euroendocrine peptides, (a neurotensin fragment and proctolin), was measured in vitro, in the presence of tyrosinase and periodate. The authors characterized the formed dimer/trimer by UV-Vis spectrophotometry and matrix-assisted laser desorption ionization mass spectrometry. They identified the presence of di-dopa crosslinks based on the absorbance peak at 410 nm of the dimer/trimer and a weight loss of 2 Da during each coupling of dopa.[95]

O-quinone may also tautomerize to form α,β-dehydro derivatives of catechols, which may further react to form crosslinks (Fig. 2.25). The presence of α,β-dehydro derivatives has been identified.[96-98] Rzepeki and Waite studied the oxidation of N-acetyl-dopa ethyl ester (NADEE) in the presence of sodium periodate using UV-Vis spectrometry.[97] Upon

oxidation, *o*-quinone formed, as evidenced by a characteristic peak at 392 nm. This quinone peak decayed, accompanied by the emergence of a peak at 320 nm, that is characteristic for the α,β-dehydro derivative of NADEE.[96,97] α,β-dehydro derivatives may further react with other functional groups to form crosslinked networks. However, a clear mechanism is still lacking.

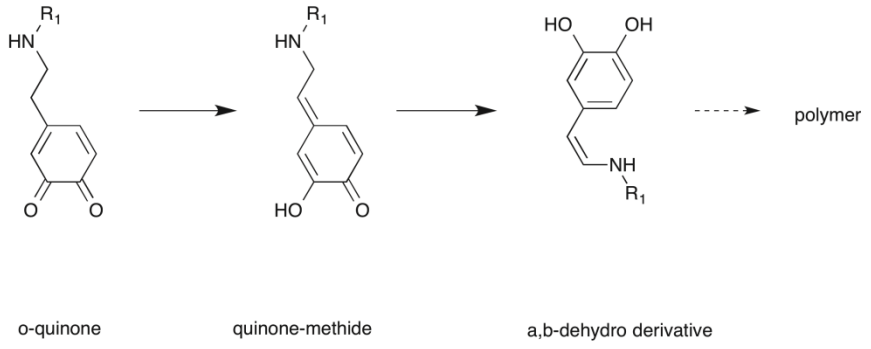

Figure 2.25. Tautomerization of *o*-quinone to α,β-dehydro derivative

To summarize, as indicated in Fig. 2.26, *o*-quinones can undergo dismutation with catechols to form *o*-semiquinone radicals, which further can couple to form crosslinks. The kinetics of this pathway is dependent on the presence of extra oxidants. In addition, *o*-quinones may also tautomerize to form α,β-dehydro derivatives, which further react to form crosslinks.

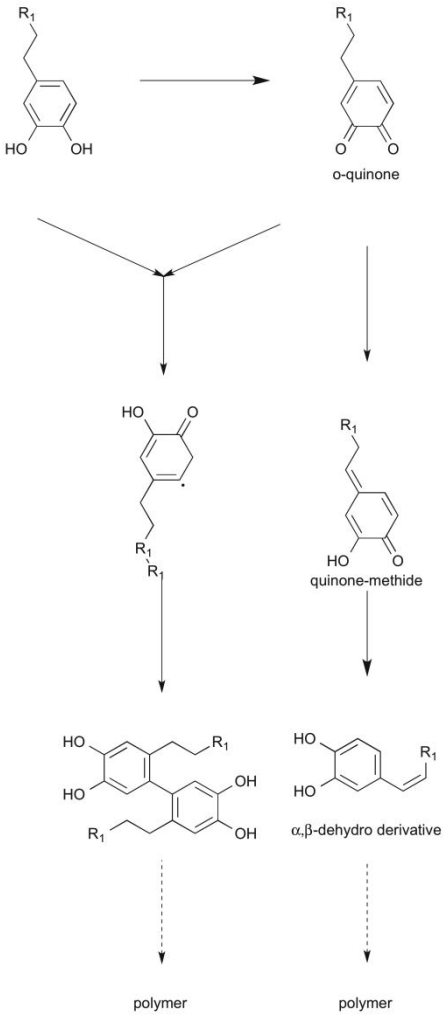

Figure 2.26. *o*-quinone forms crosslinks via two pathways: dismutation and tautomerization

2.3 Polydopamine formation mechanism and possible structures

Catecholamines can undergo oxidative self-polymerization under mild alkaline condition to form homopolymers[20,99]. The most famous example is polydopamine (PDA). PDA is insoluble in water (acid, neutral and basic), and in almost all common organic solvents and can be deposited onto any

type of substrate.[100] This versatility, together with the reactivity of catechol with other functional groups (e.g. amines, thiols) has aroused a lot of interest in different applications, such as surface modification, biomineralization, anti-fouling coatings, water purification membranes, biotechnology and biomedicine.[20,99,101,102]

Despite the extensive applications of PDA, the molecular mechanism of formation is still ambiguous. Initially, PDA formation was believed to resemble the formation mechanism of melanin that occurs in living organisms (Fig. 2.27). It was proposed that the oxidation of dopamine at basic pH leads to the formation of dopamine quinone, which subsequently goes through intramolecular cyclisation to form leucodopaminechrome. The leucodopaminechrome is further oxidized to form dopaminechrome. Thereafter, dopaminechrome rearranges to form 5,6-dihydroxyindole (DHI), which is further oxidized to form 5,6-indolequinone. DHI and 5,6-indolequinone can subsequently go through reverse dismutation reactions to form crosslinks. [31]

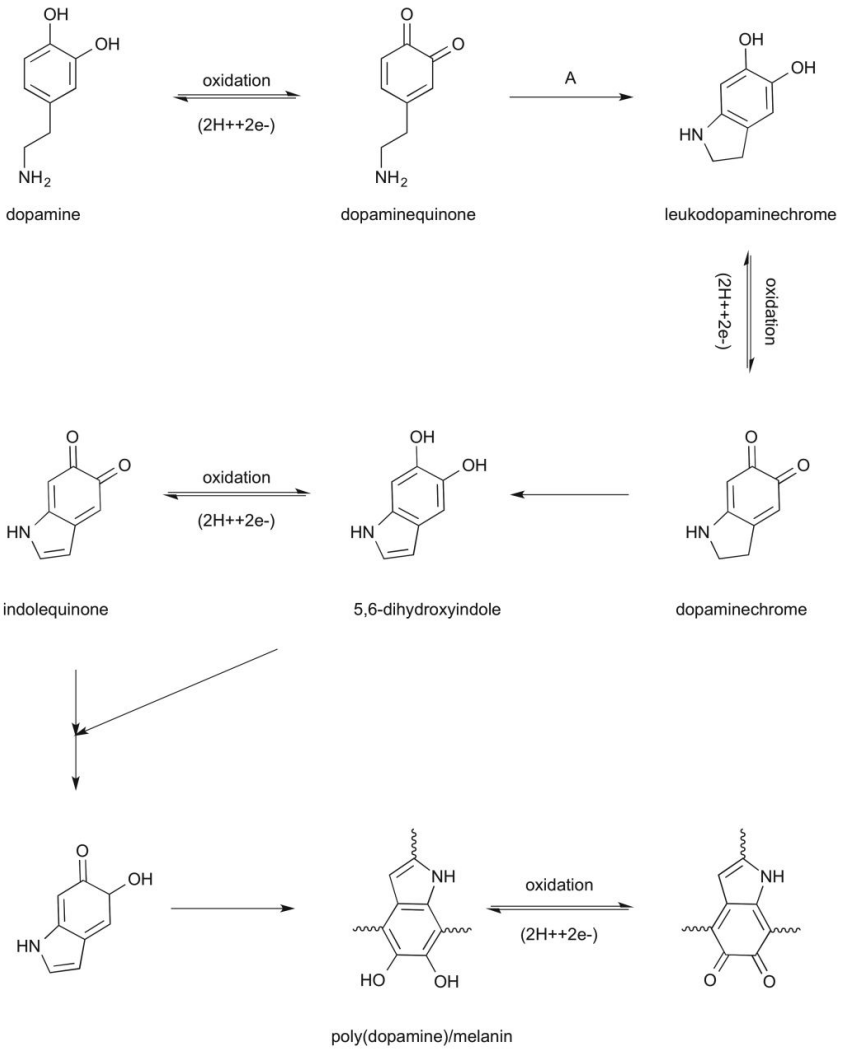

Figure 2.27. Reaction mechanism of melanin formation by dopamine oxidation.[155] Reproduced with permission from ref. 155. Copyright 2013, WILEY-VCH Verlag GmbH & Co. KGaA, Weinheim.

Bielawski and co-workers proposed that the structure of PDA is a supramolecular aggregate of monomers (consisting of mainly DHI and its dione derivatives) instead of made up of covalent bonds among dopamines (Fig. 2.28).[100] They employed a variety of solid state spectroscopic and

crystallographic techniques to analyze the isolated product from the polymerization of 3-hydroxytyramine hydrochloride under aerobic conditions, in tris(hydroxymethyl)aminomethane (TRIS) buffer at pH 8.5. They proposed that the PDA is an aggregate held together by strong non-covalent forces including hydrogen bonding, π-stacking, and charge transfer.

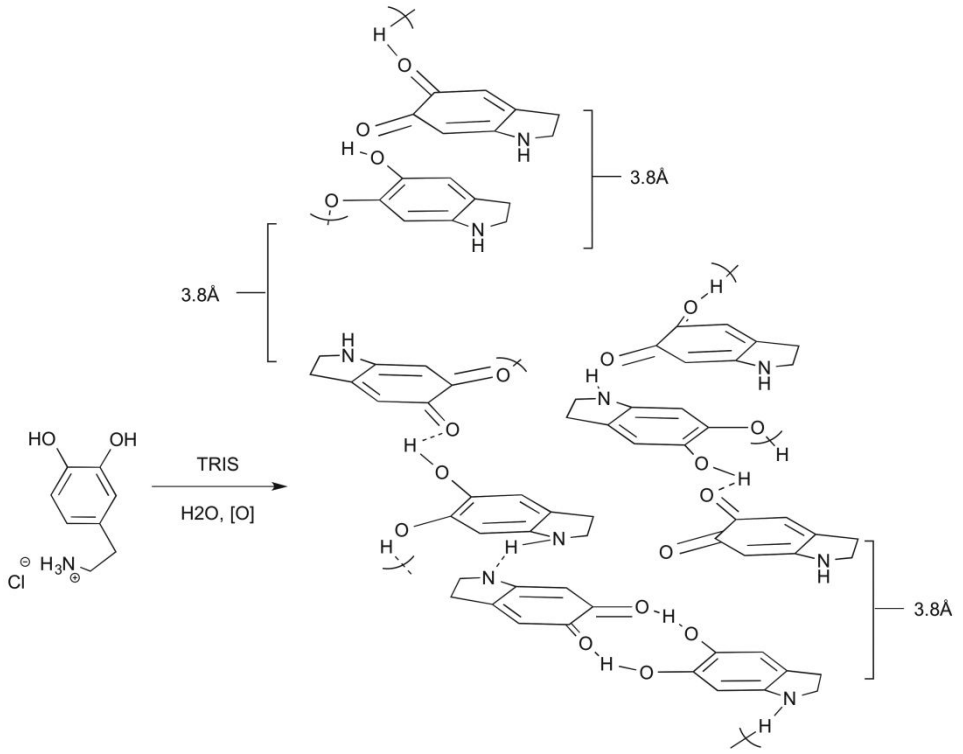

Figure 2.28. The PDA material is proposed to be comprised of intra- and interchain noncovalent interactions, including hydrogen bonding, π-stacking, and charge transfer. [100] Reprinted from ref. 100, Copyright 2010, with permission from Elsevier.

Recently, it has also been proposed that both covalent and non-covalent interactions (Fig. 2.29)[103] co-contribute to PDA formation. The proposed covalent interactions are similar to the pathway stated in Fig. 2.27. The

dopamine goes through oxidative polymerization via DHI to form a DHI-DHI dimer, or dopamine-DHI-DHI trimer conjugates, which ultimately assembles to form polymeric aggregates. D'Ischia and co-workers reported three possible components in PDA, namely uncyclized catecholamine, cyclized indole units, and novel pyrrolecarboxylic acid moieties (Fig. 2.30).[104] Moreover, the PDA has also been proven to arise from a physical, self-assembled trimer of $(dopamine)_2$/DHI. The trimer complex was found to be so tightly trapped within polydopamine, that it barely escapes from the dopamine complex.[103] However, Buehler and co-workers reported that a non-covalent DHI aggregate did not contribute to PDA formation.[105] They developed a computational model of PDA and performed nano-indentation experiments on the prepared PDA film. They found that the Young's modulus from both studies were 4.1-4.4, and 4.3-10.5 GPa, respectively. The high Young's modulus excludes the possibility of PDA being formed from physically self-assembled aggregates. We should point out, however, that all these models have been proposed rather than fully proven.

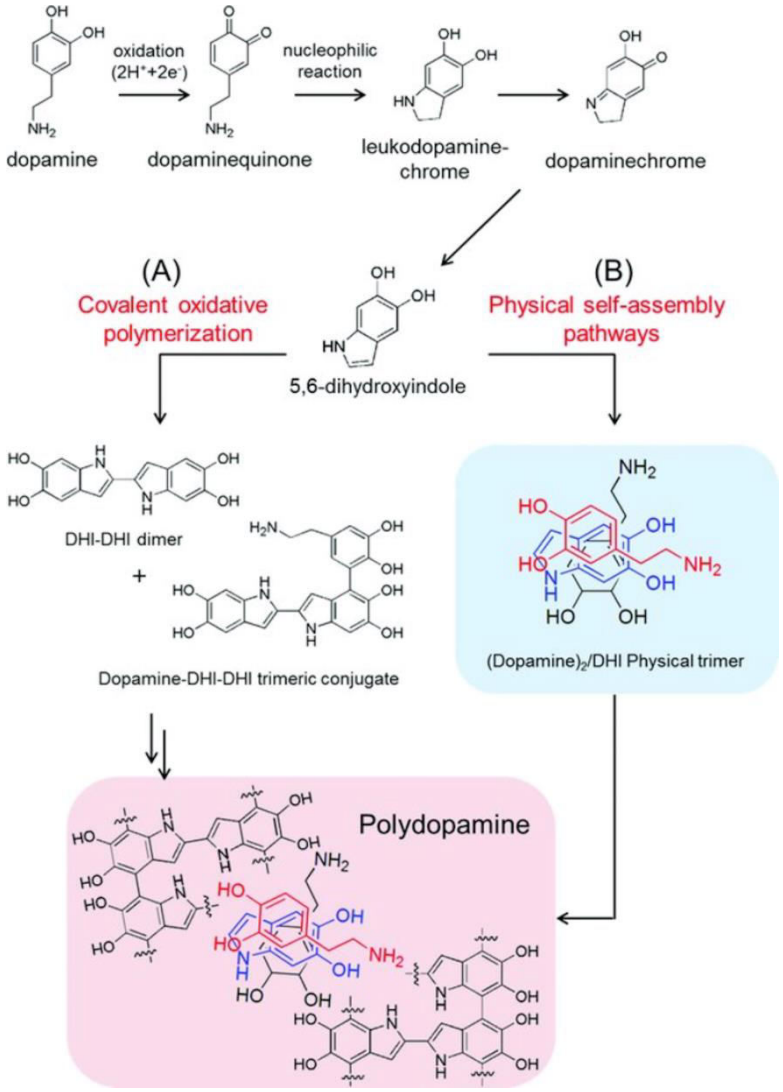

Figure 2.29. Polydopamine synthesis occurs via two pathways.[103] Reprinted with permission from ref. 103. Copyright (1982) American Chemical Society.

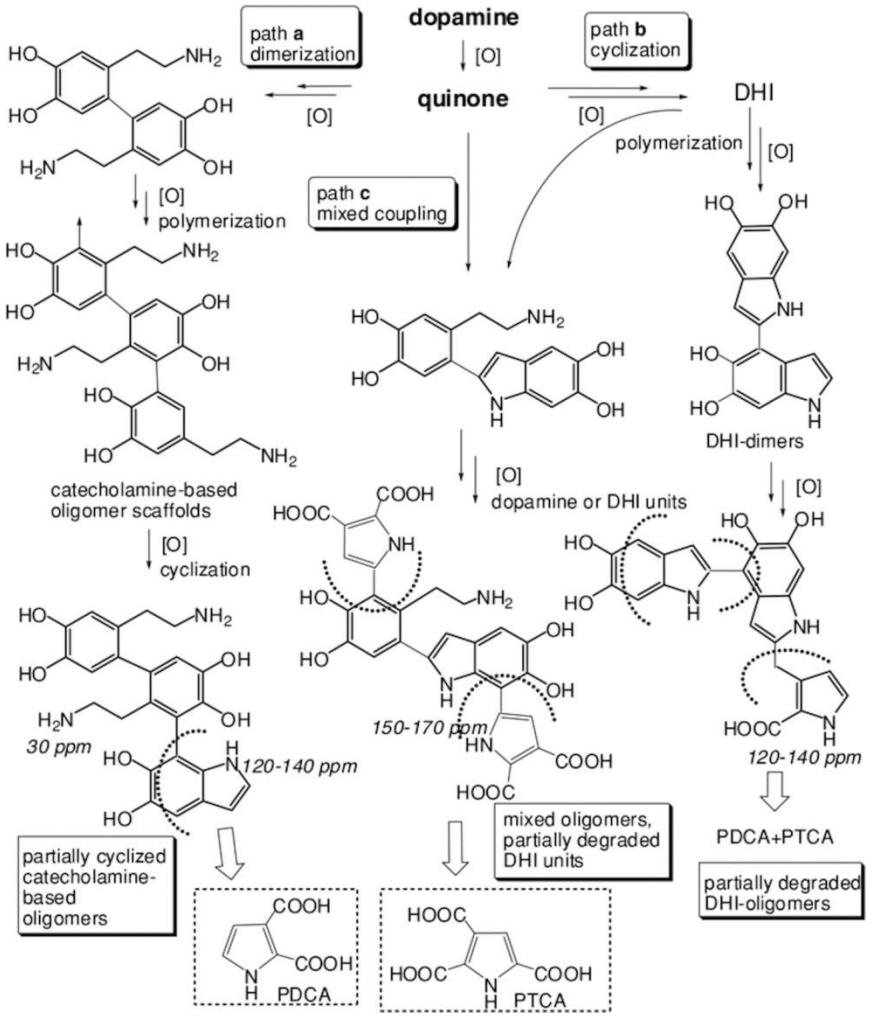

Figure 2.30. Simplified overall view of main reaction pathways involved in polydopamine formation. [104] Reproduced with permission from ref. 104. Copyright 2012, WILEY-VCH Verlag GmbH & Co. KGaA, Weinheim.

Based on the proposed mechanisms, PDA, in analogy to eumelanin,[106,107] can be interpreted as supramolecular aggregates assembled from the oligomers of DHI, rather than a conventionally recognized polymer. This aggregate structure of PDA, similar to eumelanin, is thought to give rise to

the PDA broadband absorption spectrum and enhanced absorption intensity at the higher-energy end.[107] The combination of these absorption characteristics and catechol binding functionality that PDA exhibits, results in striking optical, adhesive and mechanical properties. Lu, et al. has reported a comprehensive review on the physicochemical properties and applications of PDA.[23]

Parameters influencing polydopamine formation

The PDA formation is affected by several parameters, such as the dopamine concentration, buffer type, pH, the presence of oxidant, preparation method, etc. In the following, these parameters will be discussed one by one.

The starting concentration of dopamine affects the final composition of PDA. d'Ischia and co-workers studied the polymerization of dopamine at pH 8.5 in TRIS, $NaHCO_3$, or phosphate buffer solutions, respectively.[108] They found that when the quinone was generated by auto-oxidation in the presence of a high dopamine concentration (e.g. $10*10^{-3}$ M), the generated quinone might be efficiently trapped, yielding mainly dimers. In contrast, when the concentration of dopamine is low (e.g. $0.5*10^{-3}$ M), the quinone was formed more slowly, so that the quinones were less trapped. In this way, the chances for intramolecular cyclization to give DHI were increased. The degree of polymerization of the DHI indole units was also higher than those proposed from dopamine at a higher concentration (e.g. $10*10^{-3}$ M). Ruch and co-workers also investigated the influence of dopamine concentration on the kinetics of polymerization deposition.[109] They investigated the polymerization of dopamine in TRIS buffer at pH 8.5 for different dopamine concentrations. An exponential decay function was used to describe the deposition kinetics. $d(t) = d_0 + d_{max}(1\text{-}e^{(-kt)})$, in which $d(t)$ is the time-dependent film thickness of polydopamine; d_{max} is the maximal

thickness, and k is the kinetic constant. They found that d_{max} increased linearly with the dopamine initial concentration in the range of 0.1-5 g/L. In the presence of dopamine at 2 g/L and at pH 8.5, the film thickness was limited to 45 nm, as observed by Lee et al. and other researchers. However, by increasing the initial dopamine concentration to 3 and 5 g/L, the film thickness limitation could be overcome. Before the film deposition reached equilibrium, the film thicknesses were already 50 (for 3 g/L) and 70 nm (for 5 g/L), respectively. The thicker films also gave a higher roughness.

The polymerization of dopamine is also influenced by the buffer that is used. When dopamine is polymerized in TRIS buffer, as indicated by ^{13}C solid state NMR, the TRIS was incorporated into the polydopamine. Therefore, the intramolecular cyclization of dopamine/quinone was inhibited, which resulted in a longer reaction time (e.g. 72h) but led to the same precipitates as compared to those prepared from phosphate or hydrogen carbonate buffers.[108] Ruch and co-workers have also reported the incorporation of TRIS in PDA during the reaction.[110] They ascribed this incorporation to the presence of primary amino groups. Moreover, they found that for the polymerization of dopamine at pH 8.5 in phosphate buffer, the film could reach a thickness of up to 100 nm, whereas one obtains a thickness of 45 nm in the TRIS buffer. At pH 8.5, the phosphate was predominately present in the form of HPO_4^{2-}, and could form hydrogen bonds with the hydroxyl groups of polydopamine, resulting in a film with higher thickness. In addition, the film thickness limitation in the single-step polymerization in TRIS of pH 8.5 can be overcome by using a multistep deposition.[34] The multistep deposition consists of an initial immersion of the substrate in a basic dopamine solution, followed by drying the film with a nitrogen stream, and re-initiating the oxidation process of the film by immersing it back into

the starting polydopamine solution. This way, the film thickness can be grown from a few nanometers to the few hundred-nanometer.

The polymerization of dopamine largely depends on the pH. Ruch reported that d_{max} and the kinetic constant in the deposition kinetics $d(t) = d_0 + d_{max}(1\text{-}e^{(-kt)})$, were largely affected by pH. In the pH range of 5-8.8, the result which unfortunately featured large error bars showed that d_{max} increased with pH, and leveled off after pH 8.5, while k increased with pH in the range of 7.0-10.2 in a reproducible way.

PDA can be formed not only under mild basic conditions; the reaction can also proceed in the presence of other oxidants, such as ammonium persulfate, sodium periodate, sodium chlorate, or Cu^{2+}.[111] It has been found that the nature of the oxidant also affects PDA formation. If the dopamine was incubated under acidic conditions, no PDA could be formed.[110] However, by adding Cu^{2+} (Cu^{2+}: dopamine molar ratio 3), the PDA film thickness grew linearly to 60 nm within 80 h. Moreover, the initial growth of the film thickness was also slower than that from PDA formation in TRIS buffer at pH 8.5. The resulting film showed different optical properties from that prepared from TRIS buffer. The UV spectra of the film using Cu^{2+} as the oxidant showed a distinct peak at 370 nm and a small peak at 320 nm. In contrast, a film prepared using O_2 as the oxidant showed a similar spectrum to that of melanin. The authors attributed these differences to local changes in the branching between adjacent DHI due to the presence of Cu^{2+}.

To summarize, dopamine undergoes oxidative self-polymerization under mild alkaline conditions to form PDA (Fig. 2.31). The detailed mechanism of the polymerization as well as the structure of final PDA is still under debate. In general, both covalent and non-covalent bonds are involved in

the formation of PDA. The PDA formation is influenced by several factors, such as dopamine concentration, buffer type, pH, the presence of oxidant, preparation method, etc. By tuning these parameters, the deposition thickness of PDA on various types of substrates can be optimized.

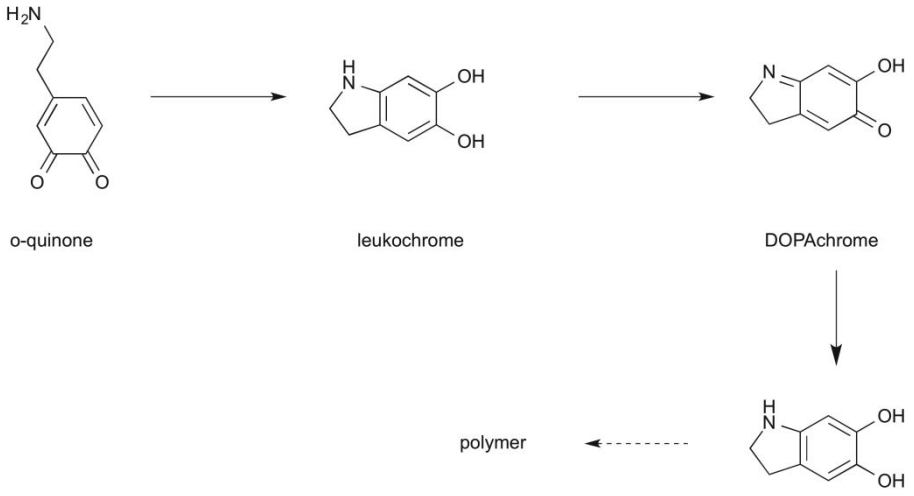

Figure 2.31. Polydopamine formation

3. Role of metal ions in adhesive curing

It has been proposed that metal ions play a key role in the cross-linking process of mussel proteins and other natural systems. In mussel adhesive, iron and other metals are present at remarkably high concentrations. The content in the organisms can be10,000 times higher than in the open sea.[112-115] Holten-Andersen et al. demonstrated that in *M. galloprovincialis* mussel byssal threads iron and dopa are colocated in the cuticle, which is the robust protective coating covering the threads (Fig. 2.32).[116] The cuticle exhibits both high hardness and high extensibility.[117,118] The colocalization of dopa and metal ions coupled with the remarkable mechanical properties of byssal threads suggest that metals ions play an important role in mussel foot

cohesion. Another natural example is the marine worm *Bdelloura candida* producing a dopa-protein, which is believed to contribute to the curing of the primary, inner layer of its eggshells.[119,120] During the hardening and darkening of the eggshell, the metal levels (e.g., iron, copper, zinc, and lead) increase, suggesting the occurrence of a metal-dependent curing process.

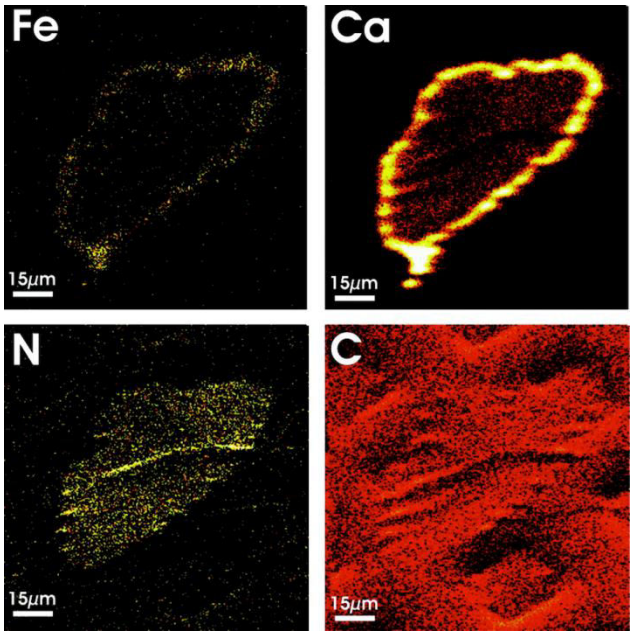

Figure 2.32: Maps of Fe, Ca, N, and C distributions in a transverse cross-section of a mussel thread generated using secondary ion mass spectroscopy (SIMS).[116] Reprinted with permission from ref. 116. Copyright (2009) American Chemical Society

It has been proposed that metal ions either chelate with catechols to form coordination complexes or mediate covalent crosslinking. In section 3.1 the formation of metal-catechol coordination complexes are discussed and the influence of different parameters such as pH, catechol: metal ion ratio and ring substituents. Growing evidence supports the role of metal-mediated covalent crosslinking in both natural and synthetic systems, which is discussed in

section 3.2. We will focus our discussion on iron ions, because most of the work done so far was based on iron. In section 3.3 the influence of other metal ions on catechol crosslinking will be discussed.

3.1 Fe^{3+}-catechol coordination

Catecholic hydroxyls in dopa can chelate with Fe^{3+} ions to form reversible non-covalent complexes in a variety of natural organisms such as marine worm eggshells, sea squirt wound plugs, and marine mussel adhesives.[121-129] For instance, some microorganisms contain molecules called siderophores that contain catechols to facilitate the solubilization and transportation of iron. One important example is enterobactin, which is produced by enteric bacteria and strongly chelates with Fe^{3+} with a stability constant of 10^{49}.[130,131]

A chelate is formed when a catechol donates a nonbonding electron pair to the iron ion. The non-covalent complexes are formed in three different modes: mono, bis and tris catechol-Fe^{3+} complexes (Fig. 2.33).[129] The stoichiometry of catechol-Fe^{3+} complexes seems to be controlled by pH via the deprotonation of catecholic hydroxyls. The stoichiometric transitions were measured using a catechol functionalized polyethylene glycol polymer solution with $FeCl_3$ in a catechol: Fe molar ratio of 3: 1. The mono catechol-Fe^{3+} complexes dominate at pH < 5.6, bis at 5.6 < pH < 9.1, and tris at pH > 9.1 (Fig. 2.34).[132] These measurements were in agreement with earlier measurements on Fe^{3+} catechol complex formation using UV-Vis spectroscopy.[133] The data was also corroborated by the observation from Taylor et al. that at pH 7 both bis and tris catechol-Fe^{3+} complexes were present in *Mytilus edulis* adhesive protein, mfp-1[134]. Zeng et al. proposed that the complexation mode (tris, bis, or mono complex) depends on the iron concentration.[135] At low Fe^{3+}, the tris complex formed; while at high Fe^{3+}, the mono complex formed. This dependence is was in agreement with their study

on the adhesion between mfp-1 films in the presence of Fe^{3+}. In the presence of low Fe^{3+} concentration (10 μM), a number of tris complexes were formed, and significant and reversible adhesion was detected when two mfp-1 layers were brought into contact and immediately separated. In contrast, at higher Fe^{3+} concentration (100 μM), only mono complexes were formed, resulting in poor adhesion.[135]

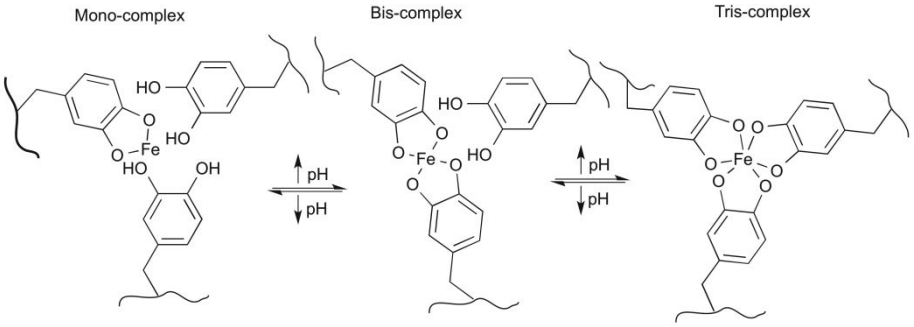

Figure 2.33: pH dependent stoichiometry of Fe^{3+}. [132]

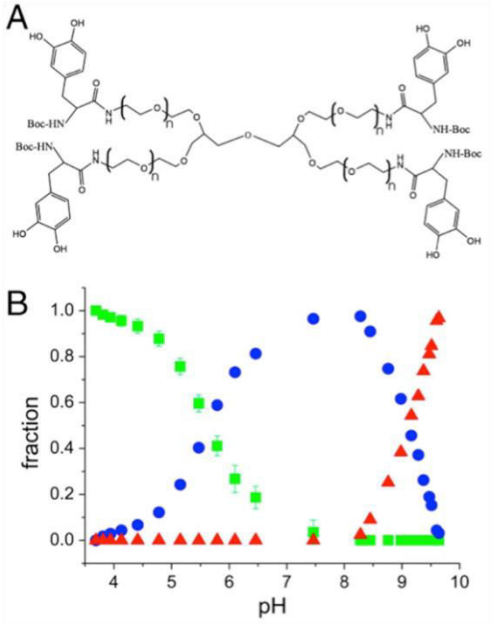

Figure 2.34: Catechol functionalized polyethylene glycol polymer. Relative fractions of mono bis and tris catechol-Fe3+ complexes in solutions with catechol-PEG with $FeCl_3$ (catechol: Fe molar ratio of 3:1) as a function of pH.[132]

It is important to note, that the solubility of Fe^{3+} is very low, especially at high pH. Therefore, to obtain bis and tris complexes in synthetic catechol functionalized polymer systems it was necessary to prebind Fe^{3+} in mono catechol-Fe^{3+} complexes at low pH before raising pH.[132] Analogously, it was proposed by Holten-Andersen et al. that in mussel byssal threads, Fe^{3+} is prebound in mono-dopa-Fe^{3+} complexes by mfp-1 in secretory granules at pH ≤ 5. Upon secretion into the seawater the pH increases which could cause the spontaneous physical crosslinking by bis- and/or tris-dopa-Fe^{3+} complex formation.[132]

The substitution groups on the catecholic aromatic ring affect the catechol-Fe^{3+} coordination by changing the pK_a values of the catechol analogues.

Studies on natural siderophores have established that catechol protonation is the rate-determining step in the dissociation of Fe^{3+}-catechol complexes.[136] Catechol derivatives exhibiting higher stability constants upon chelating with Fe^{3+} also exhibit a higher proton affinity, i.e., a higher pK_a value. Therefore, when the substitution group is electron-withdrawing, e.g., $-NO_2$, it withdraws the electron density from the catechol moiety, resulting in lower pK_a values (pK_a for nitrocatechol is 6.7 and 10.3; for catechol is 9.1 and 14).[137-139] Thereby, nitro-substituted catechols are easier to chelate, i.e., nitrocatechol chelates with Fe^{3+} and forms crosslinks at lower pH values than catechols. This statement is confirmed by Menyo and co-workers. They studied the crosslinking of 4-arm PEG, end-functionalized with catechol, or nitrocatechol with Fe^{3+} at pH 9. The nitrocatechol-based hydrogels, as indicated from UV-Vis spectrophotometry data, are predominately tri-coordinated, while catechol-based gels have a great number of bis-coordinated complexes.[140]

The ability to form bis and tris catechol complexes implicates the role of iron ions as non-covalent cross-linking agents. Iron is particularly interesting, because the stability constants of bis- and tris-catechol-Fe^{3+} complexes are among the highest known for metal-ligand chelates. [121,129,134] Single molecule force measurements showed that the catechol-Fe^{3+} bond is only slightly weaker than a covalent bond under identical loading conditions[71]. It was also shown that the catechol-Fe^{3+} bonds can spontaneously reform after breaking, providing intrinsic self-healing properties to the material.[71]

In addition, the loss of material stiffness and hardness upon metal removal (using the chelating agent ethylenediaminetetra-acetic acid (EDTA)) observed for both synthetic and natural materials is strongly suggestive of a non-covalent crosslinking role.[141] Nevertheless, there is growing evidence that Fe^{3+}

does not only lead to non-covalent complex formation, but also plays a key role in covalent crosslinking. This will be the topic of the next section.

3.2 Covalent crosslinking mediated by Fe^{3+}

Besides coordination bond formation, Fe^{3+} may also facilitate catechol oxidation, because oxidation of catechol and reduction of Fe^{3+} occur at similar potentials (~0.75 V) [142]. Upon further reaction of the oxidized catechol, covalent crosslinks may be formed. Wilker et al. proposed [143,144] that tris dopa-Fe^{3+} complexes undergo a valence tautomerisation in which Fe^{3+} is reduced to Fe(II), while dopa is oxidized to semiquinone radicals (Fig. 2.35). The semiquinone may further react with O_2 to generate a radical species which may persist or convert to other radicals. Radical-radical coupling can occur to provide crosslinking. This mechanism is based on insights from spectroscopic studies on whole adhesive plaques performed by Wilker et al. Electron paramagnetic resonance (EPR) spectra were obtained for plaques and showed clear signals for both an organic radical species and Fe^{3+}. In addition, they collected an EPR spectrum of extracted dopa containing adhesive proteins (mfp-1 and mfp-2) before deposition and crosslinking, which displayed no significant signal. Addition of Fe^{3+} to a solution of these proteins resulted in immediate precipitation and the EPR spectrum of the precipitate indicated a radical species and a Fe^{3+} signal. They concluded that the radical found in plaques thus appeared to arise from Fe^{3+} mediated oxidation of the protein.[114]

Additional evidence for covalent crosslinking was provided by Messersmith et al.[145] Gel permeation chromatography (GPC) was used to provide direct evidence of Fe^{3+} mediated covalent crosslinking for catechol functionalized polyethylene glycol polymers. GPC data showed that the extent and rate of catechol-catechol covalent bond formation mediated by Fe^{3+} were highest at low pH. In addition, at pH 9 after 24 h in the absence of Fe^{3+} larger aggregates

were found than in the presence of Fe^{3+}. The authors suggested that the Fe^{3+} may stabilize catechols against auto-oxidation by coordination. The pH dependency was corroborated by treatment of the materials with a chelating agent (EDTA). The samples designed at pH 3 were stable in EDTA, while materials fabricated at pH 5, 7 and 9 almost entirely dissolved when they were exposed to EDTA. However, the rheological properties of the different materials were not completely consistent with this picture. This needs further clarification. Finally, a pH dependent dual crosslinking mechanism was proposed, with covalent catechol-catechol adducts and Fe^{3+} catechol coordination dominating at acidic and basic conditions, respectively (Fig. 2.36).[145] The presence of catechol-catechol covalent bond has been, recently, directly observed for the reaction between 3-(3,4-dihydroxyphenyl)propionic acid (DHPA) and Fe^{3+} at acidic pH using NMR.[146] The protection of catechol against auto-oxidation at basic pH in the presence of Fe^{3+} has also been observed for the reaction between DOPA-containing peptide (Ac-Ser-DOPA-NH_2) and Fe^{3+}. By using HPLC-MS, at pH 9, no dimers of dipeptide were detected.[146]

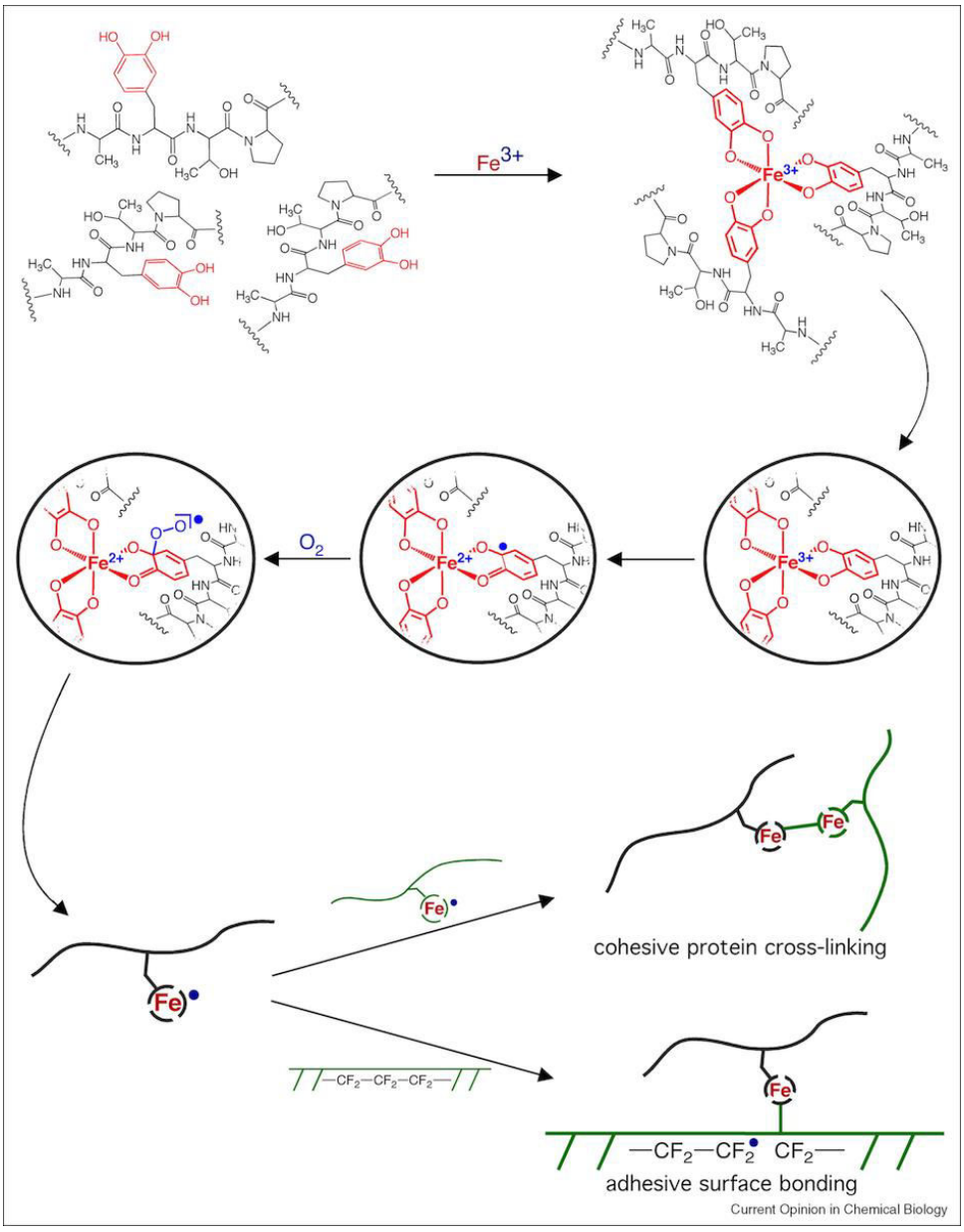

Figure 2.35. Proposed mechanism of iron mediated catechol crosslinking.[143]

Reprinted from ref. 143, Copyright 2010, with permission from Elsevier.

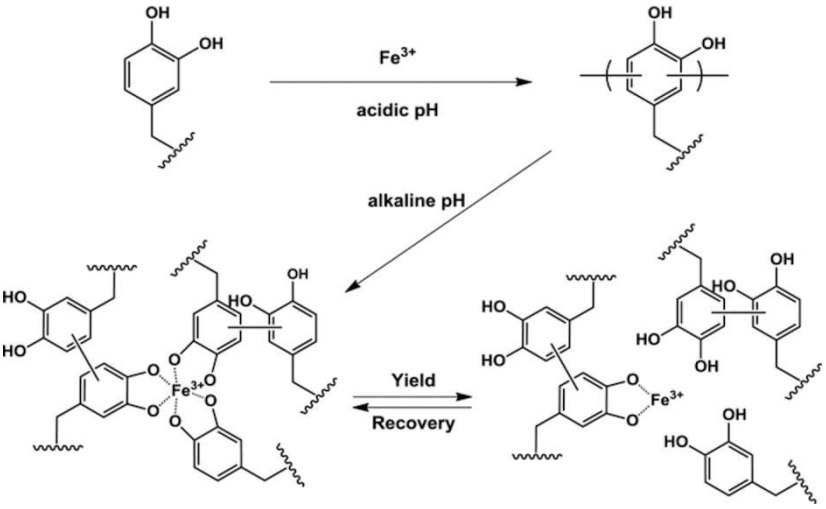

Figure 2.36: Proposed pH dependence of covalent and coordination bond formation mediated by Fe^{3+} in catechol functionalized polymers.[145] Reproduced with permission from ref. 145. Copyright 2013, WILEY-VCH Verlag GmbH & Co. KGaA, Weinheim.

As the catechol Fe^{3+} complexes are in dynamic equilibrium,[129] Xu et al. suggested that the ratio of coordination to covalent bonds may shift over time from coordination bond to covalent bonds.[147] The authors reported that at shorter contact times (10 min) and low Fe^{3+} concentration (10μM), reversible interactions between catechol and Fe^{3+} were formed. This resulted in a relatively low work of adhesion between two mfp-1 coated surfaces. With longer contact times (100 min), the redox activity of Fe^{3+} facilitates catechol oxidation by one-electron oxidation, resulting in covalent bond formation and higher adhesion (20 mN/m).[135,144] The dynamic nature of tris-complexes, i.e., the tendency to oxidize has also been observed for Al^{3+}. Different from Fe^{3+}, Al^{3+} does not have Al^{2+} state, and the one-electron oxidation does not exist. Nevertheless, it was shown that, at pH 12, the catechol-ended 4-arm PEG hydrogel changed from pure colorless (freshly prepared hydrogel) to brown in

one week. This color change implies the auto-oxidation of tris-chelated catechol under ambient conditions.[132,140]

By combining the insights gained, a picture emerges of a dual crosslinking mechanism: in the presence of iron, catechol-containing polymers seem to cure by a combination of coordination and covalent crosslinking. By controlling the amount and distributions of both bonds excellent cohesive properties may be obtained.

3.3 Interaction between catechol and other metal ions

In addition to Fe^{3+}, catechol can also interact with other transition metal ions. Wilker used a catechol-containing model system, i.e., acetyl-alanine-dopa-threonine-proline-$CONH_2$ peptide, to study catechol complexation with first-row transition metals.[122] UV-Vis spectrometry was used to track the complexation formation during base titration (pH in the range of 3 to 11). They found that low-valent metals (i.e., Cu^{2+}, Co^{2+}, Ni^{2+}) formed 1:1 and 1:2 complexes, while high-valent ions (i.e. Fe^{3+}, V^{3+}, VO^{2+}) formed 1:1, 1:2, and 1:3 complexes.[122] This suggests that these metal ions may also contribute to the curing of dopa proteins in natural systems. The different metal-catechol complexation stoichiometry has also been reported for Fe^{3+} and V^{3+} at pH 8.[148] Holten-Andersen et al. investigated the complexation of catechol end-functionalized 4-arm PEG with Fe^{3+} and V^{3+}, respectively. The UV-Vis spectra and Raman spectroscopy data showed that at pH 8, Fe^{3+} interacts with catechol via bis- coordination, while V^{3+} via tri-coordination.

Hight and Wilker found that metal ions in their reduced state, i.e., Fe^{2+}, V^{3+}, or Mn^{2+}, interact with catechols to form a weak coordination bond.[149] The weak bonding may be enhanced by the addition of oxidants, e.g., hydrogen peroxide or sodium periodate. By adding both metal ions (reduced state) and oxidants

to catechol-based derivatives, the reduced metal ions (e.g. Fe^{2+}) may first be oxidized to its oxidized state (Fe^{3+}), which further complexes with the catechols to form strong crosslinks. This enhancement due to the oxidants, as reported by Sever and Wilker, has been observed in a study on the influence of oxidants on the curing of dopa proteins in mussel adhesive by metal ions.[149] They found that, by adding oxidants (H_2O_2 or $NaIO_4$)[150,151], the resulting crosslinks from Mn^{2+}, V^{3+} and Fe^{2+} showed higher penetration forces compared to that in the absence of the oxidants, indicating a higher extent of curing. They ascribed this enhanced curing due to the oxidation of Mn^{2+}, V^{3+} and Fe^{2+} to Mn^{7+}, V^{5+}, and Fe^{3+}, respectively. The enhancement has also been observed for Ga^{3+} by adding IO_4^-. However, Ga^{3+} is not redox chemistry active except under extreme conditions. Therefore, under ambient conditions, the mechanism of crosslinking enhancement for Ga^{3+} is still not understood.

4 Conclusions and Outlook

Catechol crosslinking relies on the versatile chemistry of catechols. They can react with a variety of functionalities, e.g., amines, thiols, and metal ions. A schematic overview of all reactions is shown in Fig. 2.37.

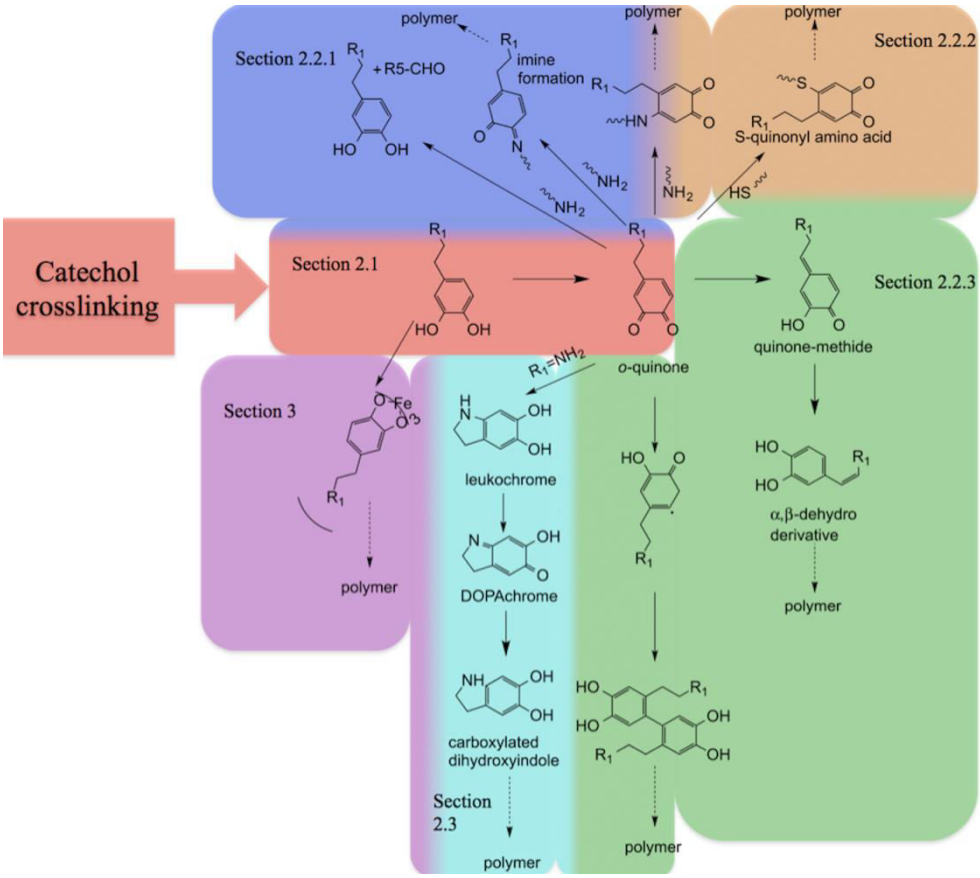

Figure 2.37. Crosslinking pathways of catechol-containing proteins

Catechol-containing polymers or proteins are cross-linked either by forming covalent or non-covalent bonds. In general, the covalent crosslinking pathways start from the oxidation of catechols either by oxygen, enzymes or chemical oxidants to form *o*-quinone. The formed *o*-quinone is highly reactive and electrophilic and, therefore, susceptible for reaction with nucleophiles such as thiols and amines. The reaction either proceeds through a Michael addition or a Schiff base reaction. In addition, *o*-quinone can also undergo dismutation reactions with catechols to form *o*-semiquinone, which then form di-dopa crosslinks by phenol radical coupling. In these reactions, the *o*-quinone formation has been well studied;

and the presence of di-dopa crosslinks, thiol-catechol and amine-catechol adducts have been detected in either natural organisms or synthetic polymers. The reaction kinetics of these reactions are dependent on a variety of parameters such as pH, type of oxidant (e.g. enzymes or chemical oxidant), type of ring substituents on the aromatic ring on catechols and the nucleophilic strength of thiols/amines. By tuning these parameters, the reaction kinetics can be optimized. Dopa-analogues containing both catechol and free amines in one molecule, e.g. dopamine, can undergo oxidative self-polymerization under mild conditions by intramolecular cyclization. Several mechanisms have been proposed. This process is affected by pH, dopamine concentration, type of oxidant used, etc.

In addition, catechols can also complex with metal ions (e.g., Fe(III)) by forming coordination bonds. The modes of complexation are highly dependent on the pH. At high pH (pH > 10), tris-dopa-Fe(III) is formed. At moderate pH (e.g., 6 < pH < 8), bis-dopa-Fe(II) is formed; and at pH 5, mono-dopa-Fe(III) is formed. Fe(III) can also oxidize catechols to form *o*-quinone, which then can form crosslinks by covalent bonding. Parameters that can be tuned to optimize the (non-covalent) crosslinking are pH, concentration of metal ions, the type of metal ions, etc.

In conclusion, the chemistry of catechols is very versatile. By using simplified catechol containing models, some parameters that affect the reaction pathways have been identified. However, detailed mechanisms for the different crosslinking reactions are still lacking. Much more research is needed to better understand the secondary reactions of *o*-quinone as well as the dual function of metal ions, i.e., coordination bond formation and redox chemistry.

References:

(1) Miserez, A.; Schneberk, T.; Sun, C. J.; Zok, F. W.; Waite, J. H. *Science* **2008**, *319*, 1816.

(2) Zhao, H.; Sun, C.; Stewart, R. J.; Waite, J. H. *Journal of Biological Chemistry* **2005**, *280*, 42938.

(3) Yu, J.; Wei, W.; Danner, E.; Ashley, R. K.; Israelachvili, J. N.; Waite, J. H. *Nature Chemical Biology* **2011**, *7*, 588.

(4) Floriolli, R. Y.; Langen, J.; Waite, J. H. *Marine Biotechnology* **2000;2**, 352.

(5) Chandra, S.; Gonzalez de Mejia, E. *J Agr. Food Chem.* **2004**, *52*, 3583.

(6) Korver, O.; Wilkins, C. K.; Collier, P. *J Soc. Chem. Ind. (London)* **1973**, *93*, 89.

(7) Purr, A.; Springer, R.; Morcinek, H. *I. Rev. Int. Chocolat.* **1964**, *19*, 398.

(8) Pilizota, V.; Subaric, D. *Food Tech. Biotech.* **1998**, *36*, 219.

(9) Waite, J. H.; Tanzer, M. L. *Science* **1981**, *212*, 1038.

(10) Lee, B. P.; Messersmith, P. B.; Israelachvili, J. N.; Waite, J. H. *Annu. Rev. Mater. Res.* **2011**, *41*, 99.

(11) Waite, J. H.; Qin, X. *Biochemistry* **2001**, *40*, 2887.

(12) Bandara, N.; Zeng, H. B.; Wu, J. P. *Journal of Adhesion Science and Technology* **2013**, *27*, 2139.

(13) Crisp, D. J.; Walker, G.; Young, G. A.; Yule, A. B. *J. Colloid. Interface Sci.* **1985**, *104*, 40.

(14) Ye, Q.; Zhou, F.; Liu, W. *Chemical Society Reviews* **2011**, *40*, 4244.

(15) Burzio, L. A.; Waite, J. H. *Biochemistry* **2000**, *39*, 11147.

(16) Yu, M.; Hwang, J.; Deming, T. J. *Journal of the American Chemical Society* **1999**, *121*, 5825.

(17) Yamamoto, H.; Ogawa, T.; Nishida, A. *Journal of Marine Biotechnology* **1997**, *5*, 133.

(18) Lee, H.; Lee, B. P.; Messersmith, P. B. *Nature* **2007**, *448*, 338.

(19) Shafiq, Z.; Cui, J.; Pastor-Pérez, L.; San Miguel, V.; Gropeanu, R. A.; Serrano, C.; del Campo, A. *Angew. Chem. Int. Ed.* **2012**, *51*, 4332.

(20) Lee, H.; Dellatore, S. M.; Miller, W. M.; Messersmith, P. B. *Science* **2007**, *318*, 426.

(21) Dreyer, D. R.; Miller, D. J.; Freeman, B. D.; Paul, D. R.; Bielawski, C. W. *Chemical Science* **2013**, *4*, 3796.

(22) Lynge, M. E.; van der Westen, R.; Postma, A.; Stadler, B. *Nanoscale* **2011**, *3*, 4916.

(23) Liu, Y.; Ai, K.; Lu, L. *Chemical Reviews* **2014**.

(24) Sedo, J.; Saiz-Poseu, J.; Busque, F.; Ruiz-Monlina, D. *Adv. Mater.* **2013**, *25*, 653.

(25) Faure, E.; Falentin-Daudré, C.; Jérôme, C.; Lyskawa, J.; Fournier, D.; Woisel, P.; Detrembleur, C. *Progress in Polymer Science* **2013**, *38*, 236.

(26) Waite, J. H. *Comp. Biochem. Physiol.* **1990**, *97B*, 19.

(27) Nagai, A.; Yamamoto, H. *Bull. Chem. Soc. Jpn.* **1989**, *62*, 2410.

(28) Yamamoto, H.; Kuno, S.; Nagai, A.; Nishida, A.; Yamauchi, S.; Ikeda, K. *Int. J. Biol. Macromol.* **1990**, *12*, 305.

(29) Bittner, S. *Amino Acids* **2006**, *30*, 205.

(30) Wagreich, H.; Nelson, J. M. *J. Biol. Chem.* **1936**, *115*, 459.

(31) Felix, C. C.; Sealy, R. C. *Journal of the American Chemical Society* **1982**, *104*, 1555.

(32) Felix, C. C.; Sealy, R. C. *Photochemistry and Photobiology* **1981**, *34*, 423.

(33) Yamazaki, I. *Free radicals in biology*; W. Pryor ed.; Academic Press: New York, 1977; Vol. 3.

(34) Wardman, P. *J. Phys. Chem. Ref. Data* **1989**, *18*, 1637.

(35) Wood, P. M. *Trends in Biochemical Sciences* **1987**, *12*, 250.

(36) Ilan, Y. A.; Meisel, D.; Czapski, G. *Israel J. Chem.* **1974**, *12*, 891.

(37) McDowell, L. M.; Burzio, L. A.; Waite, J. H.; Schaefer, J. *The Journal of Biological Chemistry* **1999**, *274*, 20293.

(38) Decker, H.; Terwilliger, N. *J. Exp. Biol.* **2000**, *203*, 1777.

(39) Garcia-Borron, J. C.; Solano, F. *Pigment Cell Res.* **2002**, *15*, 162.

(40) Gerdemann, C.; Eicken, C.; Krebs, B. *Acc. Chem. Res.* **2002**, *35*, 183.

(41) Land, E. J.; Ramsden, C. A.; Riley, P. A. *Acc. Chem. Res.* **2003**, *36*, 300.

(42) Solomon, E. I.; Lowery, M. D. *Science* **1993**, *259*, 1575.

(43) Ramsden, C. A.; Riley, P. A. *Arkivoc* **2010**, 248.

(44) Asimov, I.; Dawson, C. R. *Journal of the American Chemical Society* **1950**, *72*, 820.

(45) Robinson, M. E.; McCance, R. A. *Biochem. J.* **1925**, *19*, 251.

(46) Dawson, C. R.; Nelson, M. J. *J. Am. Chem. Soc.* **1938**, *60*, 250.

(47) Ludwig, B. J.; Nelson, J. M. *J Am. Chem. Soc.* **1939**, *61*, 2601.

(48) Wright, C. I.; Mason, H. S. *J. Biol. Chem.* **1946**, *165*, 45.

(49) Heacock, R. A. *Chem. Rev.* **1959**, *59*, 181.

(50) Bors, W.; Saran, M.; Michael, C.; Lengfelder, E.; Fuchs, C.; Spottl, R. *Int. J. Radiat. Biol.* **1975**, *28*, 353.

(51) Bors, W.; Michael, C.; Saran, M.; Lengfelder, E. *Biochem. Biophys. Acta* **1978**, *540*, 162.

(52) Cooksey, C. J.; Garratt, P. J.; Land, E. J.; Pavel, S.; Ramsden, C. A.; Riley, P. A.; Smit, N. P. M. *J. Biol. Chem.* **1997**, *272*, 26226.

(53) Danilewicz, J. C. *Am. J. Enol. Vitic.* **2003**, *54*, 73.

(54) Yu, M.; Deming, T. J. *Macromolecules* **1998**, *31*, 4739−4745.

(55) Zhang, L.; Wu, J. J.; Wang, Y. X.; Long, Y. H.; Zhao, N.; Xu, J. *J. Am. Chem. Soc.* **2012**, *134*, 9879.

(56) Kalyanaraman, B.; Felix, C. C.; Sealy, R. C. *J. Biol. Chem.* **1984**, *259*, 354.

(57) Sealy, R. C.; Puzyna, W.; Kalyanaraman, B.; Felix, C. C. *Biochimica et Biophysica Acta (BBA) - General Subjects* **1984**, *800*, 269.

(58) Weidman, S. W.; Kaiser, E. T. *Journal of the American Chemical Society* **1966**, *88*, 5820.

(59) Kaiser, E. T.; Weidman, S. W. *Tetrahedron Letters* **1965**, *9*, 497.

(60) Liu, B.; Burdine, L.; Kodadek, T. *Journal of the American Chemical Society* **2006**, *128*, 15228.

(61) Manthey, M.; Pyne, S.; Truscott, R. *Australian Journal of Chemistry* **1989**, *42*, 365.

(62) Kutyrev, A. A. *Tetrahedron* **1991**, *47*, 8043.

(63) Miserez, A.; Rubin, D.; Waite, J. H. *J. Biol. Chem.* **2010**, *285*, 38115.

(64) Kramer, K. J.; Kanost, M. R.; Hopkins, T. L.; Jiang, H. B.; Zhu, Y. C.; Xu, R. D.; Kerwind, J. L.; Tureceke, F. *Tetrahedron Letters* **2001**, *57*, 385.

(65) Christensen, A. M.; Schaefer, J.; Kramer, K. J.; Morgan, T. D.; Hopkins, T. L. *Journal of the American Chemical Society* **1991**, *113*, 6799.

(66) Merritt, M. E.; Christensen, A. M.; Kramer, K. J.; Hopkins, T. L.; Schaefer, J. *Journal of the American Chemical Society* **1996**, *118*, 11278.

(67) Schaefer, J.; Kramer, K. J.; Garbow, J. R.; Jacob, G. S.; Stejskal, E. O.; Hopkins, T. L.; Speirs, R. D. *Science* **1987**, *235*, 1200.

(68) Weeks, W. W.; Campos, M. P.; Moldoveanu, S. *J Agric. Food Chem.* **1993**, *41*, 1321.

(69) Weeks, W. W.; Campos, M. P.; Moldoveanu, S. *J Agric. Food Chem.* **1995**, *43*, 2247.

(70) Nematollahi, D.; Afkhami, A.; Mosaed, F.; Rafiee, M. *Res. Chem. Intermed.* **2004**, *30*, 299.

(71) Lee, H.; Scherer, N. F.; Messersmith, P. B. *PNAS* **2006**, *103*, 12999.

(72) Khalafi, L.; Rafiee, M.; Shahbak, M.; Shirmohammadi, H. *Journal of Chemistry* **2012**, *2013*, 1.

(73) Nematollahi, D.; Hesari, M. *Journal of Electroanalytical Chemistry* **2005**, *577*, 197.

(74) Aveldaño, M. I.; Sprecher, H. *J. Biol. Chem.* **1987**, *262*, 1180.

(75) Mason, H. S.; Peterson, E. W. *Biochimica et Biophysica Acta (BBA) - General Subjects* **1965**, *111*, 134.

(76) Klein, R. F. X.; Bargas, L. M.; Horak, V.; Navarro, M. *Tetrahedron Letters* **1988**, *29*, 851.

(77) Tian, Y.; Cao, Y.; Wang, Y.; Yang, W.; Feng, J. *Advanced Materials* **2013**, *25*, 2980.

(78) Hurrell, R. F.; Finot, P. A. *Adv. Exp. Med. Biol.* **1984**, *177*, 423.

(79) Manthey, M. K.; Pyne, S. G.; Truscott, R. J. W. *Aust. J. Chem.* **1989**, *42*, 365.

(80) Faure, E.; Falentin-Daudré, C.; Lanero, T. S.; Vreuls, C.; Zocchi, G.; Van De Weerdt, C.; Martial, J.; Jérôme, C.; Duwez, A. S.; Detrembleur, C. *Adv. Funct. Mater.* **2012**, *22*, 5271.

(81) Yaylayan, V. A. *Food Sci Tech Res* **2003**, *9*, 1.

(82) Saito, S.; Kawabata, J. *Journal of Agricultural and Food Chemistry* **2004**, *52*, 8163.

(83) LaVoie, M. J.; Ostaszewski, B. L.; Weihofen, A.; Schlossmacher, M. G.; Selkoe, D. J. *Nat. Med.* **2005**, *11*, 1214.

(84) Zhao, H.; Waite, J. H. *J. Biol. Chem.* **2006**, *281*, 26150.

(85) Zhao, H.; Waite, J. H. *Biochemistry* **2005**, *44* 15915.

(86) Ohkawa, K.; Nagai, T.; Nishida, A.; Yamamoto, H. *J. Adhes.* **2009**, *85*, 770.

(87) Brandes, N.; Schmitt, S.; Jacob, U. *Antioxid. Redox Signal* **2009**, *11*, 997.

(88) Jensen, K. S.; Hansen, R. E.; Winther, J. R. *Antioxid. Redox Signal* **2009**, *11*, 1047.

(89) Kim, H. S.; Ham, H. O.; Son, Y. J.; Messersmith, P. B.; Yoo, H. S. *Journal of Materials Chemistry B* **2013**, *1*, 3940.

(90) Lee, Y. H.; Chung, H. J.; Yeo, S. H.; Ahn, C. H.; Lee, H.; Messersmith, P. B.; Park, T. G. *Soft Matter* **2010**, *6*, 977.

(91) Nikolantonaki, M.; Jourdes, M.; Shinoda, K.; Teissedre, P.-L.; Quideau, S.; Darriet, P. *Journal of Agricultural and Food Chemistry* **2012**, *60*, 2647.

(92) Charles-Bernard, M.; Kraehenbuehl, K.; Rytz, A.; Roberts, D. D. *Journal of Agricultural and Food Chemistry* **2005**, *53*, 4417.

(93) Nikolantonaki, M.; Chichuc, I.; Teissedre, P.-L.; Darriet, P. *Analytica Chimica Acta* **2010**, *660*, 102.

(94) Haemers, S.; Koper, G. J. M.; Frens, G. *Biomacromolecules* **2003**, *4*, 632.

(95) Burizio, L. A.; Waite, J. H. *Protein Science* **2001**, *10*, 735.

(96) Sugumaran, M. *AdV. Insect Phys.* **1998**, *27*, 230.

(97) Rzepecki, L. M.; Waite, J. H. *Arch. Biochem. Biophys.* **1991**, *285*, 27.

(98) Lee, B. P.; Dalsin, J. L.; Messersmith, P. B. *Biomacromolecules* **2002**, *3*, 1038.

(99) Kang, S. M.; Rho, J. S.; Choi, I. S.; Messersmith, P. B.; Lee, H. *J. AM. CHEM. SOC.* **2009**, *131*, 13224.

(100) Dreyer, D. R.; Miller, D. J.; Freeman, B. D.; Paul, D. R.; Bielawski, C. W. *Langmuir* **2012**, *28*, 6428.

(101) Lee, H.; Rho, J. S.; Messersmith, P. B. *Adv. Mater.* **2009**, *21*, 431.

(102) Xu, L. Q.; Yang, W. J.; Neoh, K. G.; Kang, E. T.; Fu, G. D. *Macromolecules* **2010**, *43*, 8336.

(103) Hong, S.; Na, Y. S.; Choi, S.; Song, I. T.; Kim, W. Y.; Lee, H. *Adv. Funct. Mater.* **2012**, *22*, 4711.

(104) Vecchia, N. F. D.; Avolio, R.; Alfè, M.; Errico, M. E.; Napolitano, A.; d'Ischia, M. *Adv. Funct. Mater.* **2013**, *23*, 1331.

(105) Lin, S. C.; Chen, C. T.; Bdikin, I.; Ball, V.; Graciob, J.; Buehler, M. J. ***Soft Matter*** **2014**, *10*, 457.

(106) Chen, C. T.; Ball, V.; de Almeida Gracio, J. J.; Singh, M. K.; Toniazzo, V.; Ruch, D.; Buehler, M. J. *ACS Nano* **2013**, *7*, 1524.

(107) Chen, C.-T.; Chuang, C.; Cao, J.; Ball, V.; Ruch, D.; Buehler, M. J. *Nature Communications* **2014**, *5*, 3839.

(108) Della Vecchia, N. F.; Avolio, R.; Alfè, M.; Errico, M. E.; Napolitano, A.; d'Ischia, M. *Advanced Functional Materials* **2013**, *23*, 1331.

(109) Ball, V.; Frari, D. D.; Toniazzo, V.; Ruch, D. *Journal of Colloid and Interface Science* **2012**, *386*, 366.

(110) Bernsmann, F.; Ball, V.; Addiego, F. d. r.; Ponche, A.; Michel, M.; Gracio, J. J. d. A.; Toniazzo, V. r.; Ruch, D. *Langmuir* **2011**, *27*, 2819.

(111) Wei, Q.; Zhang, F.; Li, J.; Li, B.; Zhao, C. *Polymer Chemistry* **2010**, *1*, 1430.

(112) Coombs, T. L.; Keller, P. J. *Aquat Toxicol* **1981**, *1*, 291.

(113) Rzepecki, L. M.; Waite, J. H. *Bioorganic marine chemistry*; Springer-Verlag: New York, 1991.

(114) Sever, M. J.; Weisser, J. T.; Monahan, J.; Srinivasan, S.; Wilker, J. J. *Angew Chem Int Ed* **2004**, *43*, 448.

(115) George, S. G.; Pirie, B. J. S.; Coombs, T. L. *J. Exp. Mar. Bio. Ecol.* **1976**, *23*, 71.

(116) Holten-Andersen, N.; Mates, T. E.; Toprak, M. S.; Stucky, G. D.; Zok, F. W.; Waite, J. H. *Langmuir* **2009**, *25*, 3323.

(117) Holten-Andersen, N.; Fantner, G. E.; Hohlbauch, S.; Waite, J. H.; Zok, F. W. *Nat. Mater.* **2007**, *6*, 669.

(118) Harrington, M. J.; Masic, A.; Holten-Andersen, A.; Waite, J. H.; Fratzl, P. *Science* **2010**, *328*, 216.

(119) Swann, C. P.; Waite, J. H.; Huggins, L. G. *Nucl. Instrum. Methods Phys. Res., Sect. B* **1996**, *109/110*, 301.

(120) Huggins, L. G.; Waite, J. H. *J. Exp. Zool.* **1993**, *265*, 549.

(121) Taylor, S. W.; Luther III, G. W.; Waite, J. H. *Inorg. Chem.* **1994**, *33*, 5819.

(122) Sever, M. J.; Wilker, J. J. *Dalton Trans.* **2006**, 813.

(123) Dorsett, L. C.; Hawkins, C. J.; Grice, J. A.; Lavin, M. F.; Merefield, P. M.; Parry, D. L.; Ross, I. L. *Biochemistry* **1987**, *26*, 8078.

(124) Oltz, E. M.; Bruening, R. C.; Smith, M. J.; Kustin, K.; Nakanishi, K. *J. Am. Chem. Soc.* **1988**, *110*, 6162.

(125) Taylor, S. W.; Hawkins, C. J.; Winzor, D. J. *Inorg. Chem.* **1993**, *32*, 422.

(126) Taylor, S. W.; Ross, M. M.; Waite, J. H. *Arch. Biochem. Biophys.* **1995**, *324*, 228.

(127) Smith, M. J.; Ryan, D. E.; Nakanishi, K.; Frank, P.; Hodgson, K. O. *Met. Ions Biol. Syst.* **1995**, *31*, 423.

(128) Taylor, S. W.; Kammerer, B.; Bayer, E. *Chem. Rev.* **1997**, *97*, 333.

(129) Avdeef, A.; Sofen, S. R.; Bregante, T. L.; Raymond, K. N. *J. Am. Chem. Soc.* **1978**, *100*, 5362.

(130) Dertz, E. A.; Raymond, K. N. *Comprehensive coordnation chemistry II*; Elsevier Pergamon: Boston, 2003; Vol. 8.

(131) Loomis, L. D.; Raymond, K. N. *Inorg. Chem.* **1991**, *30*, 906.

(132) Holten-Andersen, N.; Harrington, M. J.; Birkedal, H.; Lee, B. P.; Messersmith, P. B.; Lee, K. Y. C.; Waite, J. H. *PNAS* **2011**, *108*, 2651.

(133) Severa, M. J.; Wilker, J. J. *Dalton Trans.* **2004**, 1061.

(134) Taylor, S. W.; Chase, D. B.; Emptage, M. H.; Nelson, M. J.; Waite, J. H. *Inorg. Chem.* **1996**, *35*, 7572.

(135) Zeng, H. B.; Hwang, D. S.; Israelachvili, J. N.; Waite, J. H. *PNAS* **2010**, *107*, 12850.

(136) Monzyk, B.; Crumbliss, A. L. *J Am. Chem. Soc.* **1982**, *104*, 4912.

(137) Nurchi, V. M.; Pivetta, T.; Lachowicz, J. I.; Crisponi, G. *J. Inorg. Biochem.* **2009**, *103*, 227.

(138) Burgess, J.; Rangel, M. *Adv. Inorg. Chem.* **2008**, *60*, 167.

(139) Zhou, T.; Ma, Y.; Kong, X.; Hider, R. C. *Dalton Trans.* **2012**, *41*, 6371.

(140) Menyo, M. S.; Hawker, C. J.; Waite, J. H. *Soft Matter* **2013**, *9*, 10314.

(141) Broomell, C. C.; Mattoni, M. A.; Zok, F. W.; Waite, J. H. *J. Exp. Biol.* **2006**, *209*, 3219.

(142) Kipton, H.; Powell, J. *Aust. J. Chem.* **1982**, *35*, 739.

(143) Wilker, J. J. *Curr. Opin. Chem. Biol.* **2010**, *14*, 276.

(144) Monahan, J.; Wilker, J. J. *Chemical Communications* **2003**, 1672.

(145) Barrett, D. G.; Fullenkamp, D. E.; He, L. H.; Holten-Andersen, N.; Lee, K. Y. C.; Messersmith, P. B. *Adv. Funct. Mater.* **2013**, *23*, 1111.

(146) Fullenkamp, D. E.; Barrett, D. G.; Miller, D. R.; Kurutz, J. W.; Messersmith, P. B. *RSC Adv.* **2014**, *4*, 25127.

(147) Xu, H.; Nishida, J.; Ma, W.; Wu, H.; Kobayashi, M.; Otsuka, H.; Takahara, A. *ACS Macro Lett.* **2012**, *1*, 457.

(148) Holten-Andersen, N.; Jaishankar, A.; Harrington, M. J.; Fullenkamp, D. E.; DiMarco, G.; He, L. H.; McKinley, G. H.; Messersmith, P. B.; Lee, K. Y. C. *J. Mater. Chem. B* **2014**, *2*, 2467.

(149) Sever, M. J.; Wilker, J. J. *J Mater. Sci.* **2007**, *42*, 8934.

(150) Lide, D. R. *CRC handbook of chemistry and physics*; CRC Press: Boca Raton, 1992.

(151) Bratsch, S. G. *J. Phys. Chem. Ref. Data* **1989**, *18*, 1.

(152) Kalyanaraman, B.; Felix, C. C.; Sealy, R. C. *Environmental Health Perspectives* **1985**, *64*, 185.

(153) Decker, H.; Tuczek, F. *Trends Biochem. Sci.* **2000**, *25*, 392.

(154) Inaba, K. *Genes to cells* **2010**, *15*, 935.

(155) Yu, F.; Chen, S. G.; Chen, Y.; Li, H. M.; Yang, L. J.; Chen, Y. Y.; Yin, Y. S. *Journal of Molecular Structure* **2010**, *982* 152.

Chapter 3

Reaction pathways in catechol/primary amine mixtures: a window on crosslinking chemistry

Abstract

In this chapter, we aim at exploring the crosslinking chemistry of catechol and primary amine. To simplify the system, yet to capture the essential chemistry, model compounds 4-methyl catechol (4-MC) and propylamine (PA) were used. We carried out the reaction of 4MC with PA in the presence of $NaIO_4$ in 10 mM Na_2CO_3 aqueous solution. We used a variety of spectroscopic and chromatographic methods such as ^{1}H NMR, LC-MS, and UV-VIS, to track the reaction, and identify the products/intermediates. We found that the crosslinking chemistry of catechol and amine is both fast and complicated. Within five minutes, more than 60 products were formed. These products encompass 19 different masses ranging from 179 to 704. By combining time-dependent data, we infer the dominant reaction pathways: the majority are formed via aryloxyl-phenol coupling and Michael-type addition, whereas a small fraction of products is formed via Schiff base reactions.

This chapter is based on publication:
Juan Yang, Vittorio Saggiomo, Aldrik Velders, Martien A.Cohen Stuart, Marleen Kamperman, *Journal of the American Chemical Society*, in preparation.

Introduction

Catecholic compounds are widely distributed among natural animal and plant systems[1-3]. One famous example of a catecholic compound is 3,4-Dihydroxyphenylalanine (DOPA). When exposed to air, DOPA is prone to oxidation. The formed *o*-quinones may further react with a variety of nucleophiles in various pathways to form crosslinks[4]. A well-known nucleophile is the amine that may react with *o*-quinones to form adducts either by Michael addition or Schiff base reaction (Scheme 3.1)[4].

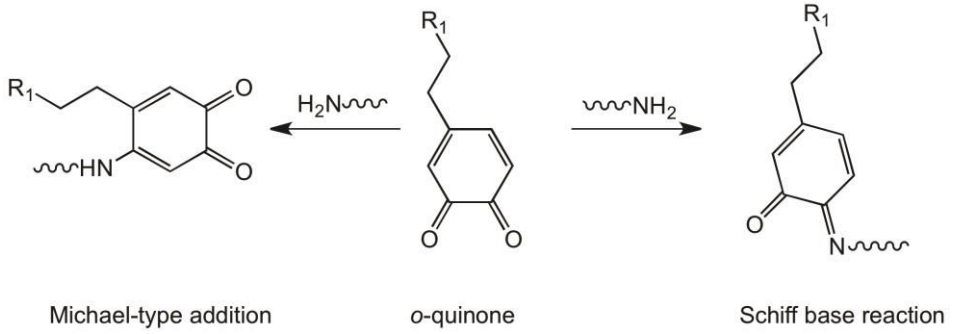

Scheme 3.1. Reaction of amines with *o*-quinones via Michael-type addition or Schiff base reaction

The reaction between catechols and amines is of vital importance in natural biological processes, such as the crosslinking of adhesive proteins by marine organisms[5], the formation of cytoskeleton by insects[6] and the biosynthesis of melanin[7]. For instance, in blue mussels, both DOPA and *l*-lysine are present in large quantities in mussel adhesive foot proteins (mfps)[8]. It has been proposed that the -NH_2 group in lysine side chains in mfps may react with the carbonyl groups of *o*-quinones to form Schiff-base adducts[9]. The reaction between catechols and amines, together with all other possible reactions involving catechols, contribute to the fast solidification of freshly secreted mfps to form a tough and robust cuticle[9]. Similar *o*-quinone-amine adducts have also been identified in insect

sclerotization. By isolation and proteolysis of the natural proteins from beak cutouts of squid Dosidicus gigas, Waite et al. has identified the presence of multimers (dimers, trimers and tetramers) of catechol–histidine adducts[1,10]. The catechol-amine chemistry occurring in natural organisms has attracted much attention in material science[11-13]. Several research groups have developed water-soluble polymers that form a gel or water-resistant film upon reaction between a catechol and an amine. For instance, Lee et al. synthesized a poly(ethylene glycol) polymer containing both catechol and amine functional groups[11]. Upon the reaction between the catechol and amine, the water-soluble polymer formed rigid hydrogels in one minute. Similarly, Xu et al. prepared a multilayered film by alternatively immersing a substrate in aqueous solutions of poly(acrylic acid-dopamine) (PAA-dopamine) and poly(allyamine hydrochloride) (PAH), respectively. After triggering the reaction of catechol and amine, a stable and robust film was obtained.[13]

Despite of the extensive literature on material development using catechol-amine reactions, the mechanism remains unclear. Several mechanistic studies have been performed to gain more fundamental understanding. For instance, Kodadek et al. studied the reaction between catechol and amines using two peptide nucleic acids.[14]. They found that crosslinks were formed through Michael addition between amines with *o*-quinones. In addition, they formulated two premises that should be fulfilled for the reaction to proceed: i) close proximity of *o*-quinone intermediate and amine nucleophiles, and ii) the presence of sodium periodate. Waite et al. also studied the reaction mechanism by using natural decapeptides derived from mfp1, which contains both DOPA and lysines. They started the reaction by adding oxidants such as sodium periodate, or tyrosine. By using HPLC,

MALDI-TOF, and amino acid analysis, they observed that lysine is likely to contribute to intramolecular crosslinking with DOPA, rather than to intermolecular crosslink formation.[9] These studies showed that the reaction mechanism differs strongly depending on the specific reaction conditions.

The mechanistic studies mentioned above have given valuable insights in the crosslinking chemistry of catechols and amines. However, a thorough understanding of the mechanisms based on detailed product identification is still missing, resulting in uncontrollable crosslinking in many bio-mimetic materials. The difficulty in exploring the crosslinking chemistry in natural systems is related to the complexity of full-length proteins, and to ambiguities in tyrosine oxidation to DOPA or *o*-quinones. Therefore, in this study, instead of using proteins, we used small model compounds to study the crosslinking chemistry. The model compounds are 4-methyl catechol (4MC) and propylamine (PA). Sodium periodate and sodium carbonate aqueous solution (10 mM) were used as oxidant and solvent, respectively. By using HPLC and LC-MS, we found that the reaction of 4MC and PA is very fast. In less than five minutes, more than 30 products are formed. Among these products, the majority was from Michael-type addition. Additional products were mainly formed by Schiff-base reaction or phenol coupling.

Materials and Experiments

Materials

All reagents were used as received unless noted otherwise. 4-methylcatechol (95%), propylamine (99%), sodium periodate (99.8%), sodium iodate (99.5%), sodium carbonate (99.5%), acetic acid (99.99%), and silica gel 60 for chromatography were purchased from Sigma-Aldrich. Solvents used for HPLC and LC-MS analysis were acetonitrile (containing

0.1 v/v% formic acid) of HPLC grade, and water (containing 0.1 v/v% formic acid) of HPLC grade purchased from Sigma-Aldrich. Solvents used for synthesis were acetonitrile, *n*-hexane and diethyl ether of HPLC grade purchased from Biosolve.

Experiments

Synthesis of model compound

The synthesis of the model compound 4-propylamino-5-methyl-o-quinone was adapted from the procedure reported by Suyama, et al.. Sodium iodate (6 g, 30 mmol) in 60 ml of distilled water was added slowly to a mixture of 4-methyl catechol (4.97 g, 40 mmol) and propylamine (2.42 g, 41 mmol) in 80 ml of acetic acid. After one hour of reaction in an ice-bath, the reaction mixture was slowly added to 500 ml cold milli-Q water, and followed by filtration. The solid material was dissolved in 200 ml acetonitrile, and extracted three times by 300 ml *n*-hexane. The fitrate was extracted three times with 500 ml *n*-hexane. All hexane layers were collected, and concentrated using rotary evaporation. Afterwards, the red solution was collected and separated by silica gel column chromatography with a *n*-hexane/diethyl ether (8:2, v/v) mixture as eluent. Five fractions were collected and further subjected to HPLC measurements.

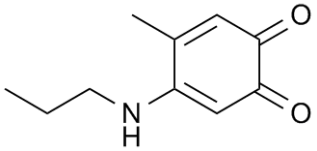

Scheme 3.2. Chemical structure of 4-propylamino-5-methyl-o-quinone

Sample preparation for HPLC and LC-MS

Reactions mixtures for HPLC and LC-MS measurements were prepared by adding 4-methyl catechol (4MC) (1.24 mg, 2 mM), propylamine (PA) (1.77 mg, 1 mM), and sodium periodate (2.14 mg, 0.5 mM) to 5ml of sodium

carbonate (10 mM) aqueous solution.

Analytical HPLC analysis

Analytic HPLC was carried out on Hewlett Packard 1100 systems coupled to UV detectors and the data were processed using HP Chemstation software. Separations were performed using a reversed-phase HPLC column (Alltima C18-5u, 4.6 mm, 250 mm) after injecting 10 μL of the sample. Except where otherwise stated, the chromatography was carried out using UV detection at 254, 260 and 280 nm. A flow rate of 1 mL/min was used. The mobile phase consisted of a mixture of acetonitrile and milli-Q water (both containing 0.1 % formic acid), using the following gradient: (0 min: 5 % CH_3CN; 13 min: 45 % CH_3CN; 23 min: 95% CH_3CN; 32 min: 95% CH_3CN; 35 min: 5% CH_3CN; 43 min: 5% CH_3CN).

LC-MS Analysis

LC-MS was performed using a HPLC-MS from Thermo Scientific, Finnigan LXQ series. Analyses were performed using a reversed-phase HPLC column (Alltima C18-5u, 4.6 mm, 250 mm) injecting 10 μL of the sample. A flow rate of 1 mL/min was used. A splitter was used, 0.2 ml/min entered the MS detector and 0.8 ml/min was disposed off. The mobile phase consisted of a mixture of acetonitrile and milli-Q water (both containing 0.1 % formic acid), using the following gradient: (0 min: 0 % CH_3CN; 13 min: 55 % CH_3CN; 23 min: 5% CH_3CN; 32 min: 5% CH_3CN; 35 min: 95% CH_3CN; 43 min: 95% CH_3CN). Positive ion mass spectra were acquired in ultrascan mode using electrospray ionization. MS analysis was performed using electrospray ionization (ESI) and detection in the positive mode, with a source voltage of 5.0 kV and an ion transfer tube temperature of 275°C.

Dynamic light scattering (DLS)

Dynamic light scattering was used to monitor the formation of high molecular weight products between 4MC and PA. Briefly, a reaction mixture containing 2mM 4-methyl catechol, 1 mM propylamine, and 0.5 mM sodium periodate in 5ml of 10 mM sodium carbonate aqueous solution was filtered through a 0.45 μm polyethersulfone filter. Light scattering was performed using an ALV dynamic light scattering instrument with a Cobolt Samba- 300 DPSS laser (300 mW) operating at a wavelength of 532 nm and an ALF-5000/60X0 multiple τ digital correlator. A refractive index matching bath of filtered cis-decalin surrounded the cylindrical scattering cell. All measurements were performed at a fixed angle θ of 90°, corresponding to a scattering vector $q = \frac{4\pi n}{\lambda} sin \frac{\theta}{2}$ ~ 0.02 nm^{-1}, where n is the refractive index of the solvent (water). The temperature was kept constant at 20 °C using a Haake F3-K thermostat.

^{1}H NMR spectroscopy

^{1}H NMR of the sample was performed in D_2O on a Bruker AMX-400 spectrometer (400 MHz) at 25 °C.

UV-VIS spectroscopy

UV-visible characterization was performed on a Shimadzu UV-2600 spectrophotometer. The samples were measured using a wavelength scan range of 200-600 nm in a quartz cuvet.

Results and discussion

Reaction system design

The crosslinking chemistry of catechols and amines is complicated and the mechanisms are still under dispute. Generally, it is accepted that the nucleophilic amines attack oxidized catechols by either Michael-type

addition or Schiff-base reaction. However, a detailed understanding of the identities of the products is still missing. In this study, we used several techniques to identify the products of catechol-amine crosslinking reactions. The proper choice of reaction system and reaction conditions is important. In material science, most often large molecular weight molecules are linked together with catechol and amine reactions. However, in this mechanistic study, ^{1}H NMR is one of the techniques we used. It is thus desirable to keep the system as simple as possible to avoid possible peak broadening and overlapping. For this reason, we chose the simplest form of catechol and α-amino derivatives, i.e. 4-methyl catechol (4MC) and propylamine (PA), respectively. By using these two model compounds, we expect to capture the essential chemistry between catechol and amine. This essential chemistry would facilitate a better understanding of the catechol-amine crosslinking mechanism in polymer systems as studied in Chapter 4. To precisely identify the reaction products, the reaction conditions should fulfill the following requirements. Firstly, it is generally accepted that, for primary amines to work effectively as nucleophiles, they should not be charged[15]. Therefore, pH is an essential parameter. In our case, since the pKa of PA is 10.71, we maintained the pH of the reaction medium above 11 using 10 mM aqueous sodium carbonate solution as the solvent. Secondly, as reported, the reaction rate of catechol oxidation at high pH is the rate-determining step that affects further reactions. Therefore, we add an oxidant $NaIO_4$ (0.5 equivalent to catechol) to form enough *o*-quinones.[16] Thirdly, generally, the reaction between amines and *o*-quinones is slightly slower than that of aryloxyl coupling.[17] To increase the likelihood of reacting *o*-quinones with amines, we set the PA/4MC molar ratio to 3. This excess of amines with respect to catechols may well represent the polymer system we

studied in chapter 4, in which the polymer poly(dopamine acrylamide-*co*-2-aminoethyl metharylamide) contains more amines than catechols. Finally, at high temperatures *o*-quinones may react with amines via Strecker degradation to produce aldehydes and 2-aminocarbonyl compounds. However, the crosslinking of catechols and amines for polymer systems as described in Chapter 4 usually proceeds at ambient conditions. Therefore, we set the reaction temperature at 20 °C.

^{1}H NMR analysis

The reaction of 4MC, PA and $NaIO_4$ in 10 mM Na_2CO_3 aqueous solution was monitored by ^{1}H NMR measurements. To have a clear understanding of the role of PA, we also studied two reference reactions: 4MC in 10 mM Na_2CO_3 (aq) and 4MC in the presence of $NaIO_4$ in 10 mM Na_2CO_3 (aq). For 4MC in 10 mM Na_2CO_3 (aq), and after 26 h, the reaction solution shows a pinkish color, and no precipitates were observed. The pinkish color indicates that some reactions might have been taking place. This indication is supported by the observation in Fig. 3.1(b), that the aromatic proton peaks are gradually shifted downfield. The shift might be due to the formation of *o*-quinones, in which the electron-withdrawing property of the carbonyl groups has a "deshielding" effect on the aromatic protons. Moreover, as shown in Fig. 3.1(a), little change is observed in the intensity of the methyl peaks (δ = 2.2 ppm) and the aromatic peaks (δ = 6.5-6.8 ppm) over time (Fig. 3.1(a)). The little change indicated that the reaction proceeded at a very slow rate. The slow rate might be due to slow catechol oxidation, which has been identified to be the rate-determining step under these conditions.[16] To speed up the reaction, $NaIO_4$ was added, and the reaction solution immediately turned dark red. In less than one hour, dark red precipitates were observed, which could not be detected by liquid ^{1}H

NMR. As shown in Fig. 3.2, the aromatic peaks (δ =6.5-6.8 ppm) and methyl peaks (δ = 2.2 ppm) decreased significantly over time. Meanwhile, a very broad peak at around δ = 1.5 ppm emerged, indicating the formation of oligomer-like structures. Therefore, addition of $NaIO_4$ has significantly increased the reaction rate.

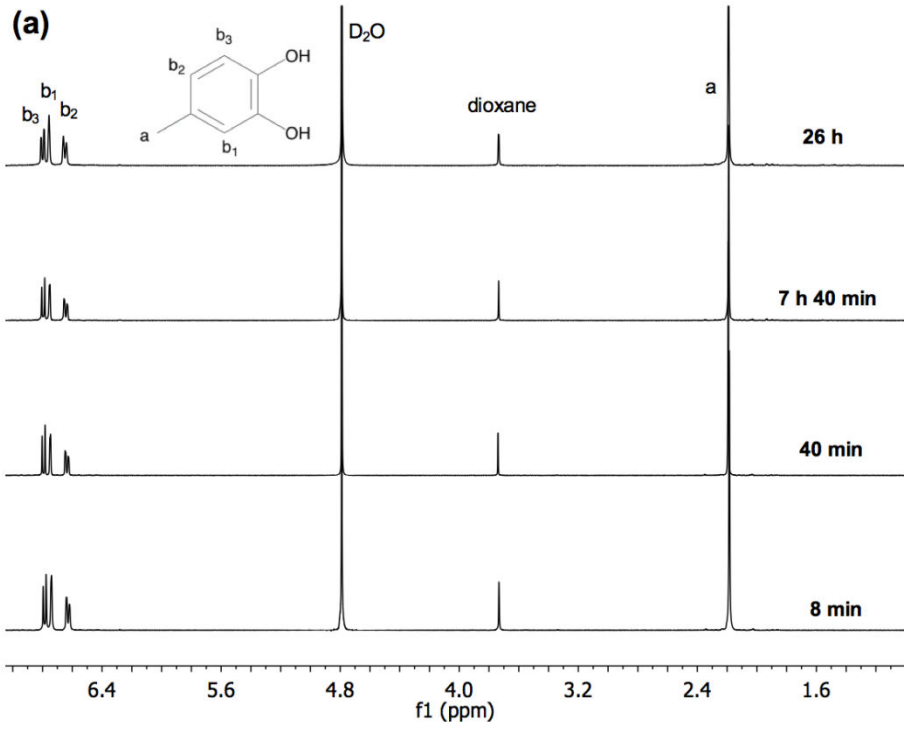

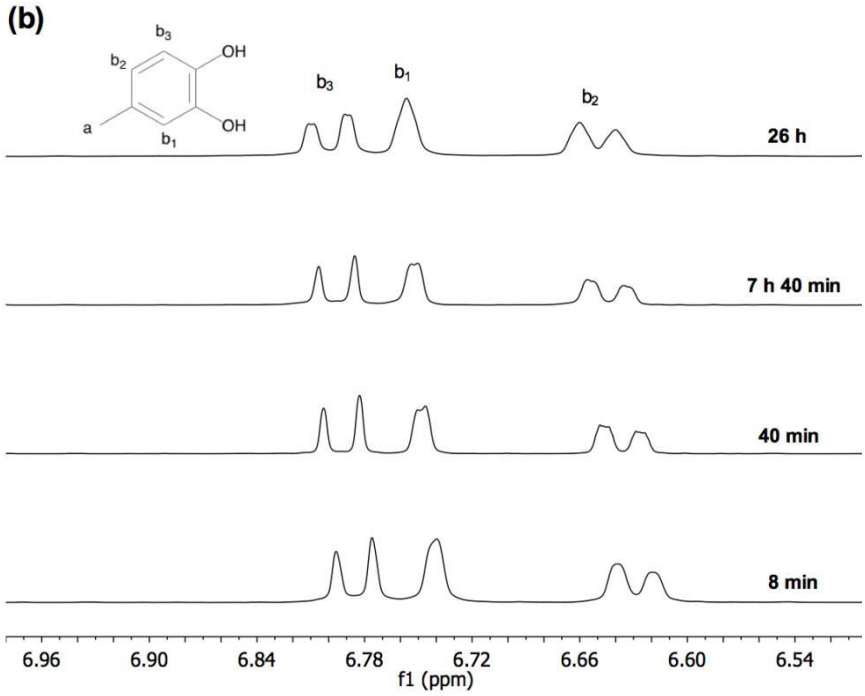

Figure 3.1. ^{1}H NMR spectra monitoring the reaction of 4MC in 10mM Na_2CO_3/D_2O with time. Dioxane was used as a reference. (a) Full overview of the ^{1}H NMR spectra (b) ^{1}H NMR spectra in the aromatic region.

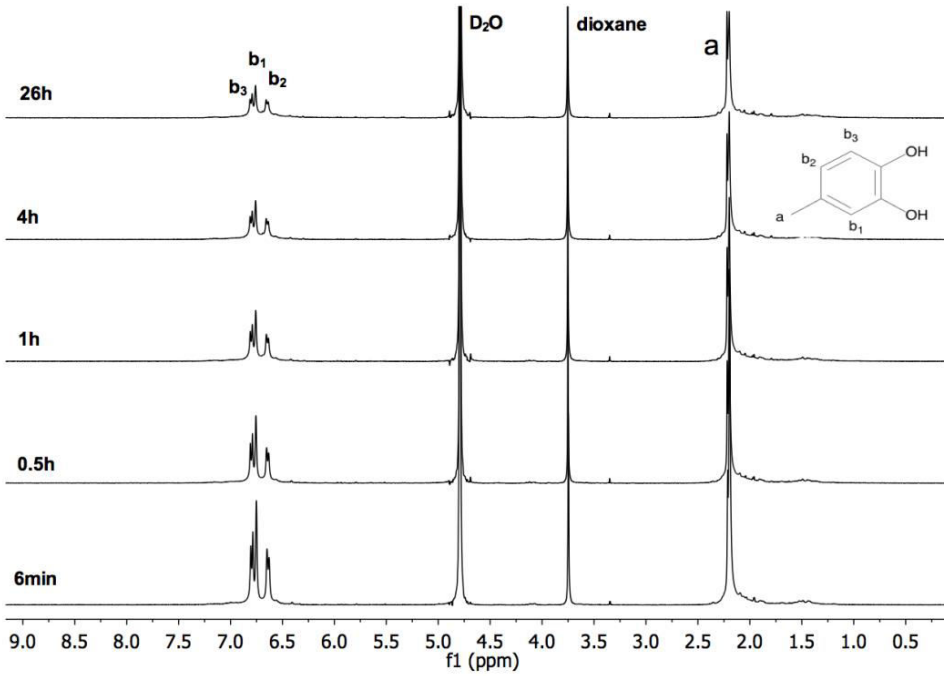

Figure 3.2. ^{1}H NMR spectra monitoring the reaction of 4MC and $NaIO_4$ in 10mM Na_2CO_3/D_2O with time. The molar ratio between 4MC and $NaIO_4$ is 0.5. Dioxane was used as a reference.

Fig. 3.3 shows representative ^{1}H NMR spectra of the reaction of 4MC, PA and $NaIO_4$ in 10mM Na_2CO_3 aqueous solution. As soon as the reagents were mixed, the solution turned dark red. After one hour of reaction, dark red precipitates appeared. As shown in Fig. 3.3, the peaks related to 4MC, namely, the aromatic peaks at δ of 6.3-6.75 ppm, and methyl peaks at δ = 2.1 ppm both decreased significantly in two hours. Moreover, broad peaks close to δ = 2.1 ppm and δ =7.0 ppm appeared within 11 min, and decreased again over time. The peaks related with PA, namely, δ of 0.9, 1.48, and 2.65 ppm also decreased with time. Meanwhile, three small peaks (marked in red) appeared. These three peaks were shifted downfield and showed

similar shapes as the peaks related with the alkyl groups of PA (positions e, d, and c). The integrated area ratio of these peaks is 3:2:2, which is the same ratio as the PA protons. This observation might indicate that the alkyl groups in PA are connected to the aromatic group in 4MC to form an amine-catechol adduct. In other words, PA reacted indeed with 4MC under the current reaction conditions.

Collectively, the ^{1}H NMR measurements suggest that oxidation of 4MC at high pH is slow and sodium periodate is needed to speed up the catechol oxidation. The oxidized 4MC may react with PA to form catechol-amine adducts. However, ^{1}H NMR could not detect the precipitates observed in the reaction mixture, and additional techniques are needed to identify the reaction products.

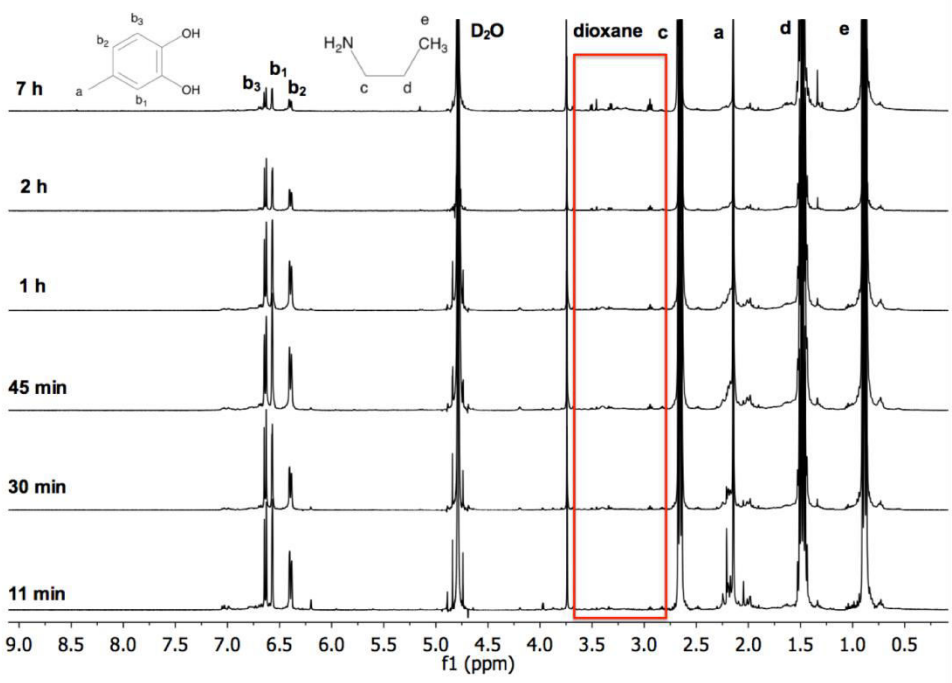

Figure 3.3. ^{1}H NMR spectra monitoring the reaction of 4MC, PA and $NaIO_4$ in 10mM Na_2CO_3/D_2O with time. The molar ratio between 4MC, PA and $NaIO_4$ is 1:3:0.5. Dioxane was used as a reference.

UV-VIS measurements

UV-vis spectroscopy is a technique often used in catechol-related literature to follow catechol-involving reactions. Therefore, in this study, to gain additional insights into the reaction of 4MC with PA, we monitored the reaction mixture over time using UV-VIS spectroscopy. Two reference reactions were also studied.

As shown in Fig. 3.4, 4MC in Milli-Q water showed a single characteristic absorbance peak at λ_{max}=280 nm, which is attributed to unreacted catechols. Upon adding 4MC to 10mM Na_2CO_3, the transparent aqueous solution turned to pink immediately. The characteristic peak of catechol at λ_{max}=280 nm disappeared, along with the appearance of two new peaks at λ_{max}= 240 and 448 nm. These two peaks might reveal the formation of *o*-quinones by catechol oxidation.[9] As the reaction proceeded, the peaks at λ_{max}= 240 nm and λ_{max}= 448 nm decreased, with the simultaneous appearance of peaks at 277 nm (after 15 min). These changes suggest that the *o*-quinones react further to form other products. The new peaks at 277 nm gradually shifted to 283 nm within 50 min, along with a gradual intensity increase, which might be an indication of the formation of di-DOPA crosslinks.[9]

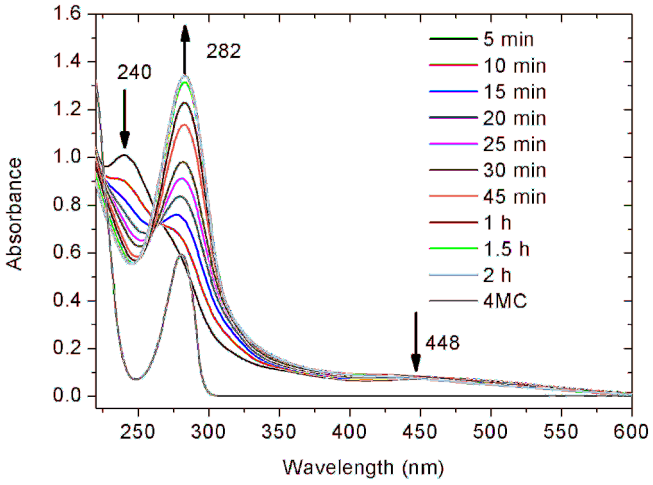

Figure 3.4. UV-VIS absorbance monitoring the reaction of 4MC in 10mM Na_2CO_3 aqueous solution.

Similar UV-VIS spectra were also obtained for the reaction of 4MC in 10mM Na_2CO_3 aqueous solution in the presence of $NaIO_4$, as shown in Fig. 3.5. The difference with the reaction without $NaIO_4$ is that the peak at around λ_{max}= 240 nm was hardly visible at 5 min, which means that *o*-quinones had already reacted further on that time scale. Apart from that, the spectra showed similar changes as those in Fig. 3.4. That is to say, the peaks at λ_{max}= 441 nm decreased with time; and a new peak at λ_{max}= 277 nm appeared (after 20 min), which gradually shifted back to λ_{max}= 282 nm (after 1 h 5 min) and intensified over time. These changes also indicate that the *o*-quinones reacted further to form other products. It is unclear, however, what the reason is of the longer time taken for the appearance and shift of the peak at λ_{max}= 277 nm. Perhaps, it is related to the increased *o*-quinone concentration on the kinetics of further reactions. Nevertheless, the presence of $NaIO_4$ did not alter the essential chemistry of the 4MC reaction.

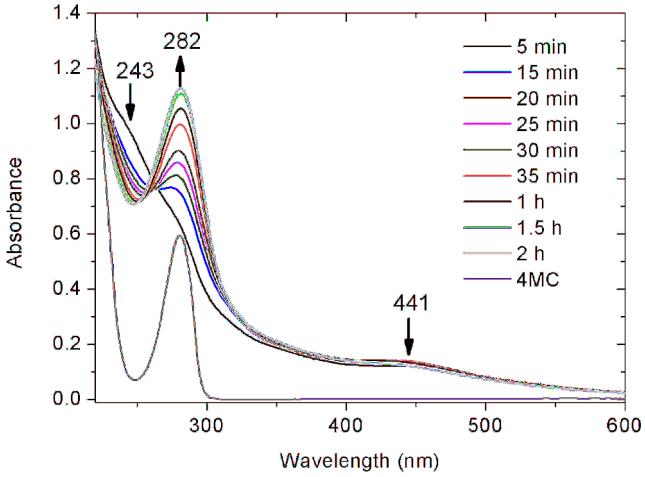

Figure 3.5. UV-VIS absorbance monitoring the reaction of 4MC and $NaIO_4$ in 10mM Na_2CO_3. The molar ratio between 4MC and $NaIO_4$ is 0.5.

The UV-VIS spectrum of 4MC and PA together in the presence of $NaIO_4$ in 10mM Na_2CO_3 aqueous solution is shown in Fig. 3.6. By comparing to the spectra for 4MC only, or 4MC with $NaIO_4$, some similarities can be seen, i.e., the initial disappearance of the characteristic catechol peak at λ_{max}= 280 nm; and the gradual peak shift from 277 nm (observed at 15 min) to 280 nm (observed after 35 min). These similarities suggest that in all cases oxidation of catechol to *o*-quinones proceeds immediately. In contrast, new peaks appeared at λ_{max}= 358 and 488 nm, which gradually decreased somewhat over time, and concurrently, the intensity of the peak at 280 nm increased significantly. These changes indicate the occurrence of subsequent reaction of *o*-quinones. The increased absorbance at wavelengths higher than 500 nm has been associated in the literature with the formation of products from Michael type addition of catechol and amines.[18]

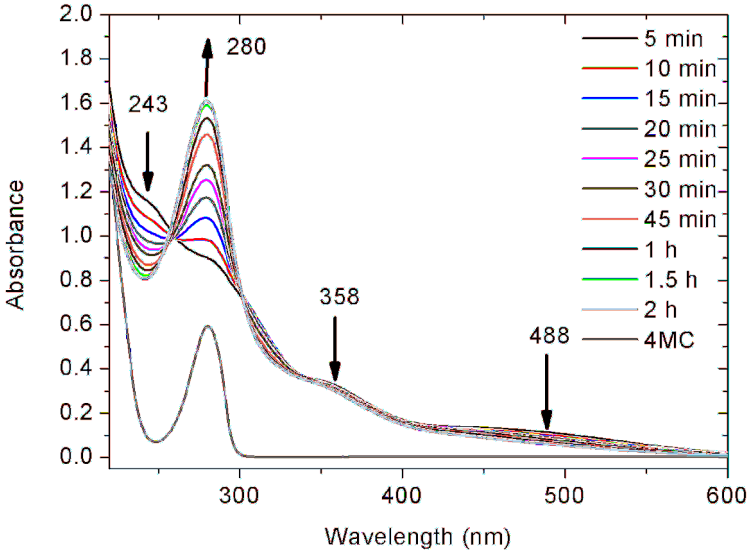

Figure 3.6. UV-VIS absorbance monitoring the reaction of 4MC, PA and $NaIO_4$ in 10mM Na_2CO_3. The molar ratio between 4MC, PA and $NaIO_4$ is 1:3:0.5.

HPLC

Collectively, the ^1H NMR and UV-VIS data suggest that 4MC reacts differently in the presence of PA than without. It is generally accepted that multiple reactions of 4MC and PA may take place. The presence of multiple reactants/products brings difficulty in interpreting the UV-VIS data. Therefore, in the following, we use HPLC to separate the reactants/products from the reaction mixture, and to study the time dependence of the reaction (Fig. 3.7).

As shown in Fig. 3.7, the reaction proceeds very fast, as evidenced by multiple peaks already emerging in 5 min after mixing the reagents. Under the chromatographic conditions employed, $NaIO_4$ eluted from the column

almost immediately, which is assumed to quench the reaction effectively. Unreacted 4MC did not show a signal (which should, as we checked, elute at a retention time of 12.2 min) in Fig. 3.7, suggesting that all 4MC has undergone oxidation. Since PA does not respond to UV, and 4MC has already reacted to *o*-quinones, the peaks shown in Fig. 3.7 must be considered as evidence of products/intermediates. The peaks at retention times around 6.34 and 6.5 min (after 5 min of reaction) disappeared after one hour of reaction, indicating that the corresponding compounds must be highly reactive intermediates. After one hour of reaction, two peaks at retention times of 3.1 and 7.0 min started to emerge, and they increased until the longest recorded reaction time of 24 h. Aside from these two peaks, all the other peaks decreased with time. Therefore, the elution patterns of 5 min and one hour already represent the majority of the products/intermediates. Therefore, these two chromatographic profiles were further characterized by mass spectroscopy.

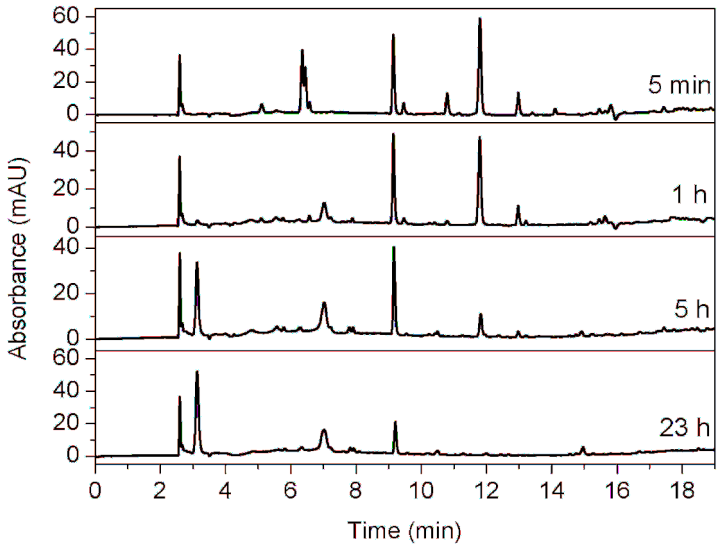

Figure 3.7. HPLC-UV chromatograms (monitored at 254 nm) of the reaction mixture of 4MC, PA, and $NaIO_4$ with time. The ratio of 4MC, PA and $NaIO_4$ is 1:3:0.5.

LC-MS analysis for peak identification

To identify the possible intermediates/products in HPLC, we obtained mass spectra for the observed peaks in HPLC using mass spectroscopy. Here one should note that all the peaks in the elution profile of Fig. 3.7 are slightly shifted due to equipment differences as shown in Fig. 3.8. However, this shift does not alter the chemistry of the reaction.

In general, as discussed previously in Scheme 3.1, the reaction between oxidized catechol and amine in basic aqueous conditions can proceed via two pathways: 1) Michael-type addition of amine to *o*-quinone; 2) Schiff base reaction of amine to *o*-quinone. Moreover, *o*-quinones may also react with catechols via dismutation to form catechol-catechol crosslinks. As seen in Scheme 3.3, the phenol radical coupling generally takes place at

positions 3, 6, and possibly at positions 1 and 2. Coupling of two catechols would lead to a mass loss of 2 Da [9] at position 3 and 6 and a mass loss of 16 Da at position 1 or 2. For Michael-type addition, the nucleophilic amine, generally attacks position 4 or 6 on the *o*-quinone by 1,6-addition, and position 3 by 1,4-addition, both leading to a mass loss of 2 Da.[9] For Schiff-base reactions, the substitution usually takes places at positions 1 or 2, resulting in a mass loss of 16 Da. Therefore, the mass of the prominent peaks *m* in the chromatogram should be related to the mass of (oxidized) 4MC (m_{4MC}) and PA (m_{PA}) by the following equation:

$$m = n_1 m_{4MC} + n_2 m_{PA} - 2n_3 - 16n_4$$

in which n_1, n_2, n_3, n_4 are integers. Based on this equation and the mass we obtained from mass spectroscopy, we can postulate the structures corresponding to the peaks.

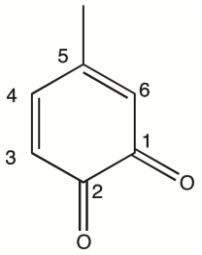

Scheme 3.3. Chemical structure of 4MC with numbers indicating the position of C atoms on the aromatic ring.

In total, we have identified around 20 m/z values for all these peaks. Here we will elaborate on a few examples for the major peaks at different retention times. As shown in Fig. 3.8, the peak at retention time of 10.28 min showed a strong signal in the mass spectrum (Fig. 3.8(c)) at m/z = 180.10. This value matches the structure of 4-*n*-propylamino-5-methyl-1,2-benzoquinone (PMB) (Fig. 3.8(e)). To further verify the structure of the compound, we attempted to isolate PMB by collecting the fraction with

retention time 10.28 min from HPLC elution. However, after freezing and lyophilization of the collected fractions, the HPLC chromatogram of the sample showed a different retention time. Moreover, the ^{1}H NMR spectrum of the fraction did not match the structure, indicating that the compound had degraded. The degradation might be due to two possible reasons. Firstly, during lyophilization, formic acid became more concentrated with time, leading to higher acidity, which may have hydrolyzed PMB. Secondly, PMB may have further reacted to form higher molecular weight products due to its high reactivity. If the first reason is the most important, it might be possible to obtain pure PMB via a different route for NMR structural analysis. For this reason, we tried to synthesize PMB directly from the reaction of 5-methyl-1, 2-benzoquinone and PA in acetic acid, which was modified from a reported protocol.[19] Although we kept the pH of the reaction medium slightly acidic to prevent PMB hydrolysis, this strategy proved to be unsuccessful. The product is unstable and dark brown precipitates were observed when the product was concentrated in organic solvent (e.g. hexane, diethyl ether) during purification. The instability has been reported for a similar compound, 4-*n*-butylamino-5-methyl-1,2-benzoquinone.[20] Additionally, the UV-VIS spectra of eluted PMB showed distinct peaks at 294, and 504 nm, which matched the UV-VIS spectra of the amine-catechol adduct reported in literature.[19,20] Nevertheless, one might argue that we did not observe these two distinct peaks in Fig. 3.6. We ascribed this to the fact that Fig. 3.6 presents collective spectra of so many products/intermediates in the reaction mixture, that peaks of individual species are obscured.

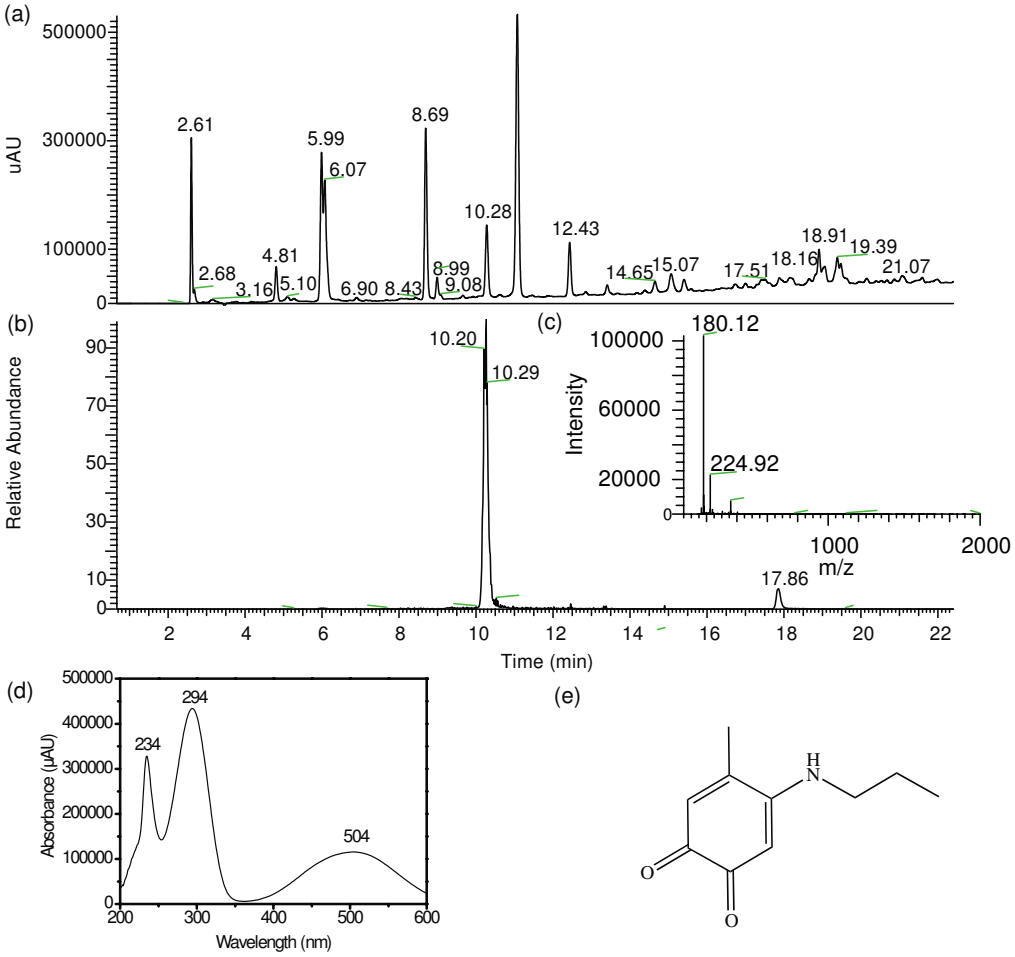

Figure 3.8. a) LC-UV chromatograms (monitored at 254 nm) of the reaction mixture of 4MC, PA, and $NaIO_4$ over time. The ratio of 4MC, PA and $NaIO_4$ is 1:3:0.5. b) Extracted ion chromatogram (positive ion mode) corresponding to PMB (m/z = 179.5-180.5) c) ESI-MS spectra [m/z 50-2000] summed over the 10.00-10.53 min retention time window; d) Extracted UV spectra corresponding to the 10.00-10.53 min retention time e) Proposed representative chemical structure of product.

Fig. 3.9 shows the complete structural details of the possible product at retention time 11.07 min. As shown in Fig. 3.9(b), the mass m/z = 440.31 was detected at more than one retention time, e.g., 10.00, 11.00, 19.33 min, indicating that multiple products/isomers with m/z of 440.31 were formed. The products from Fig. 3.9(e) were formed via a combination of Michael-type addition and Schiff base reaction. The UV-VIS data exhibited two maxima in absorbance around λ = 265 and 384 nm.

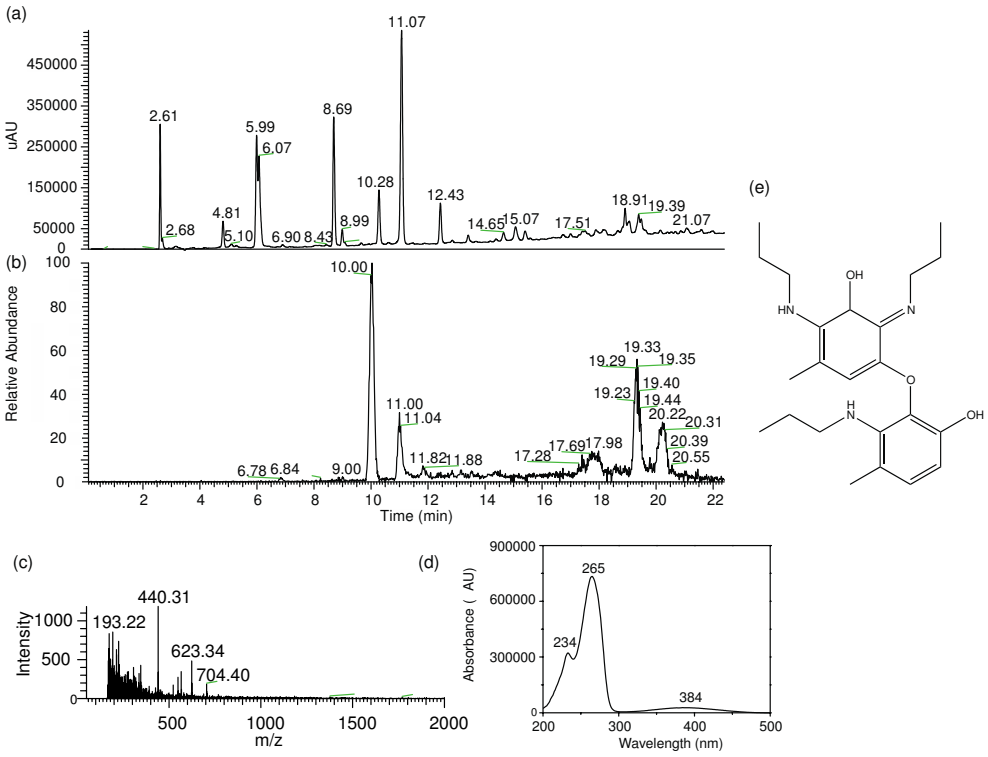

Figure 3.9. a) LC-UV chromatograms (monitored at 254 nm) of the reaction mixture of 4MC, PA, and $NaIO_4$ over time. The ratio of 4MC, PA and $NaIO_4$ is 1:3:0.5. b) Extracted ion chromatogram (positive ion mode) corresponding to product with m/z = 439.5-440.5 c) ESI-MS spectra [m/z 50-2000] summed over the 11.00-11.10 min retention time window; d)

Extracted UV spectra corresponding to the 11.00-11.10 min retention time e) Proposed representative chemical structure of product.

Similarly, for all the major peaks in the chromatogram, we have identified the mass spectra, UV-VIS spectra and the existence of possible isomers. From this, we construct a list of hypothetical structures for these products. All the details are listed in Fig. 3.10, 3.11, and 3.12. Finally, we scanned over the whole HPLC chromatogram, and identified around 60 products in addition to the major peaks (Table 3.1 and Fig. 3.13), which are associated with small peaks in the HPLC chromatogram. The intensity of each peak is an indication of the relative amount of the product. Therefore, these products, as listed in Table 1, were formed in a limited amount.

Proposed reaction mechanisms of 4MC and PA

Using the assignments from LC-MS, we found that the reaction between 4MC and PA under the current reaction conditions is very fast and many products are formed. Within 5 min, more than 60 products covering the mass range from 179 to 704 were identified. These products are categorized into 19 groups based on their mass (Table 3.1 and Fig. 3.13). It is clear that for each of the products, more than one isomer was formed, which indicates the complexity of the mechanism. The proposed structures in Fig. 3.14 reveal that the majority of the products were formed via aroxyl phenol coupling and Michael-type addition. Only a very small portion was formed by Schiff base reaction.

Using HPLC, we investigated the time dependence of the reaction between 4MC and PA (Fig. 3.7). As time progressed, most of the multiple HPLC peaks that had appeared after 5 min decreased with time, except for two peaks that eluted at retention times of 3.1 and 7.0 min. The intensity of these two peaks increased over 24 h, indicating net formation of these two

products. From the identification of MS, these two products showed signals at m/z of 578 (retention time 3.1 min) and 230 (7.0 min), respectively. The mass of m/z = 578 corresponds to compound 15 shown in Fig. 3.14, while the structure corresponding to m/z = 230 remains unidentified. Finally, from the observation that the increasing trend of the two peaks at 3.1 and 7.0 min coincides with a decreasing trend of all other major peaks, we infer a hypothetical pathway of the reaction between 4MC and PA. Upon mixing 4MC with PA in the presence of $NaIO_4$, 4MC was first quickly oxidized to *o*-quinone. The highly reactive *o*-quinone either formed crosslinks with catechol, or reacted with nucleophilic amines in PA to form low molecular weight adducts. For instance, PMB was formed after 5 min of reaction, and due to its instability, it disappeared already after one hour of reaction. The low molecular weight intermediates react further with *o*-quinone or PA or other intermediates to form higher molecular weight products. In the course of time, the coupling of these products resulted in low concentrations of less soluble polymeric structures.

To verify this hypothesis, we performed dynamic light scattering to elucidate more details of this mechanism. Fig. 3.14 shows the scattered intensity of the reaction mixture as a function of time. Generally, larger aggregates scatter more light than small ones. From Fig. 3.14, it is clear that the intensity initially increased significantly, reaching a maximum around 24 h. This increase in intensity suggests the formation of large particles when the reaction proceeds. These large particles, in turn, might be due to the formation of high molecular weight poorly soluble adducts from the reaction of 4MC and PA. The formation of large particles is also verified by the diffusion coefficient of the reaction mixture over time, as shown in Fig. 3.15 (a) and (b). As the reaction progressed, the diffusion coefficient

gradually shifted to lower values, indicating the formation of larger particles. After 16 h, two populations of particles with very different sizes, as indicated by the different diffusion coefficients, were formed. The new population of slowly diffusing particles arises most likely as a result of physical aggregation of the least soluble reaction products. This verifies our hypothesis that the low molecular weight intermediates gradually transformed into high molecular weight products. After 24 h, there is a decrease in intensity as shown in Fig. 3.14. This is likely due to sedimentation of the large particles.

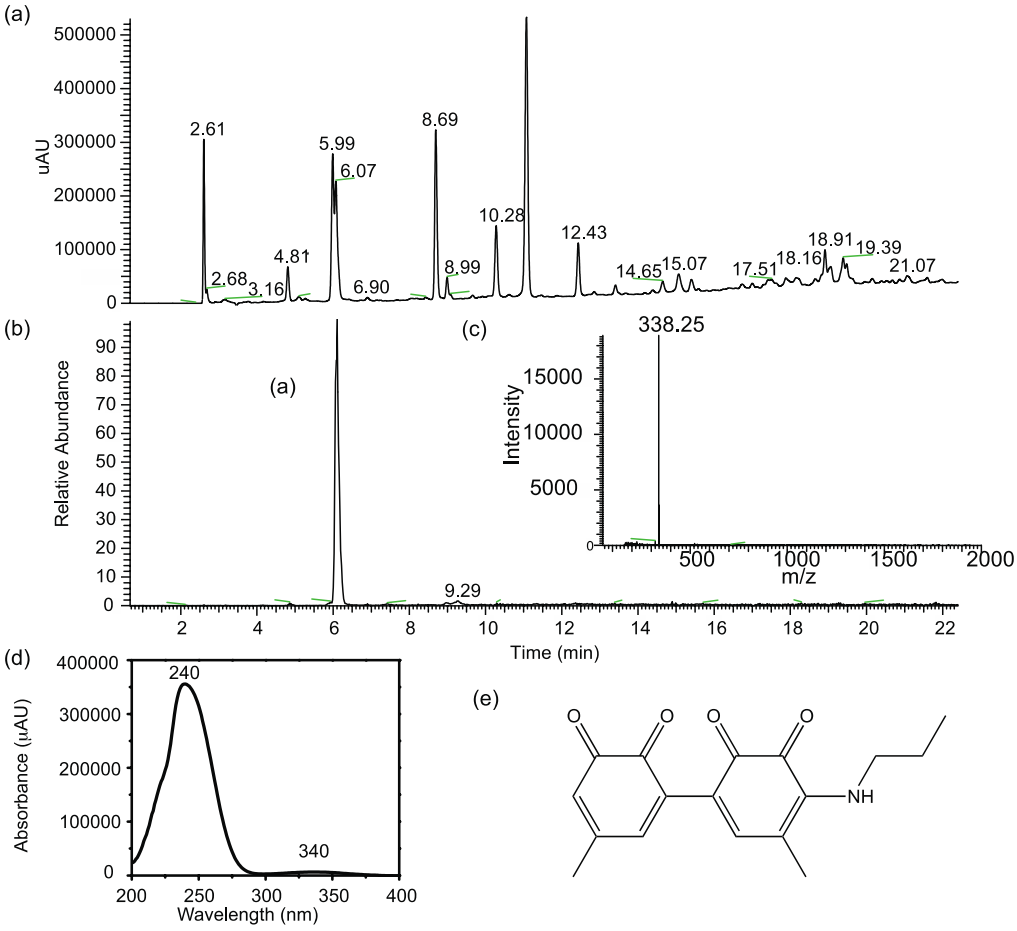

Figure 3.10. a) LC-UV chromatograms (monitored at 254 nm) of the

reaction mixture of 4MC, PA, and $NaIO_4$ over time. The ratio of 4MC, PA and $NaIO_4$ is 1:3:0.5. b) Extracted ion chromatogram (positive ion mode) corresponding to m/z = 337.5-338.5 c) ESI-MS spectra [m/z 50-2000] summed over the 5.93-6.15 min retention time window; d) Extracted UV spectra corresponding to the 5.93-6.15 min retention time e) Proposed representative chemical structure of product.

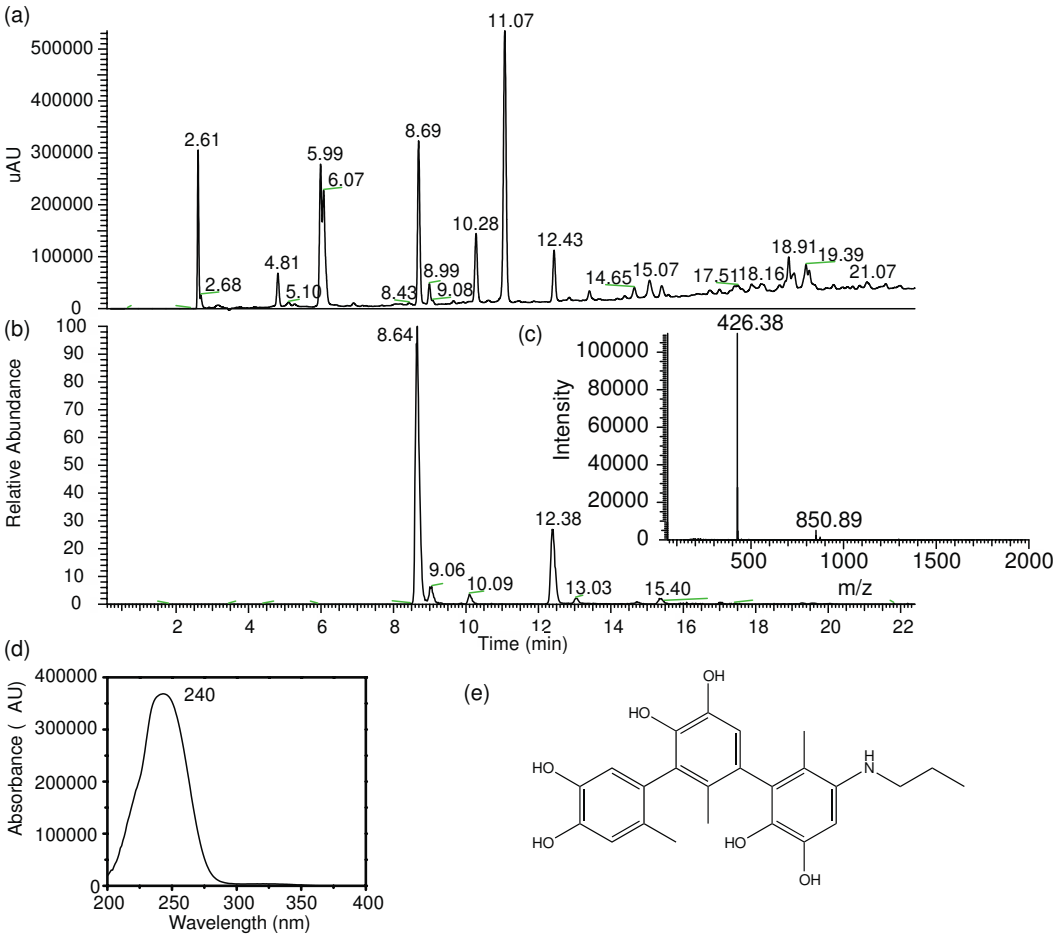

Figure 3.11 a) LC-UV chromatograms (monitored at 254 nm) of the reaction mixture of 4MC, PA, and $NaIO_4$ over time. The ratio of 4MC, PA and $NaIO_4$ is 1:3:0.5. b) Extracted ion chromatogram (positive ion mode)

corresponding to m/z = 425.5-426.5 c) ESI-MS spectra [m/z 50-2000] summed over the 8.6-8.91 min retention time window; d) Extracted UV spectra corresponding to the 8.6-8.91 min retention time e) Proposed representative chemical structure of product.

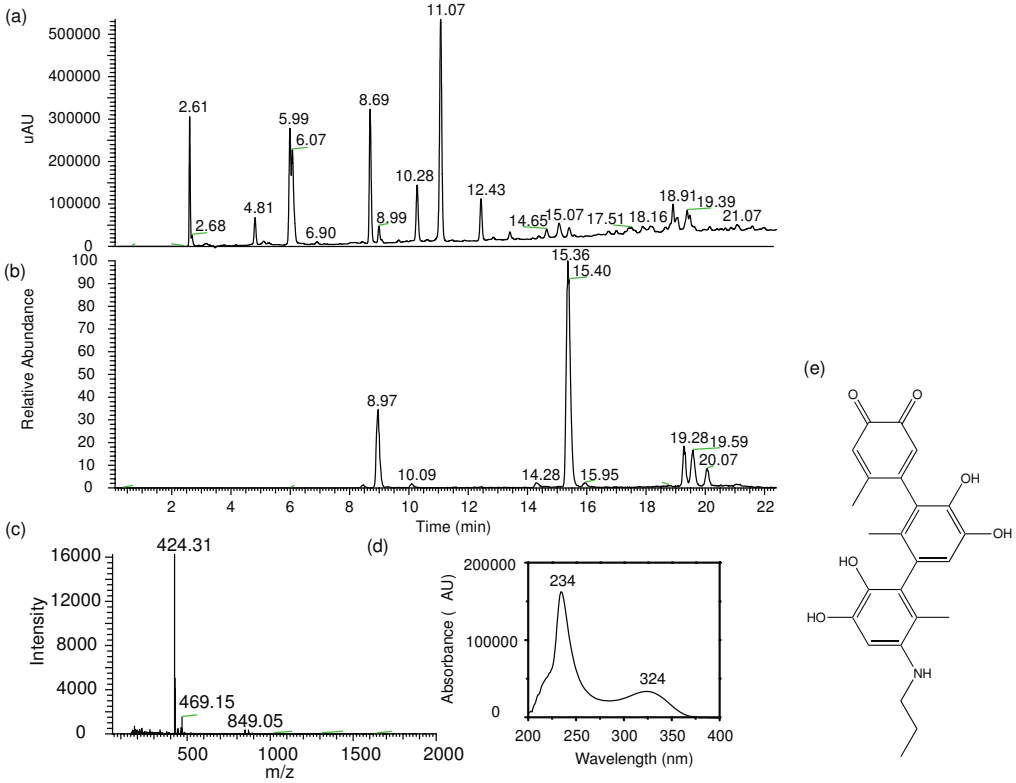

Figure 3.12. a) LC-UV chromatograms (monitored at 254 nm) of the reaction mixture of 4MC, PA, and $NaIO_4$ over time. The ratio of 4MC, PA and $NaIO_4$ is 1:3:0.5. b) Extracted ion chromatogram (positive ion mode) corresponding to m/z = 423.5-424.5 c) ESI-MS spectra [m/z 50-2000] summed over the 8.70-9.20 min d) Extracted UV spectra corresponding to the 8.70-9.20 min retention time e) Proposed representative chemical structure of product.

Table 3.1.Identification of peaks in LC-MS, based on MS and UV-VIS data

Entry	Retention time (min)	M/Z	Ion type	UV(λ_{max})	Product number
1	17.86	180	$[M+H]^+$	236,272,355	1
2	13.19	261	$[M+Na]^+$	235,281	2
3	15.06	261	$[M+Na]^+$	235,265(329)	2
4	14.62	302	$[M+H]^+$	235,285	3
5	18.61	302	$[M+H]^+$	236,330,441	3
6	9.57	304	$[M+H]^+$	234	4
7	10.41	304	$[M+H]^+$	234,276	4
8	10.56	304	$[M+H]^+$	234,264	4
9	14.73	304	$[M+H]^+$	235,281	4
10	17.82	304	$[M+H]^+$	236,267,353	4
11	6.31	322	$[M+K]^+$	234	5
12	7.24	322	$[M+K]^+$	234,338	5
13	9.52	322	$[M+K]^+$	234	5
14	9.69	322	$[M+K]^+$	234,278,309	5
15	10.27	359	$[M+H]^+$	235,294,504	6
16	22.68	359	$[M+H]^+$	236	6
17	8.97	424	$[M+H]^+$	235,324	7
18	15.36	424	$[M+H]^+$	235,264,355,384	7
19	8.66	426	$[M+H]^+$	235	8
20	9.06	426	$[M+H]^+$	234	8
21	12.38	426	$[M+H]^+$	235	8
22	10.04	440	$[M+K]^+$	234	9
23	17.98	440	$[M+K]^+$	236,283,347	9
24	19.33	440	$[M+K]^+$	236,281,382	9
25	20.22	440	$[M+K]^+$	236	9
26	9.23	444	$[M+Na]^+$	234	10
27	9.89	444	$[M+Na]^+$	234	10
28	13.76	444	$[M+Na]^+$	235	10
29	14.39	444	$[M+Na]^+$	235	10
30	6.86	458	$[M+K]^+$	234,276	11
31	10.04	458	$[M+K]^+$	234	11
32	16.43	458	$[M+K]^+$	235(354)	11
33	17.55	458	$[M+K]^+$	236(346)	11
34	13.71	548	$[M+H]^+$	235	12
35	18.61	548	$[M+H]^+$	236,333,441	12

36	19.89	548	$[M+H]^+$	236,346	12
37	20.81	548	$[M+H]^+$	236,350	12
38	12.3	564	$[M+Na]^+$	235	13
39	17.84	564	$[M+Na]^+$	236,268,355	13
40	19.1	564	$[M+Na]^+$	236,346	13
41	19.44	564	$[M+Na]^+$	236,281,399	13
42	11.09	566	$[M+Na]^+$	233,265,384	14
43	17.82	566	$[M+Na]^+$	236,267,353	14
44	17.65	578	$[M+K]^+$	236	15
45	17.97	578	$[M+K]^+$	236,347	15
46	19.48	578	$[M+K]^+$	236,283,396	15
47	19.56	578	$[M+K]^+$	236,349	15
48	14.28	605	$[M+H]^+$	235	16
49	14.53	605	$[M+H]^+$	235	16
50	16.17	605	$[M+H]^+$	235(352)	16
51	17.93	670	$[M+H]^+$	236,352	17
52	19.01	670	$[M+H]^+$	236,346	17
53	20.35	670	$[M+H]^+$	236(346)	17
54	16.5	702	$[M+K]^+$	235(352)	18
55	16.96	702	$[M+K]^+$	236(346)	18
56	18.36	702	$[M+K]^+$	236(354)	18
57	10.95	704	$[M+K]^+$	234,264	19
58	11.48	704	$[M+K]^+$	235,276	19
59	17.07	704	$[M+K]^+$	236(346)	19
60	16.96	704	$[M+K]^+$	236(346)	19

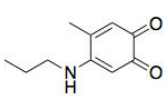

1

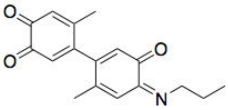

2

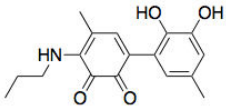

3

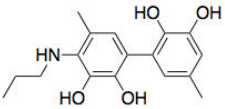

4

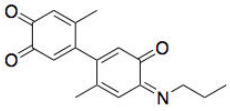

5

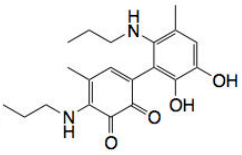

6

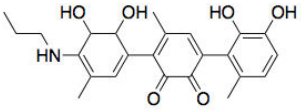

7

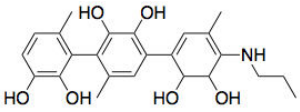

8

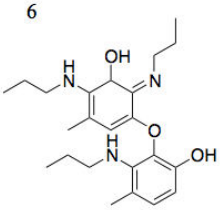

9

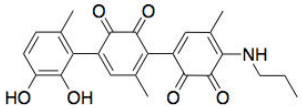

10

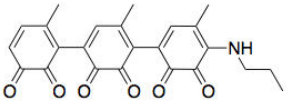

11

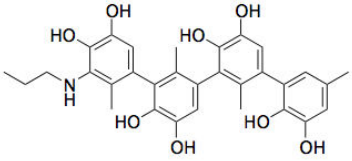

12

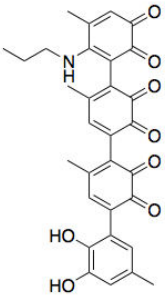

13

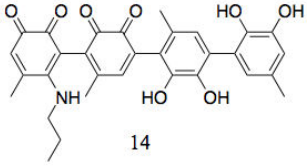

14

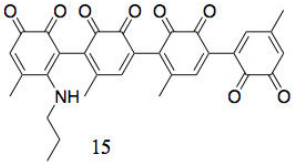

15

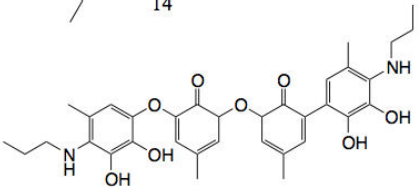

16

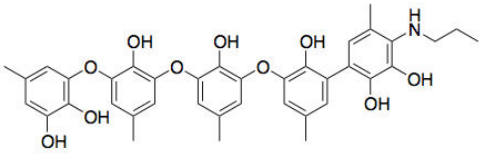

17

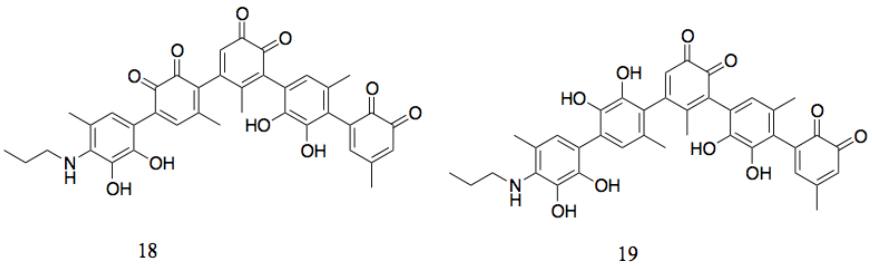

Figure 3.13. An overview of the proposed structures of the products. The number under each structure corresponds to the number in Table 1.

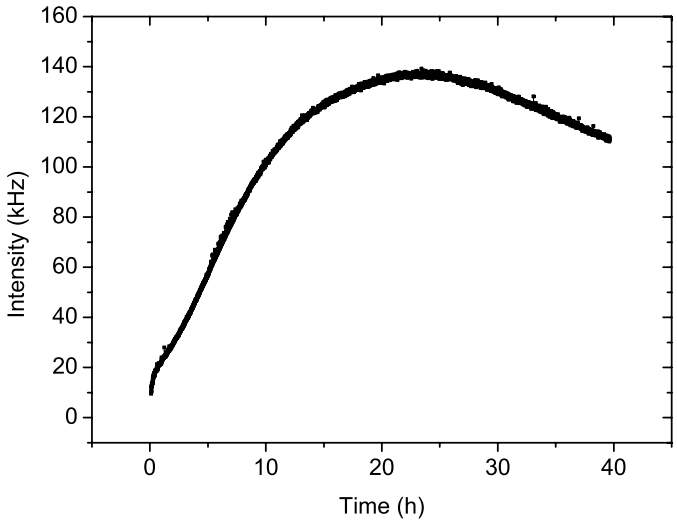

Figure 3.14. DLS measurement of the reaction system as a function of time: Intensity as a function of time, b) the diffusion coefficient as a function of time within 4h, c) the diffusion coefficient as a function of time within 24h.

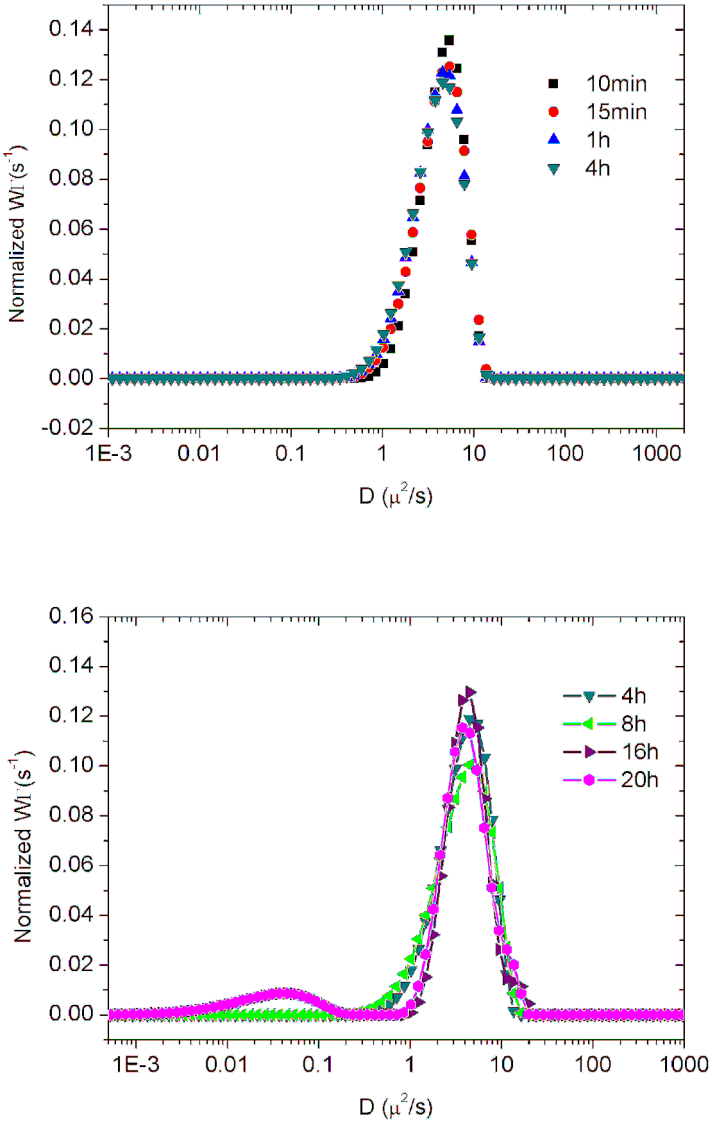

Figure 3.15. DLS measurements of the reaction system as a function of time: a) the diffusion coefficient as a function of time within 4h; b) the diffusion coefficient as a function of time within 24h.

Conclusions

In this study, we have investigated the crosslinking chemistry of catechol and primary amine using model compounds 4MC and PA by spectroscopic and chromatographic methods. We carried out the reaction of 4MC and PA at 20 °C in the presence of $NaIO_4$ at high pH using 10 mM Na_2CO_3 aqueous solution. By separating and identifying the products using HPLC-MS, we found that the crosslinking chemistry of catechol and amine is both fast and complicated. Within five minutes, more than 60 products were formed. These products encompass 19 masses ranging from 179 to 704. The majority of these products are formed via aryloxyl phenol coupling and Michael-type addition; a small fraction are formed via Schiff base reactions. Given the complexity of the system, a systematic investigation of relevant parameters, such as pH, the amount of $NaIO_4$ and temperature would require a large effort beyond our resources. Nevertheless, the results presented here highlight major reaction pathways and can hopefully be used to design better crosslinking strategies and material properties. By regulating these parameters, we may control the rate of reaction and follow the kinetics. But the analysis will take a lot of efforts.

References

(1) Miserez, A.; Schneberk, T.; Sun, C.; Zok, F. W.; Waite, J. H. *Science* **2008**, *319*, 1816.

(2) Yu, J.; Wei, W.; Danner, E.; Ashley, R. K.; Israelachvili, J. N.; Waite, J. H. *Nat. Chem. Biol.* **2011**, *7*, 588.

(3) Floriolli, R. Y.; Langen, J.; Waite, J. H. *J. Mar. Biotechnol.* **2000**, *2*, 352.

(4) Yang, J.; Cohen Stuart, M. A.; Kamperman, M. *Chem. Soc. Rev.* **2014**, *43*, 8271.

(5) Zhao, H.; Waite, J. H. *Biochemistry* **2005**, *44*, 15915.

(6) Kramer, K. J.; Kanost, M. R.; Hopkins, T. L.; Jiang, H. B.; Zhu, Y. C.; Xu, R. D.; Kerwin, J. L.; Turecek, F. *Tetrahedron* **2001**, *57*, 385.

(7) Land, E. J.; Ramsden, C. A.; Riley, P. A. *Accounts of Chemical Research* **2003**, *36*, 300.

(8) Holl, S. M.; Hansen, D.; Waite, J. H.; Schaefer, J. *Arch. Biochem. Biophys.* **1993**, *302*, 255.

(9) Burzio, L. A.; Waite, J. H. *Biochemistry* **2000**, *39*, 11147.

(10) Miserez, A.; Rubin, D.; Waite, J. H. *Journal of Biological Chemistry* **2010**, *285*, 38115.

(11) Lee, B. P.; Dalsin, J. L.; Messersmith, P. B. *Biomacromolecules* **2002**, *3*, 1038.

(12) Yu, M.; Deming, T. J. *Macromolecules* **1998**, *31*, 4739.

(13) Wu, J. J.; Zhang, L.; Wang, Y. X.; Long, Y. H.; Gao, H.; Zhang, X. L.; Zhao, N.; Cai, Y. L.; Xu, J. *Langmuir* **2011**, *27*, 13684.

(14) Liu, B.; Burdine, L.; Kodadek, T. *J. Am. Chem. Soc.* **2006**, *128*, 15228.

(15) Faure, E.; Falentin-Daudré, C.; Lanero, T. S.; Vreuls, C.; Zocchi, G.; Van De Weerdt, C.; Martial, J.; Jérôme, C.; Duwez, A.-S.; Detrembleur, C. *Advanced Functional Materials* **2012**, *22*, 5271.

(16) Haemers, S.; Koper, G. J. M.; Frens, G. *Biomacromolecules* **2003**, *4*, 632.

(17) Smith, A. M.; Callow, J. A. *Biological adhesives*; Springer Berlin Heidelberg, 2006.

(18) Wang, S. X.; Mure, M.; Medzihradsky, K. F.; Burlingame, A. L.; Brown, D. E.; Dooley, D. M.; Smith, A. J.; Kagan, H. K.; Klinman, J. P. *Science* **1996**, *273*, 1078.

(19) Akagawa, M.; Suyama, K. *Biochem. Biophys. Res. Commun.* **2001**, *281*, 193.

(20) Mure, M.; Wang, S. X.; Klinman, J. P. *J. Am. Chem. Soc.* **2003**, *125*, 6113.

Chapter 4

pH-induced self-crosslinking of mussel-inspired polymer coatings

Abstract

In this chapter, we aim at developing a catecholamine polymer for water-borne coating applications. For this application, an aqueous solution of this polymer should be stable as homogeneous liquid, readily applied on a surface, and should solidify to form a water-insoluble coating during drying and curing. To achieve this aim, we synthesized a copolymer using free radical polymerization of borax-protected dopamine acrylamide (DAA-*p*) and 2-aminoethyl methacrylamide hydrochloride (AEMA) in aqueous media. The polymer is pH-responsive. At low pH (pH 2), the polymer is water-soluble. At high pH (pH 11.5), by triggering the crosslinking reaction of catechols and amines in the polymer, we successfully fabricated a crosslinked, and water-insoluble film. The homogeneity of the resulting network is affected by the polymer sequence distribution. Therefore, we studied the sequence distribution by determining at the reactivity ratios of the monomers DAA-*p* and AEMA, using an in-situ ^{1}H NMR monitoring method. The reactivity ratios of DAA-*p* and AEMA are 0 and 0.46, respectively, indicating that our polymer has a moderately alternating structure, in which, I concluded that DAA-*p* pairs cannot occur, and sequence of AEMA are not when DAA-*p*/AEMA is not too low.

This chapter is based on: Juan Yang, Inge Bos, Anthonie Stuiver, Wim J. Pranger, Aldrik Velders, Martien A.Cohen Stuart, Marleen Kamperman, Journal of Materials Chemistry A, submitted, (2015)

Introduction

Natural organisms often use coatings to protect themselves against corrosive factors in the environment, e.g. mechanical impact, moisture, and temperature. Examples include mussel byssal threads[1], squid beak[2,3], and protective cuticles on plants[4]. The production of the protective coating, generally, involves two steps: i) secretion of fluidic and pliable proteins, and ii) fast curing to form hard and tough solids[1]. For instance, mussels produce viscous liquid mussel foot proteins (mfps) at pH < 5 inside granules. Upon being secreted into the seawater, at pH 8, the mfps solidify in a few minutes to form very tough and hard cuticle[5]. The formed cuticle (~ 5 μm in thickness)[6] coats the exposed byssus surfaces, and protects the byssus against microbial attack and rough sea waves[7-9]. A similar hydrophobic coating has been observed in squid beak, i.e. *Dosidicus* beak. The beak is composed of chitin fibers, proteins and polyphenolic compounds. The polyphenolic compounds form a dense crosslinked network, providing an efficient hydrophobic coating around the soft and hydrophilic chitin nanofibers, preventing the chitin from softening by water adsorption. [2]

For mussels, the fast cuticle curing can occur due to the efficient, versatile and complicated crosslinking chemistry of mfps[10]. As reported by Waite, et al., significant amounts of catecholic amino acid 3,4-dihydroxyphenylalanine (DOPA) are present in mfps[11]. The *o*-dihydroxylphenyl/catechol moiety in DOPA forms crosslinks in a variety of pathways. Briefly, catechols are easily oxidized to form reactive *o*-quinones. The *o*-quinones can then either react with catechols via dismutation reaction, or with amines via Michael type addition or Schiff base reaction, or with thiols via Michael addition to form crosslinks[10]. In

addition, catechols can interact with transition metals by forming strong coordination bonds to give catechol-metal complexes[12]. The crosslinking of mfps happens in response to the change in environment, i.e., the higher pH in seawater, and the exposure to oxygen.

Inspired by the fascinating properties of natural coatings, and the versatile chemistry of catechols, much effort has been devoted to fabricating thin catechol-functionalized films for various applied fields such as biomedical engineering and antimicrobial coatings[13-15]. Catechols are particularly interesting because they strongly bind to various types of substrates. A common fabrication method is layer-by-layer (LBL) assembly, i.e. alternative deposition of catechol-containing polymer and amine-containing polymer on substrates. The reaction between catechol and amine is employed as a tool to ensure the stability of the multilayer films. Detrembleur and co-workers have published several very interesting articles on LBL.[16-18] For instance, they prepared films by alternatively depositing, from aqueous solution, oxidized catechol-containing polymer pox(DOPA) and amine-containing polymer poly(allylamine) (PAH). The reaction between the quinones in pox(DOPA) and primary amines in PAH yielded films with long-term durability. The films can further be modified to target different applications. By doping with silver nanoparticles, the films were used as antibacterial coatings. The films can also be grafted with enzymes (e.g. DispersinB) or poly(ethylene glycol) to have anti-biofilm and anti-adhesion properties, respectively.[16] Xu et al. have also reported similar LBL work. They prepared multilayered films by alternatively immersing a substrate in an aqueous solution of poly(acrylic acid-dopamine) (PAA-dopamine) and PAH. By immersing the final film into an aqueous solution of 1 mM $NaIO_4$, crosslinking was triggered. The crosslinked films showed

high stability under extreme conditions, e.g. extreme pH and high ionic strength. [19]

Besides LBL assembly that involves multiple-step deposition, a one-pot deposition strategy of aqueous solutions containing catecholamine-containing polymers on various substrates has also been developed. For instance, Messersmith et al. prepared films by immersing various substrates (e.g. Au, Pt, PS, PMMA) into an aqueous solution of copolymer p(N-(3,4-dihydroxyphenethyl) methacrylamide-co-aminoethylmethacrylamide) (catechol content 10.6 wt%) at pH 8.3 for 24 h. The films were further used for DNA immobilization.[20]

In this study, we aimed at reproducing the working mechanism of mussels by developing a catecholamine polymer for water-borne paint applications. The current solvent-based alkyl-paints are still considered superior in terms of rheology, but harmful for the environment since organic solvents are used. Our catecholamine polymer, in contrast, is water soluble, and should be a promising alternative having similar rheological characteristics as classical solvent-based paints. Therefore, the requirements the polymer should fulfill were 1) being able to self-crosslink in response to an external trigger such as pH; 2) being water-soluble at acidic pH; 3) being water-insoluble at basic pH. We synthesized a co-polymer by free radical polymerization of borax-protected dopamine acrylamide (DAA-*p*) and 2-aminoethylmethacrylamide hydrochloride (AEMA). The monomer reactivity of DAA-*p* and AEMA was investigated by in-situ ^{1}H NMR measurements. At low pH, the polymer is soluble in water and forms a stable solution. Polymer films were prepared by increasing the pH and casting the polymer solutions on substrates. The increase in pH triggers

crosslinking reactions, which resulted in crosslinked, water-insoluble films. The chemistry and morphologies of the films were investigated by UV-VIS, and AFM measurements.

Materials and Experiments

Materials: All reagents were used as received unless mentioned otherwise. Dopamine hydrochloride, methacrylic anhydride (94%), 2-methoxyethyl acrylate (98%), basic alumina, deuterochloroform (99.96%), tetrahydrofuran (98.5%), ethyl acetate (99%), dimethylformamide (99.8%), 2,2'-Azobis(2-methylpropionitrile) (98%), 2,2'-Azobis(2-methylpropionamidine)dihydrochloride (95%), dichloromethane (98.5%), methanol (98.5%), 3,4-dimethoxyphenethyl amine (97%) and triethylamine (>99.5%), acryloyl chloride (97%) were purchased from Sigma-Aldrich. Sodium hydroxide solution (1 M) and anhydrous magnesium sulfate ($MgSO_4$, 97%) were purchased from Merck. Hydrochloride solution (1 M) was purchased from Fluka. Hexane (p.a.) and diethyl ether (p.a.) were purchased from Biosolve. Sodium tetraborate decahydrate (p.a.) and sodium bicarbonate were purchased from J.T.Baker. 2-Aminoethyl methacrylamide hydrochloride was purchased from Polysciences.

Experiments

Dopamine acrylamide (DAA) monomer synthesis

Dopamine acrylamide (DAA) was synthesized by reaction of dopamine hydrochloride and acryloyl chloride in a mixture of tetrahydrofuran (THF) and Milli-Q water, see Scheme 4.1. 20 g of sodium tetraborate decahydrate and 8 g of sodium bicarbonate were added to 200 ml Milli-Q water. The aqueous solution was bubbled with N_2 for 20 min, followed by addition of 10 g of dopamine hydrochloride. Next, 8.6 ml of acryloyl chloride in 50 ml

of THF was added dropwise. The pH of the solution was adjusted to above 8 by adding drops of 1 M NaOH solution. The reaction mixture was stirred overnight (around 14 h) under continuous N_2 bubbling at room temperature. After the reaction, a slightly pinkish slurry was formed with a white solid present at the bottom of the flask. The reaction mixture was filtered by vacuum filtration and the clear, slightly pinkish solution was washed twice with 100 ml ethyl acetate. The obtained aqueous solution was acidified by 1 M HCl to a pH of around 2, followed by extraction with 100 ml ethyl acetate repeated three times. The brownish organic solution obtained from extraction was collected and dried over $MgSO_4$. Afterwards, the volume of the solution was reduced to around 50 ml by rotary evaporation and precipitated into 500 ml hexane. The formed suspension was stored at 4 °C overnight to aid crystallization. After 14 h, the resulting brownish solids were collected, dissolved in 100 ml ethyl acetate and precipitated in 1000 ml hexane. The final solid obtained by filtration of the suspension was dried in a vacuum oven overnight at room temperature and the yield was 54%.

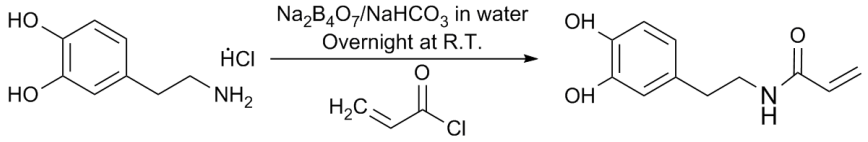

Scheme 4.1. The synthesis pathway of DAA

DAA Protection (DAA-*p*)

The protection of DAA was carried out by adding 3 g DAA dissolved in a mixture of ethanol/H_2O (10 ml ethanol and 20 ml Milli-Q water) to 289.5 ml of degassed aqueous solution of sodium tetraborate decahydrate (Scheme 4.2) (11.0420 g, 2 molar equivalents compared to catechol moieties). The reaction mixture was kept under nitrogen for one hour under

continuous stirring. After that, the product was lyophilized and used without any further purification.

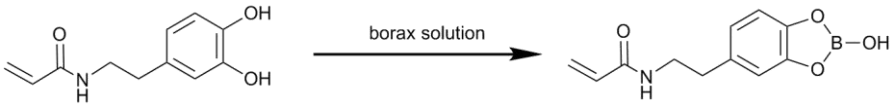

Scheme 4.2. The synthesis of protected DAA (DAA-*p*) from DAA and sodium tetraborate decahydrate solutions

Polymer synthesis

Co-polymerization of DAA-*p* and 2-aminoethyl methacrylamide hydrochloride (AEMA) was carried out by free radical polymerization at 65 °C for 10 hours, see Scheme 4.3. DAA-*p* (0.74 g), and AEMA (2.3 g, DAA-p/AEMA=8:92 mol/mol) were added to 14.06 ml Milli-Q water in a 50 ml three-neck round bottom flask. The reaction mixture was heated up to 65 °C, and after that, AIBN (0.02493 g, 0.152 mmol) in 1.7 ml DMF was added. It is important to note that at room temperature, DAA-*p* was not fully dissolved. The solubility of DAA-*p* increased significantly when the temperature reached 55 °C. After the reaction had been kept under nitrogen overnight under continuous stirring, the reaction mixture was allowed to cool down. Then 1M HCl was added to acidify the mixture to pH 1. The mixture was transferred to a dialysis membrane (MWCO = 1000 Da) and dialysed against acidic Milli-Q (0.001 M HCl) for two days. The product was lyophilized and stored at 4 °C until further use. The yield was 58%.

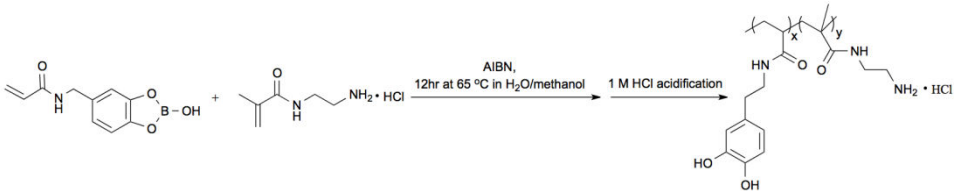

Scheme 4.3. Polymer synthesis by free radical polymerization of DAA-*p* and AEMA

Polymerization kinetics studied by ^{1}H NMR

The reactivity ratio of DAA-*p* and AEMA was determined by in-situ ^{1}H NMR, as described by Aguilar et al.[21] The experiments were carried out in a 500 Avance I NMR spectrometer, operating at 500.137 MHz, equipped with a 5 mm TXI probe. To perform quantitative experiments, the following measurement conditions were used: A pulse sequence of 9 μs equivalent to a 90° tip angle and a 53s delay time were applied to allow the total relaxation of the protons and to process the individual data. The spinning rate of the sample was set to 9 Hz during shimming, and for each datum only one acquisition (FID) was used to ensure that the measurement corresponds to instantaneous composition and not to an average. The measurement was carried out at 56 °C. A solution of DAA-*p* and AEMA (total monomer concentration is 5 wt%) in 10 mM Na_2CO_3 in D_2O (0.75 ml) was added in a screw-capped thin NMR tube under argon. Three sets of experiments were performed, and the feed molar fractions of DAA-*p* were 6, 10 and 15 mol%, respectively. Dioxane (10 μl) was added to be used as a reference. V50 (1.19 mg, 4.39 μmol) was used as the initiator.

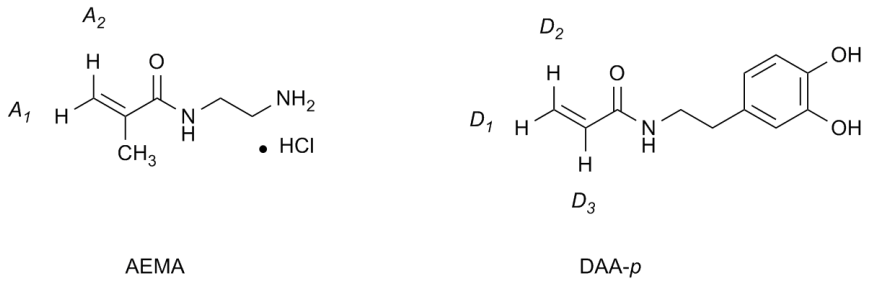

AEMA DAA-*p*

Scheme 4.4. Chemical structure of the comonomers used in the copolymerization including the nomenclature of the vinyl protons

The signals were integrated using the software Mestrenova 10.0.2. The concentrations of unreacted DAA-*p* and AEMA were determined as follows.

$$[DAA-p] = \frac{D_1 + D_2 + D_3}{3R}$$

$$[AEMA] = \frac{A_1 + A_2}{2R}$$

where D_1, D_2 and D_3 correspond to the protons assigned to the vinyl group of DAA-*p*, and A_1 and A_2 are the protons of the vinyl group of AEMA, as shown in Fig. 4.1. *R* is the reference peak of dioxane, since dioxane is not expected to react, and therefore the peak should stay constant. These values were normalized to the initial feed monomer concentration $[DAA\text{-}p]_0$ and $[AEMA]_0$.

Static light scattering (SLS)

SLS was used to determine the molar mass of the copolymer. The measurements were carried out at 20 °C with an ALV light scattering setup using an ALV5000/60X0 External Correlator with a Cobolt Samba-300 DPSS Laser operating at 100mW at a wavelength of 660 nm and an ALV / HIGH QE APD Single Photon Detector. Copolymer solutions in 1 mM HCl aqueous solution with a concentration of 0.26 g/l were measured at different angles. The angle was varied using an ALV-125 goniometer with increasing steps of 5° between 20° and 120°. The molecular weight of the copolymers was deduced from a Zimm analysis of the collected data.

^{1}H NMR spectroscopy

^{1}H NMR of the polymers was performed in 0.1 M DCl/D_2O on a Bruker AMX-400 spectrometer (400 MHz) at 298 K.

Polymer film preparation

For AFM, UV-vis measurements, optical microscopy and contact angle measurements, polymer films were prepared using a casting method. For AFM measurements, glass cover slips, 18 mm long x 18 mm wide, were used as substrates for the polymer films. A 10 mg/ml polymer solution was prepared using 0.001 M HCl (aq) as the solvent. Four polymer films were prepared under the following conditions: a) low pH; b) high pH, by adding 1M NaOH; c) high pH, in the presence of a moderate amount of $NaIO_4$ ($NaIO_4$/ catechol = 1/ 100); d) high pH, in the presence of a large amount of $NaIO_4$ ($NaIO_4$/ catechol = 1/ 10). A volume of 0.6 ml of the respective polymer solution was spread onto a pre-cleaned coverslip, and left to dry under well-ventilated conditions for more than 24 h. For UV-vis measurements, 4.5 cm long x 1.25 cm wide quartz slides were used as substrates. Polymer solutions were prepared in the same way as for the AFM measurements; 1.04 ml of polymer solution was spread onto the pre-cleaned quartz slide, and left to dry under well-ventilated conditions for more than 24 h.

UV-VIS spectroscopy

UV-visible characterization was performed on a Shimadzu UV-2600 spectrophotometer at wavelengths from 200 to 600 nm. For the calibration of the catechols, five solutions of dopamine hydrochloride in water with different concentrations (0.18 – 0.25μM) were prepared. The spectra of the samples were measured (wavelength scan) in a quartz curvet. The absorbance intensity at λ = 280 nm for the samples was used to calculate the extinction coefficient ε.

Atomic force microscopy

The roughness of the polymer films was analyzed using a Digital Instruments NanoScope V equipped with a silicon nitride probe (Veeco, NY, U.S.A.) with a spring constant of 0.4 N/m in ScanAsyst^{TM} imaging mode. Images were recorded between 1.5 Hz and 1024 samples/line. Images were further processed with Nanoscope Analysis 1.20 software (Veeco Instruments Inc. 2010, U.S.A.). A first order flattening was used for all the images.

Contact angle measurements

The wettability of the polymer films was measured by automated static water contact angle measurements with a Krüss DSA 100 goniometer. The volume of the drop of deionized water was 3.0 μL. The reported values are the average of at least two droplets, and the relative error is less than ±3°.

FTIR

A 10 mg/ml polymer solution was prepared using 0.001 M HCl (aq) as the solvent. Subsequently, four polymer samples were prepared under the following conditions: a) low pH; b) high pH, by adding 1M NaOH; c) high pH, in the presence of a moderate amount of $NaIO_4$ ($NaIO_4$/ catechol = 1/ 100); d) high pH, in the presence of a large amount of $NaIO_4$ ($NaIO_4$/ catechol = 1/ 10). The four polymer solutions were allowed to react for 24 h and lyophilized thereafter. The ATR-FTIR measurements were carried out using a Bruker Tensor 27 FTIR spectrometer.

Optical microscopy

Cross-sections of the polymer films on the glass substrates were imaged using an Olympus BX 60. Images were obtained using a 40x magnification.

Results and discussion

Polymer synthesis

In this work, we developed a catecholamine co-polymer by free radical copolymerization in aqueous conditions of two vinyl comonomers, one containing borax protected catechol (DAA-*p*) and the other amines (AEMA). An essential step is the protection of the catechols before polymerization. As reported in our previous work, using vinyl monomers containing unprotected catechols would result in the formation of a crosslinked polymer[22]. The reason is the radical scavenging effect of catechols. More specifically, during radical polymerization, the catechols in one polymer chain can react with propagating radicals in another polymer chain. Therefore, to synthesize a linear catechol-containing polymer by radical polymerization, the catechols should be protected. Different protection methods are possible, dependent on the specific requirement of the system. In our case, we have tried two methods, namely methoxy-protection and borax-protection. For the methoxy-protection, i.e., protecting the catechols with methyl groups, we have successfully synthesized the protected polymers (Fig 4.1). Deprotection requires using BBr_3 and strict control of temperature at -65 °C. This deprotection strategy brings difficulty due to the following reasons. Firstly, the catechol deprotection by BBr_3 needs to be performed in the absence of water, since BBr_3 reacts violently with water. However, our copolymer is only soluble in a mixture of water and organic solvent, thereby making the deprotection impossible. Secondly, the removal of methoxy groups requires strict control of reaction conditions, i.e. proper amount of BBr_3, only organic solvent, and very low temperature. An addition of inappropriate amount of BBr_3 may result in partial deprotection of catechols[23]. In view of these problems, we

considered borax protection as an alternative. In this work, we start from the synthesis of vinyl monomers containing borax-protected catechols DAA-*p*. The stability of the complexation of borax with catechol is dependent on pH.[24] Generally, the pH has to be high (> 9) to ensure sufficient stability of the borax-catechol complex against dissociation or oxidation. In our synthesis, we keep the pH above 9 by using 10 mM sodium carbonate aqueous solution as the solvent. After 10 h of reaction, we deprotected the borax-catechol complex by lowering the pH to around 2 using a 1 M HCl aqueous solution. After dialysis, the polymeric product was obtained. To check the effectiveness of the deprotection procedure, the polymer and DAA-*p* aqueous solutions were investigated by UV-VIS (Fig. 4.2). DAA-*p* showed a peak at 286 nm, which was ascribed to the borax-catechol complex. For the polymer, in contrast, an absorbance peak at 280 nm was detected, which is typically ascribed to free catechols[19]. Therefore, the catechol groups in our polymer have been completely deprotected.

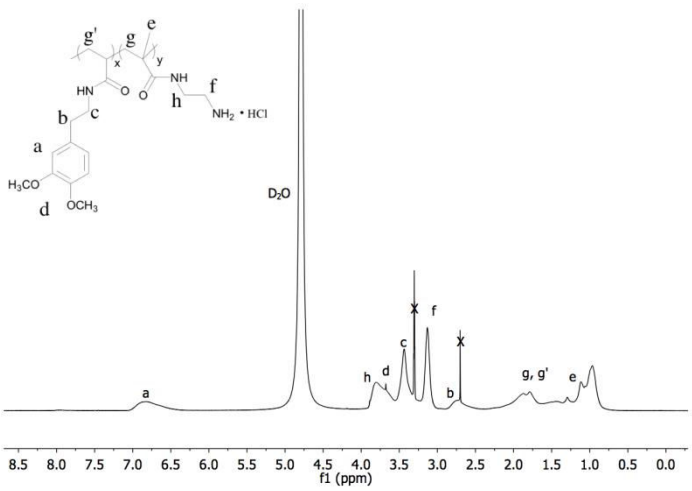

Figure 4.1. ^{1}H NMR spectra of poly(methyl-DAA-AEMA) in a mixture of MeOD/D_2O, the cross symbol ‘x’ in the spectra indicates the protons that associated with MeOD

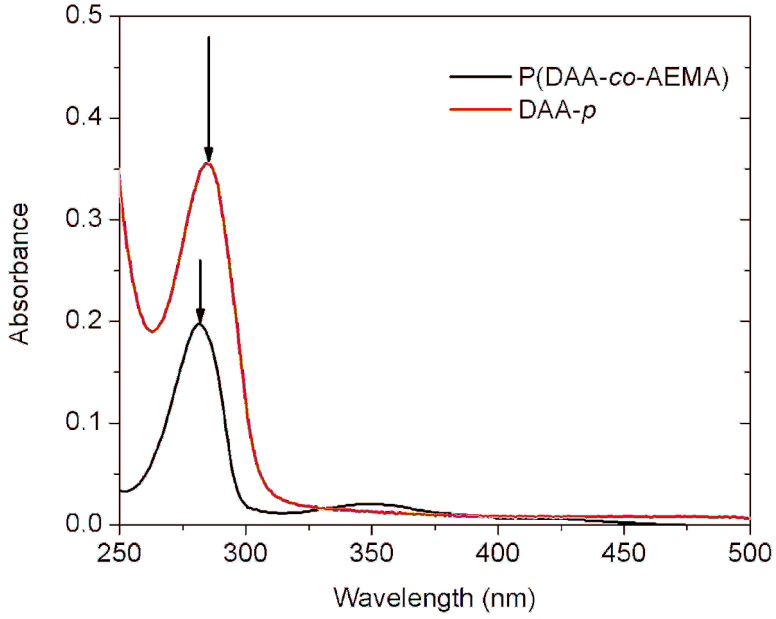

Figure 4.2. UV-vis spectra of DAA-*p* in Milli-Q water (red line) and P(DAA-*co*-AEMA) in 0.1 M HCl aqueous solution (black line)

Polymer characterization

^{1}H NMR was used to characterize the copolymer, and the spectrum is shown in Fig. 4.3. By comparing the integration area of peaks at δ = 7.2-6.6 ppm that can be assigned to the three protons of the aromatic ring in DAA (positions a), and peaks at δ = 3.75-2.8 ppm of the alkyl groups in both monomers (positions e, f, b, c), we calculated the DAA composition in the final polymer to be around 7.2 mol%. This result agrees well with that from UV-VIS, obtained as follows. To calculate the DAA composition in the final polymer, we made a calibration curve based on dopamine hydrochloride. By preparing dopamine hydrochloride solutions with different concentrations in 1 M HCl aqueous solution, we obtained the

extinction coefficient of catechol as 4688 $m^2 \cdot mol^{-1}$. By using the Lambert-beer law, the catechol concentration was obtained, and the DAA composition in the final polymer was determined to be 8.2 mol%.

The determination of the molecular weight was carried out by static light scattering. The copolymer has a weight-averaged molecular weight M_w of 4912 kg/mol, corresponding to a weight-averaged degree of polymerization of about 29140.

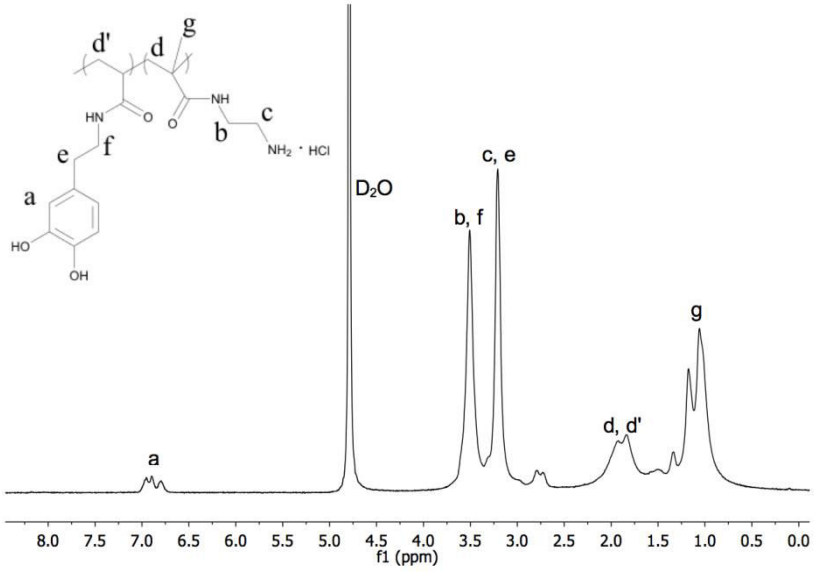

Figure 4.3. ^{1}H NMR spectra of poly(DAA-AEMA) in 0.1 M DCl/D_2O

Monomer reactivity

Generally, free radical polymerization is expected to generate random copolymers. This polymerization technique is favorable in our system, since a random copolymer would lead to an even distribution of crosslinks throughout the material. To check the randomness of the copolymer, we studied the reactivity ratios of the comonomers. The reactivity ratio *r* is a kinetic parameter that characterizes the monomer sequence distribution in a

copolymer. r_1 is defined as the ratio of the rate constant for a reactive propagating radical M_1 adding its own type of monomer M_1 to the rate constant for addition of the other monomer M_2. In our study, it was determined by in-situ ^{1}H NMR. The co-monomer concentrations were monitored as a function of time. Fig. 4.4, 4.5 and 4.6 show representative spectra of the DAA-*p*/ AEMA solutions during polymerization at different reaction times. As shown in Fig. 4.5, the peaks ascribed to the vinyl groups of DAA-*p* (δ = 6.52-6.36 ppm, and δ = 6.02-5.96 ppm) and AEMA (δ = 5.8-5.75 ppm, and δ = 6.06-6.02 ppm) decreased in time (marked in green). The aromatic peaks at δ = 7.0-6.75 ppm (marked in blue) became broader with increasing time. Meanwhile, broad peaks that can be ascribed to the -CH_2- groups in the polymer main chain, e.g., δ = 1.4-1.1 ppm (marked in blue), increased. These changes in the spectra in time clearly indicate that the polymerization takes place rapidly at elevated temperatures. We studied three reactions having feed molar ratios of DAA-*p* of 6, 10 and 15 mol%, respectively. By integrating the peaks ascribed to the vinyl groups of DAA-*p* and AEMA, as shown in Fig. 4.5, the monomer concentrations can be obtained as a function of time. From the variation of the monomer concentrations, the reactivity ratios of the comonomers can be obtained by fitting the experimental data to an integral form of the copolymer composition equation[25]:

$$\frac{M_2}{M_{20}} = \left(\frac{M_{20}M_1}{M_{10}M_2}\right)^{r_2/(1-r_2)} \times \left(\frac{(r_1-1)(M_1/M_2)-r_2+1}{(r_1-1)(M_{10}/M_{20})-r_2+1}\right)^{(r_1r_2-1)/((1-r_1)(1-r_2))} \quad (1)$$

where M_i is the instantaneous molar concentration of monomer *i* (which can be calculated by comparing the integration of the protons peaks of the vinyl groups in monomer *i* to that of dioxane), r_i is the reactivity ratio of monomer *i*, and M_{i0} is the initial molar concentration of monomer *i*.

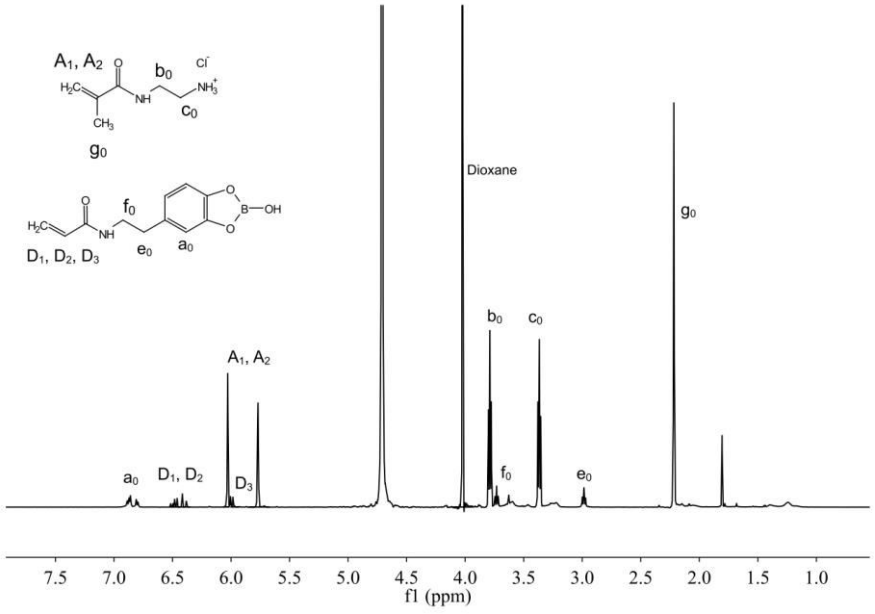

Figure 4.4. ^{1}H NMR spectra of the copolymerization reaction DAA-*p* and AEMA with an initial feed molar ratio of DAA-*p*: AEMA = 15: 85 after reaction at 56 °C for 12 min.

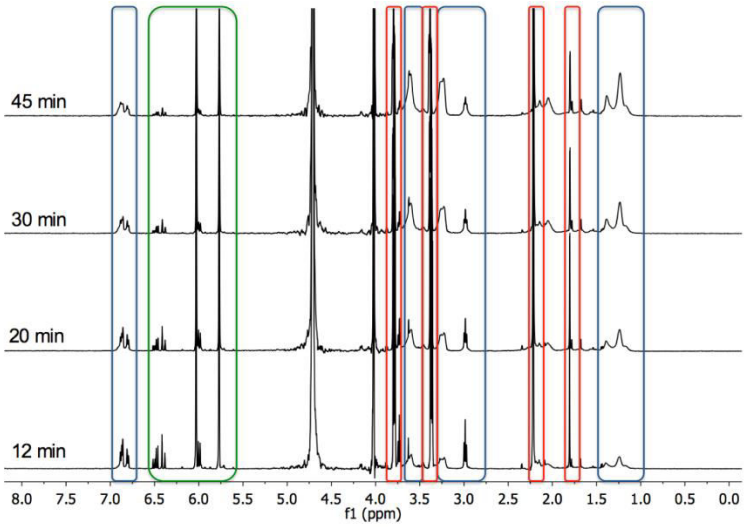

Figure 4.5. Representative ^{1}H NMR spectra of the copolymerization reaction DAA-*p* and AEMA with an initial feed molar ratio of DAA-*p*: AEMA = 15: 85. The peaks marked with green boxes indicate the vinyl

protons of the monomers; red boxes show that the protons in the alkyl groups decrease with time, and blue boxes indicate peaks that broaden.

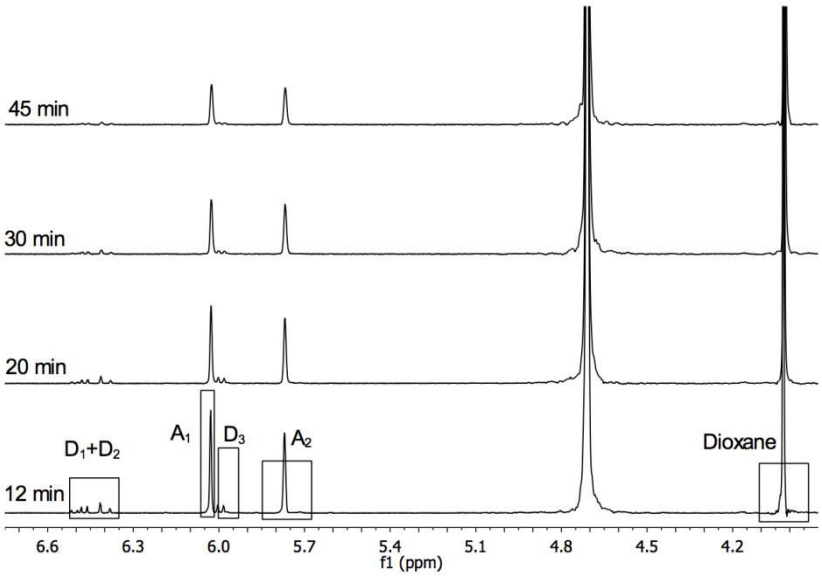

Figure 4.6. Details of the vinyl region of representative spectra for the copolymerization reaction DAA-*p* and AEMA with an initial feed molar ratio of DAA-*p*: AEMA = 15: 85.

The method takes any experimental point M_2, M_1/M_2 as starting point for the rest of the reaction. More specifically, for each reaction, the first 5-10 points were used as the initial M_{20}, M_{10}/M_{20} for the rest of the reaction. By using the least-squares optimization to fit each set of experimental data to eq (1), we obtained 5-10 reactivity ratios of $r_{DAA\text{-}p}$ and r_{AEMA}. The obtained reactivity ratios that fit each set of experimental data are highly correlated[21], and $r_{DAA\text{-}p}$ vs r_{AEMA} followed a straight line (Fig. 4.7). And for each reaction, as shown in Fig. 4.7, we obtained one straight line. The point where the lines intersect gives the final values of reactivity ratios, i.e., 0 for $r_{DAA\text{-}p}$ and

0.46 for r_{AEMA}. As all three lines intersect in one point, this indicates that a reliable reactivity ratio has been obtained. A value of 0 for the reactivity ratio of DAA-*p* indicates that the DAA-*p* propagating radicals cannot add a DAA-*p* monomer and therefore always add an AEMA monomer, while r_{AEMA} = 0.46 indicates that, AEMA propagating radicals add to DAA-*p* is about half of the cases.

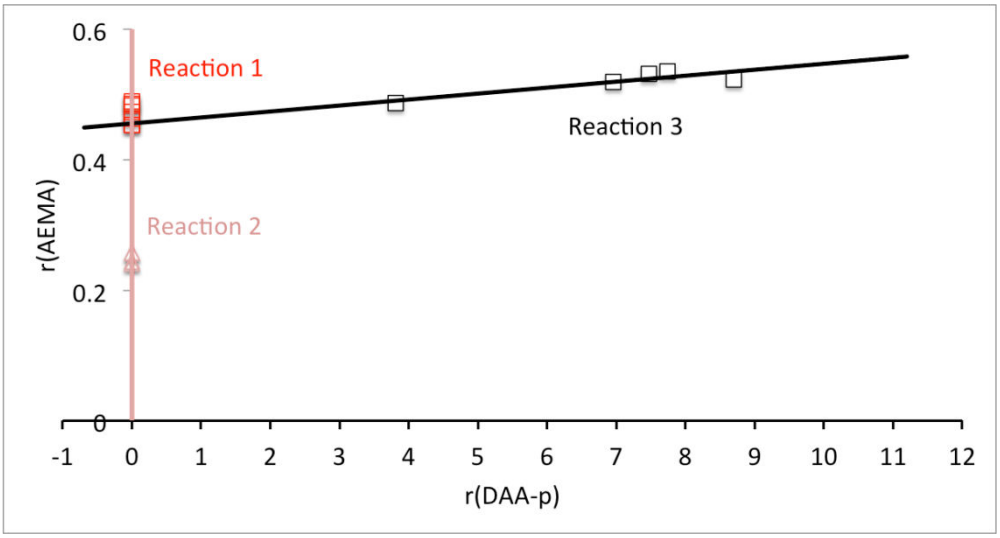

Figure 4.7. $r_{DAA\text{-}p}$ vs r_{AEMA} obtained from the method as described in the main text.

Based on the obtained reactivity ratios, we calculated the copolymer composition as a function of comonomer composition according to the following equation[25]:

$$F_1 = \frac{r_1 f_1^2 + f_1 f_2}{r_1 f_1^2 + 2 f_1 f_2 + r_2 f_2^2} \qquad (2)$$

where F_i is the mole fraction of M_i in the copolymer, and f_i is the feed molar fraction of monomer *i*. By applying the r_i we obtained above, we obtain the relation between $F_{DAA\text{-}p}$ and $f_{DAA\text{-}p}$ (Fig. 4.8). For our copolymer, the

reactivity ratios of both monomers are less than unity, and $r_{DAA\text{-}p}r_{AEMA} = 0$, giving rise to an azeotropic copolymerization. The $F_{DAA\text{-}p}$ /$f_{DAA\text{-}p}$ plots cross the line representing $F_{DAA\text{-}p} = f_{DAA\text{-}p}$. At the crossover point or azeotropic point, i.e. $f_{DAA\text{-}p} = 0.35$, the copolymerization occurs without change in the feed composition. For feed compositions near the azeotropic point, the copolymer composition distributions are narrow at low conversions. At high conversions, the copolymer composition drifts to either comonomer, depending on the initial feed, whether it contains more DAA-*p* or more AEMA. The copolymer composition distribution becomes wider when the initial feed composition deviates further from the azeotropic point. In our copolymer system, with an initial feed molar ratio of DAA-*p*: AEMA = 8: 92 as shown in Fig. 4.9, at low conversion, it is expected to present a moderate alternating structure. At high conversion, when DAA-*p* has been largely consumed, more AEMA is incorporated into the copolymer chains.

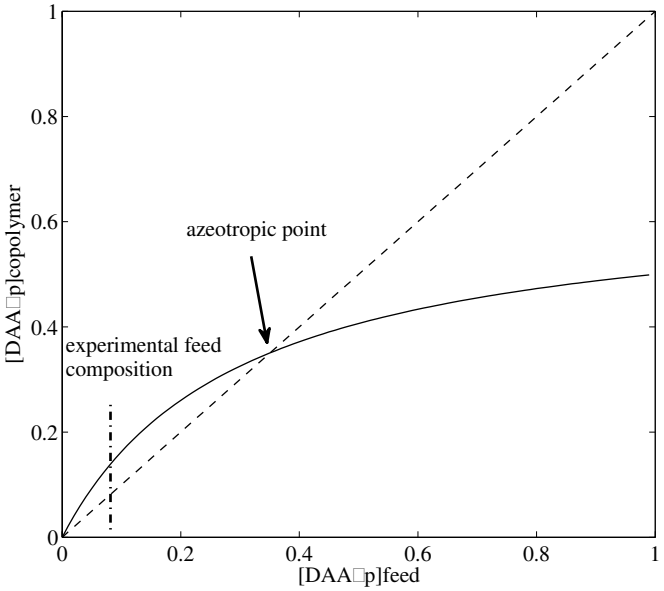

Figure 4.8. Copolymer composition as a function of monomer feed fraction for poly(DAA-*p*-AEMA) system. The dashed diagonal line represents $F_{DAA\text{-}p} = f_{DAA\text{-}p}$. The black arrow points to the azeotropic point. The dash dotted line indicates the feed composition for our copolymer with an initial DAA-*p* percentage of 8 mol%.

- At low conversion

- At high conversion

Figure 4.9. Hypothesized monomer distribution scheme in the copolymer for P(DAA-*co*-AEMA). (Schematic) Solid circle, DAA-*p*; empty triangle, AEMA.

Polymer films

We aimed at developing a linear, water-soluble polymer containing two types of functional groups, i.e., catechols and amines. By triggering the catechol crosslinking chemistry, this polymer should be able to change from water-soluble to water-insoluble. To verify the hypothesis, two polymer films were prepared on a pre-cleaned glass substrate, one at low pH (~ 2) and one at high pH (~ 11.5). The crosslinking of the polymer can be enhanced by adding the oxidizing agent sodium periodate ($NaIO_4$). To study the effect of the degree of crosslinking on the solubility behavior, two extra polymer films were prepared by adding different amounts of $NaIO_4$, i.e. 1 mol% and 10 mol% of catechol, respectively. The thickness of the four polymer films were measured by optical microscopy, and shown in Table 4.1. A representative sample is shown in Fig. 4.10.

Table 4.1. Thickness of polymer films as determined by optical microscopy. The standard deviation of the thickness of each sample is based on three measurements at different locations in the same film.

Sample	Thickness (μm)
P(DAA-*co*-AEMA) low pH	9.1 ± 0.4
P(DAA-*co*-AEMA), high pH	11.9 ± 0.7
P(DAA-*co*-AEMA), high pH, 1/100 $NaIO_4$	11.1 ± 0.2
P(DAA-*co*-AEMA), high pH, 1/100 $NaIO_4$	12.6 ± 0.5

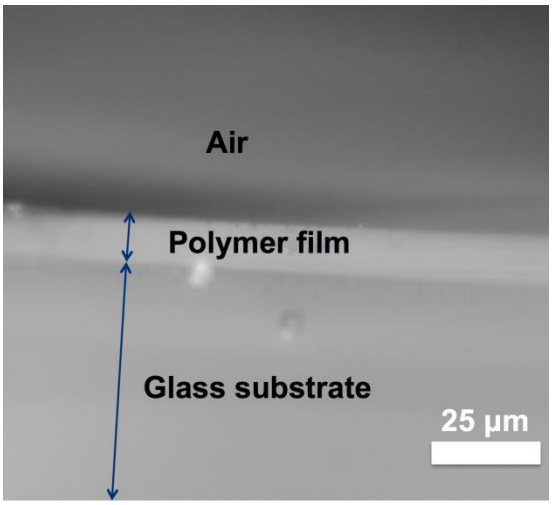

Figure 4.10. Optical microscopy image of polymer film P(DAA-*co*-AEMA) prepared at high pH) on a pre-treated glass substrate. The thickness of the polymer layer was measured with optical microscopy (× 40 magnification).

The wettability and swelling behavior of the four polymer films were studied by contact angle measurements, as shown in Fig. 4.11 and Table 4.2. Upon depositing one water droplet, the uncrosslinked film, prepared at low pH, started to absorb water, and swelled in a few seconds as shown in Fig 4.11 (a). After some time, the water droplet was fully absorbed and the polymer film assumed an irregular shape. The quick swelling behavior clearly indicates that the polymer is still soluble in water. This behavior is corroborated by UV-vis measurements. As shown in Fig. 4.12, P(DAA-*co*-AEMA) prepared at low pH exhibited a distinct peak at 280 nm, which is ascribed to unreacted catechol groups. A very broad and tiny peak at around 350 nm also appeared, which might be due to slow oxidation during the evaporation of water during film formation.

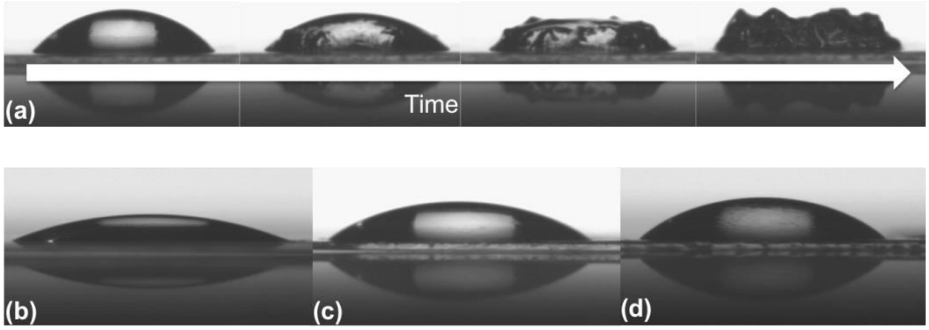

Figure 4.11. Static water contact angles of the four polymer films: a) uncrosslinked polymer film, P(DAA-*co*-AEMA) prepared at low pH (~ 2), b) slightly crosslinked polymer film, P(DAA-*co*-AEMA) prepared at high pH (~ 11.5), c) moderately crosslinked polymer film, P(DAA-*co*-AEMA), pH 11.5, $NaIO_4$/ catechol=1/100 (mol/mol), d) highly crosslinked polymer film, P(DAA-*co*-AEMA), pH=11.5, $NaIO_4$/ catechol=1/10

Table 4.2. Static water contact angle of four polymer films

Sample	Contact angle (°)
P(DAA-*co*-AEMA) low pH	-
P(DAA-*co*-AEMA), high pH	30 ± 2.4
P(DAA-*co*-AEMA), high pH, 1/100 $NaIO_4$	41 ± 0.2
P(DAA-*co*-AEMA), high pH, 1/100 $NaIO_4$	46 ± 0.2

Increasing the pH before film casting, i.e., P(DAA-*co*-AEMA) prepared at pH 11.5, resulted in a polymer film that did not swell upon loading the film

with a water droplet, as shown in Fig. 4.11(b). The polymer film was stable in the presence of water during the measurement, and exhibited a stable contact angle of around 30°. The different behavior between the low and high pH treatment can be interpreted as follows. Firstly, at high pH 11.5, when the pH is higher than the pKa of the amino group in AEMA (~ 9.6)[26], AEMA is deprotonated, and free amines are formed. The *o*-quinones formed by oxidation from the catechols, can then react with the free amines by either a Schiff-base reaction or a Michael-type addition, or with catechols by dismutation reactions.[10] We have shown in a separate study that the reaction between *o*-quinones and amine is predominant over the dismutation reaction with catechols. In the present study, we used UV-vis and FTIR measurements to corroborate this finding. As shown in Fig. 4.12, the peak at λ = 280 nm shifted to a slightly higher wavelength, λ = 288 nm. Meanwhile, a strong peak at λ = 340 nm appeared. The peak at λ = 340 nm has been ascribed to the formation of the reaction intermediate of catechol crosslinking.[27] Furthermore, in the FTIR spectrum of the polymer as shown in Fig. 4.13, the polymer prepared at low pH showed peaks at 1163 cm^{-1} ascribed to C-N stretch for aliphatic amines, and a broad peak above 3000 cm^{-1} for phenolic O-H stretch. These two peaks both decreased significantly for the other three crosslinked samples, indicating that the OH (on the aromatic ring of catechols) and amines had reacted. Secondly, in our catecholamine polymer, at low pH, the amines are protonated and charged, which favors the solubility in water. By increasing the pH, the deprotonation of the amines leads to a loss of charge, which reduces the solubility. These two reasons explain the formation of a crosslinked, water-insoluble network. Similar effects of catechol crosslinking-chemistry on the polymer solubility have also been observed in catechol-modified chitosan.

The uncrosslinked polymer was soluble in water. By exposing the polymer to $NaIO_4$ solution, the crosslinking chemistry between catechol and the amines in chitosan was triggered, resulting in a water-insoluble polymer.[28]

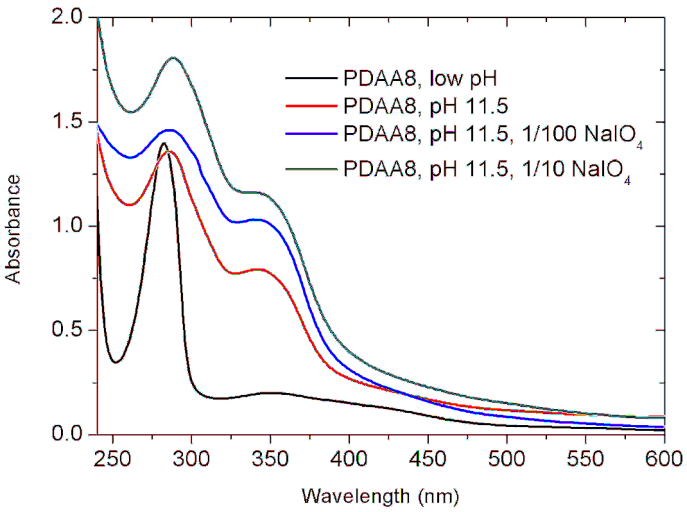

Figure 4.12. UV-vis spectra of polymer films deposited on quartz slides with different degree of crosslinking.

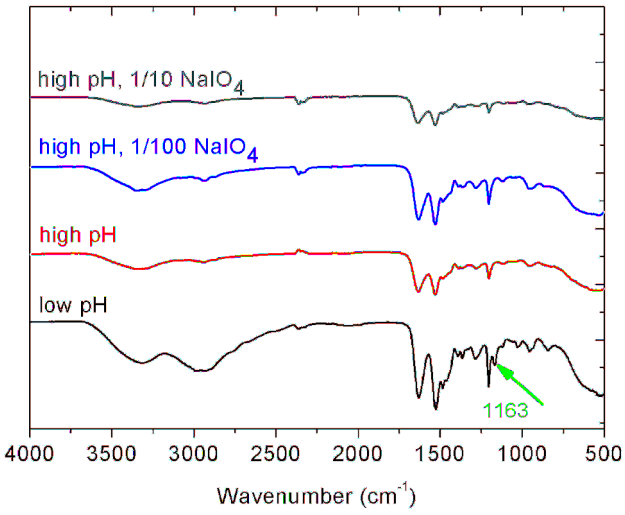

Figure 4.13. FTIR spectra of four polymers prepared at different conditions: a) at low pH (black line); b) high pH (read line); c) high pH, 1/100 $NaIO_4$ (blue line); d) high pH, 1/10 $NaIO_4$ (dark cyan line). The green arrow indicates the small peak at 1163 cm^{-1}.

The crosslinking rate of the catecholamine polymer film can be enhanced by the addition of $NaIO_4$. As shown in Fig. 4.11(c), upon adding a small amount of $NaIO_4$ ($NaIO_4$/ catechol = 1/ 100), the polymer film showed a higher static water contact angle of 41°. This increase indicated a more crosslinked polymer film. The higher degree of crosslinking is also reflected in the UV-vis spectra: the peak is shifted to the right, i.e., λ = 290 nm, and the intensity of the peak at λ = 340 nm is increased. A further addition of more $NaIO_4$ ($NaIO_4$/ catechol = 1/10) yielded a polymer film with even higher intensity of absorbance at λ = 340 nm (Fig. 4.12), and a higher static contact angle of 46° (Fig. 4.11(d)).

The effect of crosslinking on the morphology of the polymer film was studied by AFM measurements, as shown in Fig. 4.13. As shown in Fig. 4.14(a), the uncrosslinked polymer film showed a very smooth surface with negligible roughness. For the crosslinked films, however, as shown in Fig. 4.14 (b), (c) and (d), the roughness of the films increased. The roughnesses for the various crosslinked films did not differ much, indicating that a more crosslinked film does not necessarily lead to a rougher surface. It is known that the roughness of the surface has an amplifying effect on the contact angle. According to the Wenzel equation, for an intrinsic water/ air contact angle (referring to a perfectly flat surface) smaller than 90°, roughness decreases the apparent contact angle, so that the surface seems to be more hydrophilic.[29] In our case, we observed that the contact angles for crosslinked films are lower than 90°. By taking into account the amplifying effect of roughness, we can conclude that the intrinsic contact angle for the crosslinked films is most likely higher than the data we currently obtained. The effect of crosslinking on the intrinsic contact angle should still follow the same trend as the one we observed.

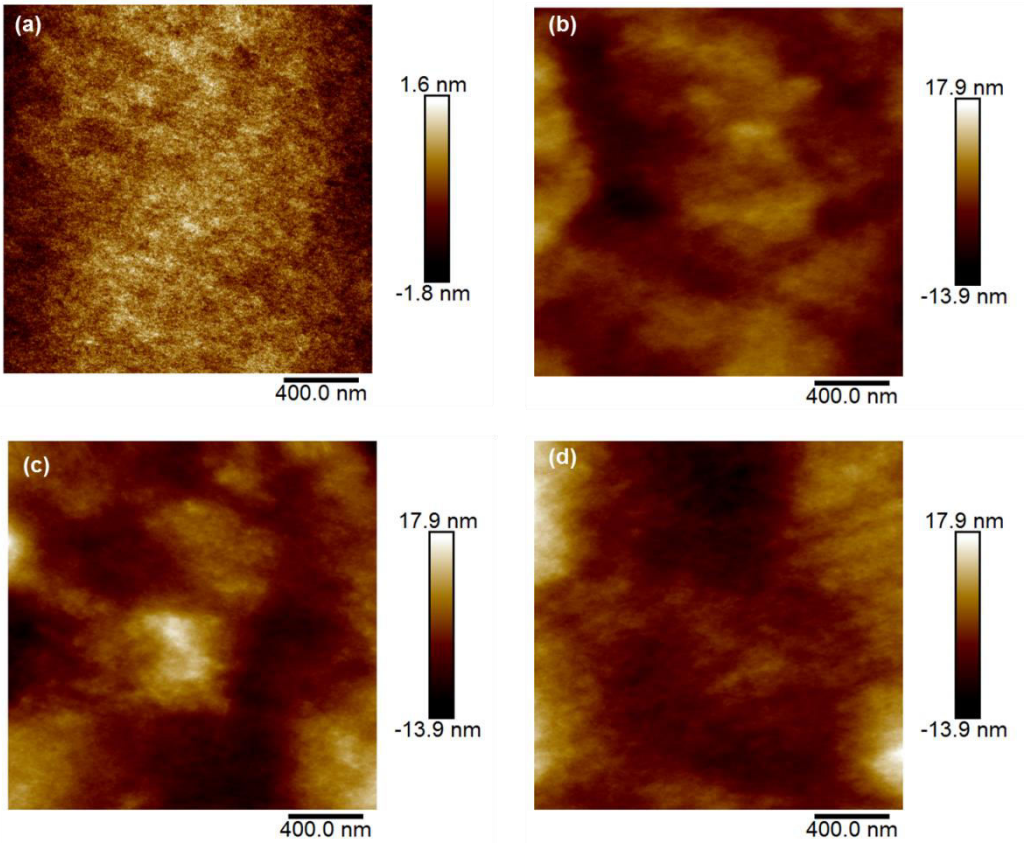

Figure 4.14. AFM images of P(DAA-*co*-AEMA) films, a) uncrosslinked film, P(DAA-*co*-AEMA) at low pH; b) slightly crosslinked film, P(DAA-*co*-AEMA), at pH 11.5; c) moderately crosslinked film, P(DAA-*co*-AEMA), pH 11.5, $NaIO_4$/ catechol=1/100; d) strongly crosslinked film, P(DAA-*co*-AEMA), pH 11.5, $NaIO_4$/ catechol=1/10.

Conclusions

In conclusion, we developed a one-pot coating system using the pH-responsive catecholamine polymer P(DAA-*co*-AEMA). We synthesized the copolymer by free radical polymerization of two monomers, DAA-*p* and AEMA, in aqueous conditions. The polymer works similarly as mussel proteins, i.e., being water-soluble at low pH (pH 2), and becoming water-

insoluble at high pH (pH 11.5). The water-solubility switch was ascribed to the self-crosslinking ability of the polymer at high pH. Moreover, the crosslinking of the polymer is affected by the polymer sequence distribution. Using an in-situ ^{1}H NMR monitoring method, we studied the sequence distribution by looking at the reactivity ratios of the monomers DAA-*p* and AEMA. Both the reactivity ratios of the monomers are lower than unity, i.e., $r_{DAA\text{-}p}$ = 0, r_{AEMA} = 0.46, giving rise to a moderately alternating polymer structure.

References

(1) Waite, J. H. *Comparative Biochemistry and Physiology Part B: Comparative Biochemistry* **1990**, *97*, 19.

(2) Miserez, A.; Rubin, D.; Waite, J. H. *Journal of Biological Chemistry* **2010**, *285*, 38115.

(3) Miserez, A.; Schneberk, T.; Sun, C.; Zok, F. W.; Waite, J. H. *Science* **2008**, *319*, 1816.

(4) Bargel, H.; Koch, K.; Cerman, Z.; Neinhuis, C. *Funct. Plant Biol.* **2006**, *33*, 893.

(5) Holten-Andersen, N.; Harrington, M. J.; Birkedal, H.; Lee, B. P.; Messersmith, P. B.; Lee, K. Y. C.; Waite, J. H. *Proc. Natl. Acad. Sci. U. S. A.* **2011**, *108*, 2651.

(6) Vitellaro Zuccarello, L. *Tissue Cell* **1981**, *13*, 701.

(7) Dreisbach, J. H.; Merkel, J. R. *J. Bacteriol.* **1978**, *135*, 521.

(8) Zardi, G. I.; Nicastro, K. R.; McQuaid, C. D.; Erlandsson, J. *Mar. Biol.* **2008**, *153*, 853.

(9) Harger, J. R. E. *Veliger* **1970**, *12*, 401.

(10) Yang, J.; Cohen Stuart, M. A.; Kamperman, M. *Chem. Soc. Rev.* **2014**, *43*, 8271.

(11) Waite, J. H.; Tanzer, M. L. *Science* **1981**, *212*, 1038.

(12) Harrington, M. J.; Masic, A.; Holten-Andersen, N.; Waite, J. H.; Fratzl, P. *Science* **2010**, *328*, 216.

(13) Ji, J.; Fu, J. H.; Shen, J. C. *Adv. Mater.* **2006**, *18*, 1441.

(14) Wang, Y. D.; Joshi, P. P.; Hobbs, K. L.; Johnson, M. B.; Schmidtke, D. W. *Langmuir* **2006**, *22*, 9776.

(15) Boudou, T.; Crouzier, T.; Ren, K. F.; Blin, G.; Picart, C. *Adv. Mater.* **2009**, *22*, 441.

(16) Faure, E.; Falentin-Daudré, C.; Lanero, T. S.; Vreuls, C.; Zocchi, G.; Van De Weerdt, C.; Martial, J.; Jérôme, C.; Duwez, A.-S.; Detrembleur, C. *Advanced Functional Materials* **2012**, *22*, 5271.

(17) Faure, E.; Lecomte, P.; Lenoir, S.; Vreuls, C.; Van De Weerdt, C.; Archambeau, C.; Martial, J.; Jerome, C.; Duwez, A.-S.; Detrembleur, C. *Journal of Materials Chemistry* **2011**, *21*, 7901.

(18) Charlot, A.; Sciannamea, V.; Lenoir, S.; Faure, E.; Jerome, R.; Jerome, C.; Van De Weerdt, C.; Martial, J.; Archambeau, C.; Willet, N.; Duwez, A.-S.; Fustin, C.-A.; Detrembleur, C. *Journal of Materials Chemistry* **2009**, *19*, 4117.

(19) Wu, J.; Zhang, L.; Wang, Y.; Long, Y.; Gao, H.; Zhang, X.; Zhao, N.; Cai, Y.; Xu, J. *Langmuir* **2011**, *27*, 13684.

(20) Ham, H. O.; Liu, Z.; Lau, K. H. A.; Lee, H.; Messersmith, P. B. *Angewandte Chemie International Edition* **2011**, *50*, 732.

(21) Aguilar, M. R.; Gallardo, A.; Fernández, M. d. M.; Román, J. S. *Macromolecules* **2002**, *35*, 2036.

(22) Yang, J.; Keijsers, J.; Heek, M.; Stuiver, A.; Cohen Stuart, M. A.; Kamperman, M. *Polym. Chem.* **2015**, *6*, 3121.

(23) Vickery, E. D.; Pahler, L. F.; Eisenbraun, E. J. *J. Org. Chem.* **1979**, *44*, 4444.

(24) Rafiee, M.; Nematollahi, D. *Electrochimi. Acta* **2008**, *53*, 2751.

(25) Odian, G. *Principles of Polymerization*; 4th ed.; Wiley-Interscience, 2004.

(26) Deng, Z. C.; Bouchekif, H.; Babooram, K.; Housni, A.; Choytun, N.; Narain, R. *J. Polym. Sci. A Polym. Chem.* **2008**, *46*, 4984.

(27) Lee, B. P.; Dalsin, J. L.; Messersmith, P. B. *Biomacromolecules* **2002**, *3*, 1038.

(28) Ryu, J. H.; Jo, S.; Koh, M.-Y.; Lee, H. *Advanced Functional Materials* **2014**, *24*, 7709.

(29) Quere, D. *Phys. A* **2002**, *313*, 32.

Chapter 5

Effect of molecular composition and crosslinking on adhesion of a bio-inspired adhesive

Abstract

In this chapter, catechol-functionalized polymers are synthesized by free radical polymerization of dopamine methacrylamide (DMA) and 2-methoxyethyl methacrylate (MEA) at 60 °C in DMF. By varying the DMA content in the polymer, it is found that during free radical polymerization, the catechol groups in DMA react with the propagating radicals, resulting in the formation of a crosslinked structure. We systematically study the effect of DMA content and crosslinking on the adhesion properties of the polymers. Under both dry and wet conditions, maximum adhesion is obtained for a polymer composed of 5 mol% DMA. This polymer exhibits an optimum balance between catechol content to strengthen the interface, compliance to ensure good contact formation and cohesive strength to resist separation. An increase in the crosslinking degree of the polymer resulted in reduced dry adhesion.

This chapter is based on publication:
Juan Yang, Jaap Keijsers, Maarten van Heek, Anthonie Stuiver, Martien A.Cohen Stuart, Marleen Kamperman, *Polymer Chemistry*, 2015, 6 (16), 3121-3130.

Introduction

The excellent underwater adhesion properties of marine organisms such as marine mussels[1, 2] and sabellariid polychaetes[3, 4] have attracted significant attention since decades. These marine organisms can achieve long-lasting and robust adhesion to various wet surfaces under harsh marine environments.[1, 5] It has been established that in holdfast proteins of several organisms, a significant amount of the catecholic amino acid L-3,4-dihydroxyphenylalanine (DOPA) is present, which contributes to the adhesion properties by forming strong covalent or non-covalent interactions with surfaces.[6-8]

The possible types and strengths of interactions between catechol and solid substrates have been extensively studied in the past few years. Liu et al. has summarized a full account of the different adhesion mechanisms.[9] Here only a few examples are listed. Frye reported that the catechol can react with organic silica to form organosilicon salts in which the silicon atom is in a penta-coordination form.[10] Lin and coworkers reported that DOPA in *Mytilus edulis* foot proteins-3 (mfp-3) interacts with mica by hydrogen bonding between the OH groups of catechol and the oxygen atoms in mica.[11] Several research groups studied the adsorption of catechol-conjugated polymers onto TiO_2 surfaces and different coordination bond configurations were proposed.[3, 5, 6, 12] The versatility of interactions between catechols and different surfaces provides the ability to strongly bind to substrates of widely varying composition.

Inspired by these versatile binding mechanisms of marine organisms, a lot of effort has been devoted to mimicking natural glues by using synthetic polymers incorporating catechol functionality.[13] One of the

most common synthesis methods is to polymerize monomers bearing unprotected catechols by free radical polymerization. This method is facile because it is a one-step synthesis and the reaction conditions are not as stringent as with other polymerization techniques such as anionic polymerization.[14, 15] However, it is expected that this method is limited by the presence of the unprotected catechols, which are known to be radical scavengers.[16, 17] During polymerization, the catechol groups can interact with the propagating polymer radicals and may form a branched or cross-linked structure. Despite this expected limitation, many reports on the free radical polymerization of unprotected monomers exist in which the potential effect of catechols on the polymer structure is not mentioned.[18-23] The first synthesis of catechol-functionalized polymers from unprotected catechol-containing monomer has been described by Messersmith and co-workers.[24] N-methacrylated DOPA monomers were copolymerized with poly(ethylene glycol) diacrylate using either ultraviolet (UV) or visible light with a photoinitiator resulting in adhesive hydrogels. Three years later, they used thermally-initiated free radical polymerization to synthesize a random copolymer poly(dopamine methacrylamide-*co*-methoxyethyl acrylate) (p(DMA-*co*-MEA)) containing 11.3 mol% DMA.[18] The polymer was coated onto a poly(dimethyl siloxane) (PDMS) pillar array. It was found that wet adhesion of the patterned surface increased 15-fold when coated with p(DMA-*co*-MEA). The adhesion of the coated structure was reversible and the adhesive strength decreased only slightly after 1000 cycles under both dry and wet conditions. A similar adhesion enhancement for patterned surfaces due to a p(DMA-*co*-MEA)-

coating was observed by Washburn and coworkers.[19] Stewart and coworkers copolymerized dopamine methacrylamide with a phosphate based monomer: 2-(methacryloyloxy) ethyl phosphate. Combining the synthesized polymer with a second polymer bearing positive charges (e.g. protonated amine polymers) in the presence of divalent cations (Ca^{2+} or Mg^{2+}) resulted in the formation of a polyelectrolyte complex.[21-23] This complex coacervate showed high underwater bond strength and may find use as biomedical adhesive.

These studies show that catechols accomplish strong and versatile interfacial interactions with different substrates and that the adhesion properties of synthetic catechol-containing polymers are promising. Therefore, one would expect that to increase the interfacial interactions the catechol content should be maximized. However, the performance of a pressure sensitive adhesive (PSA) is not only a function of its interfacial properties; the bulk mechanical properties are equally important. PSAs must be compliant and viscous to stick by simple contact, yet at the same time, must be resistant to creep, to avoid slow failure under load.[25] Therefore, the adhesion properties of catechol-containing polymers depend on the crosslinking of the polymer. As reported before, by introducing oxidant such as periodates, catechols are oxidized, and further undergo complicated crosslinking chemistry, yielding a crosslinked polymer network.[26] The altered bulk mechanical properties of the crosslinked polymer result in a different adhesion performance, as was shown by Wilker, et al, for poly[(3,4-dihydrostyrene)-*co*-styrene] (catechol content 33 mol%) systems.[6]

In this article, we systematically study the effect of catechol content in the polymer on the bulk mechanical and wet and dry adhesion properties. The potential influence of a crosslinked structure on the adhesion properties is also taken into account. Mechanical properties are measured with dynamic mechanical analysis and rheometry and the adhesion properties are studied by indentation adhesion tests.

Experimental

Materials

Dopamine hydrochloride, methacrylic anhydride (94%), 2-methoxyethyl acrylate (98%), basic alumina, deuterochloroform (99.96%), tetrahydrofuran (98.5%), ethyl acetate (99%), dimethylformamide (99.8%), 2,2'-Azobis(2-methylpropionitrile) (98%), dichloromethane (98.5%), methanol (98.5%), 3,4-dimethoxyphenethyl amine (97%) and triethylamine (>99.5%) were purchased from Sigma-Aldrich. Sodium hydroxide solution (1 M) and anhydrous magnesium sulfate ($MgSO_4$, 97%) were purchased from Merck. Hydrochloride solution (1 M) was purchased from Fluka. Hexane (p.a.) and diethyl ether (p.a.) were purchased from Biosolve. Sodium tetraborate decahydrate (p.a.) and sodium bicarbonate were purchased from J.T.Baker.

Monomer synthesis

Synthesis of dopamine methacrylamide (DMA)

Dopamine methacrylamide (DMA) was synthesized by reaction of dopamine hydrochloride and methacrylic anhydride in a mixture of tetrahydrofuran (THF) and Milli-Q water, see Scheme 5.1.[19] 30 g of sodium borate tetrahydrate and 12 g of sodium bicarbonate were added to 300 ml Milli-Q water. The aqueous solution was bubbled

with N_2 for 20 min, followed by addition of 15 g of dopamine hydrochloride. Next, 14.1 ml of methacrylic anhydride in 75 ml of THF was added dropwise. The pH of the solution was maintained above 8 by adding drops of 1 M NaOH solution. The reaction mixture was stirred overnight (around 14 h) under continuous N_2 bubbling at room temperature. After the reaction, a slightly pinkish slurry was formed with a white solid present at the bottom of the flask. The reaction mixture was filtered by vacuum filtration and the residue, a clear slightly pinkish solution, was washed twice with 150 ml ethyl acetate. The obtained aqueous solution was acidified by 1 M HCl to a pH of around 2, followed by extraction with 150 ml ethyl acetate for three times. The brownish organic solution obtained from extraction was collected and dried over $MgSO_4$. Afterwards, the volume of the solution was reduced to around 80 ml by rotary evaporation and precipitated into 800 ml hexane. The formed suspension was stored at 4 °C overnight to aid crystallization. After 14 h, the resulting brownish solids were collected, dissolved in 100 ml ethyl acetate and precipitated in 1000 ml hexane. The final solid obtained by filtration of the suspension was dried in a vacuum oven overnight at room temperature and the yield was 54%. ^{1}H NMR (400 MHz, d-DMSO, δ (ppm)): 6.62-6.42 (m, 3H, Ph), 5.92 (d, 1H, CH_2=C-), 5.27 (d, 1H, CH_2=C-), 3.23-3.18 (q, 2H, Ph-CH_2-CH_2-NH-), 2.55-2.51 (t, 2H, Ph-CH_2-CH_2-), 1.82 (s, 3H, CH_2=C(O)-CH_3). ^{13}C NMR (400 MHz, d-DMSO): δ = 167.26, 145, 143.44, 140.05, 130.25, 119.14, 118.69, 115.93, 115.43, 40.89, 34.55, 18.59.

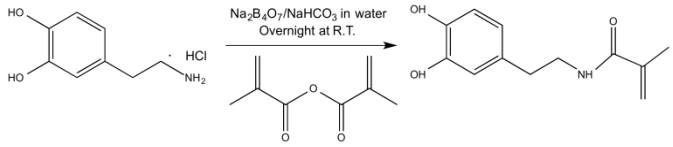

Scheme 5.1. Synthesis of DMA

Synthesis of N-(3,4-Dimethoxyphenethyl)acrylamide

N-(3,4-Dimethoxyphenethyl)acrylamide (NDMA) was synthesized by reaction of 3,4-dimethoxyphenethyl amine with acryloyl chloride in dichloromethane at room temperature, see Scheme 5.2. 7 ml of 3,4-dimethoxyphenethyl amine in 70 ml of anhydrous dichloromethane (CH_2Cl_2) was added to a 250 ml three neck round bottom flask. The solution was bubbled with nitrogen under continuous stirring for 30 min at 0 °C. Afterwards, 6.92 ml of triethylamine (TEA) was added to the reaction mixture, followed by dropwise addition of 4.01 ml acryloyl chloride in 40 ml anhydrous dichloromethane at 0 °C. The reaction mixture was stirred overnight under continuous N_2 bubbling at room temperature. After the reaction, the reaction mixture was washed with 40 ml of 0.1 M HCl solution, 0.1 M Na_2CO_3 solution and three times with brine solution. The obtained yellowish solution was dried over Mg_2SO_4 and CH_2Cl_2 was removed by rotary evaporation. The obtained sample was dried in a vacuum oven overnight at room temperature.

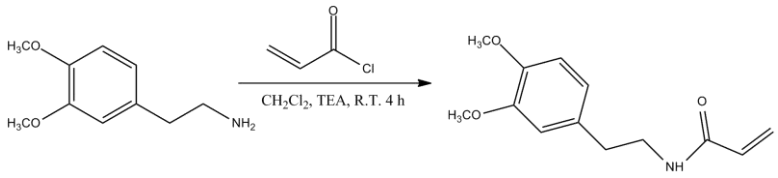

Scheme 5.2. Synthesis of N-(3,4-Dimethoxyphenethyl)acrylamide (NDMA)

Synthesis of poly(dopamine methacrylamide-co-2-methoxyethyl acrylate) p(DMA-*co*-MEA)

Five polymers with different compositions were obtained by varying the feed molar ratios of DMA and 2-methoxyethyl acrylate (MEA). The details of the polymers are described in Table 5.1. Polymers are denoted as P(DMA_x-*co*-MEA_y), where x and y are the molar percentages of DMA and MEA in the copolymer as obtained from ^{1}H NMR, respectively. Here, the synthesis of one typical copolymer is described in detail. Before polymerization, the inhibitor in MEA was removed by passing through a basic alumina column. 0.68 g DMA, 2.1 ml MEA and 42 mg of 2,2'-Azobis(2-methylpropionitrile) (AIBN) in 9.5 ml dimethylformamide (DMF) were added to a 50 ml three-neck round bottom flask, after which N_2 was bubbled through for 30 min. The reaction mixture was allowed to heat to 60 °C and was kept at this temperature for 3 h. The resulting viscous and slightly brownish mixture was diluted with 10 ml methanol, and added dropwise into 200 ml diethyl ether at 0 °C under continuous stirring. The resulting polymer was collected, dissolved in 15 ml dichloromethane and precipitated into 150 ml diethyl ether at 0 °C. After purification the polymer was dried in a vacuum oven overnight at room temperature. ^{1}H NMR (400 MHz, $CDCl_3$, δ (ppm)): 6.90-6.67 (m, 3H, Ph), 4.35 (b, 2H, -O-C*H*$_2$-CH_2-O-CH_3), 3.68 (b, 2H, -O-CH_2-C*H*$_2$-O-CH_3), 3.56 (b, 3H, -CH_2-CH_2-O-C*H*$_3$), 2.80-2.78 (br, 2H, -NH-CH_2-C*H*$_2$-Ph), 2.78-2.44 (br, 1H, -CH_2-C*H*(C=O)-CH_2-), 2.11-1.65 (br, 2H, -C*H*$_2$-C(CH_3)-C*H*$_2$-CH(C=O)CH-), 1.44-1.11 (br, 2H, -CH_2-C(C=O)-C*H*$_3$).

Synthesis of poly(N-(3,4-dimethoxyphenethyl)acrylamide) P(NDMA)

Homopolymer of N-(3,4-dimethoxyphenethyl)acrylamide was synthesized by free radical polymerization in dimethylformamide (DMF) at 60 °C using 2,2'-azobis(2-methylpropionitrile) (AIBN) as the initiator (Scheme 5.3). 3.6911 g NDMA, 34.8 mg of AIBN in 20 ml DMF were added to a 50 ml three-neck round bottom flask, after which N_2 was bubbled through for 30 min. The reaction mixture was allowed to heat to 60 °C and was kept at this temperature for 3 h. The resulting mixture was diluted with 5 ml CH_2Cl_2, and precipitated into 300 ml cold diethyl ether. The precipitated fractions were collected and redissolved into 50 ml CH_2Cl_2, followed by precipitation into 500 ml cold diethyl ether. The precipitates were collected and dried under vacuum at room temperature.

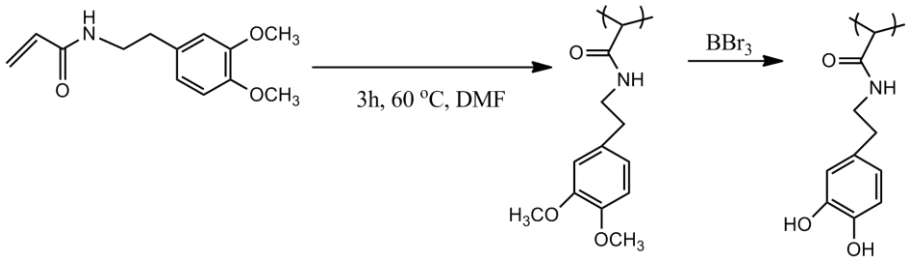

Scheme 5.3. Synthesis of *poly(N-(3,4-dihydroxyphenethyl)acrylamide)*

Synthesis of linear PDMA (l-PDMA)

1.3 g PNDMA in 110 ml CH_2Cl_2 was added to a 250 ml three-neck round bottom flask at -65 °C under continuous stirring and nitrogen bubbling

(Scheme 5.3). 18 ml 1M BBr_3 in DCM was added to the solution in a dropwise fashion. After that, the reaction mixture was slowly warmed to room temperature and stirred overnight. After the reaction, an orange slurry was formed. The slurry was added to 400 ml Milli-Q water at 4 °C under continuous stirring for 20 min. The reaction mixture was filtered and light yellow solids were obtained. The obtained solids were dried in a vacuum oven at room temperature.

Polymer characterization

All ^{1}H NMR and ^{13}C NMR measurements were carried out at 298 K on a Bruker AMX-400 spectrometer (400 MHz). Comparing the integrated area of the protons in the catechol and methoxy groups in DMA and MEA at chemical shift (δ) of 6.90-6.69 and 3.56, respectively, identified the DMA/MEA ratio in the final copolymer.

For the determination of the absolute molecular weight of the polymers and the weight-average number of branch points, a coupled size exclusion chromatography and multi-angle laser light scattering apparatus (SEC-MALLS) was used. Polymer samples (3 mg) were accurately weighed and dissolved overnight in 10 ml 0.02M potassiumtrifluoroacetate (KTFA) in 1,1,1,3,3,3-hexafluor-2-propanol (HFIP). Dissolved samples were filtered over a 0.45μm Teflon® filter prior to analysis. 0.02M potassiumtrifluoroacetate (KTFA) in 1,1,1,3,3,3-hexafluor-2-propanol (HFIP) was used as the mobile phase for SEC-MALLS. A 100μL sample was injected in a Viscotek system and separated over 2x PSS PFG analytical linear M GPC columns at 0.7 ml/min and 40 °C. The system was calibrated with a narrow

standard PolyCAL PMMA 65kD (M_w=64,368, M_n=61,304). Data collection, system handling and calculations were done with OmniSEC software V4.6. The identification of the weight-average number of branch points in the polymer is based on a log-log intrinsic viscosity vs. molecular weight plot. According to the Mark-Houwink equation, for a polymer solution, the relation between intrinsic viscosity $[\eta]$ and molecular weight M is: $[\eta] = KM^a$, in which K and a are Mark-Houwink parameters. Therefore, we get $\log[\eta] = \log K + a\log M$. By fitting the data of $\log[\eta]$ and $\log M$ to the equation, we obtained $\log K$ and a as the intercept and slope, respectively. For a branched polymer, the branching ratio g' is used to describe the degree of branching of the polymer, which is the ratio of the intrinsic viscosity of the branched polymer, $[\eta]_{branched}$, and the linear polymer, $[\eta]_{linear}$: $g = [\eta]_{branched}/[\eta]_{linear}$. The degree of branching can also be expressed using g', which is defined as: $g' = R^2_{g,branched}/R^2_{g,linear}$, where R_g is the radius of gyration of the branched or linear polymer. The relation between g and g' is given the by shape factor ε: $g' = g^{\varepsilon}$. For many polymers, ε is typically 0.7-0.8. In our study, we used 0.75. g is then applied to derive the weight-average number of branch points per molecule using the Zimm-Stockmayer equation. The copolymers studied here are random, tri-functional, and polydisperse polymers. For this class of polymers, the Zimm-Stockmayer equation becomes:

$$g = \frac{6}{B_n}\left[\frac{1}{2}\left(\frac{2+B_n}{B_n}\right)^{1/2}\ln\left(\frac{(2+B_n)^{1/2}+{B_n}^{1/2}}{(2+B_n)^{1/2}-{B_n}^{1/2}}-1\right)\right] \quad (1)$$

where B_n is the weight-average number of branch points per molecule.[27]

The thermal behavior of the polymers was measured on a Perkin Elmer Diamond Differential Scanning Calorimeter (DSC), using a temperature range from -60 to 160 °C with a heating and cooling rate of 10 °C/min. Glass transition temperatures of the polymers were determined during heating. T_g was determined using the half heat capacity (C_p) extrapolation method. [28]

Polymer film preparation

For adhesion testing, optical microscopy, and AFM measurements, polymer films were prepared using a casting method. Square glass substrates, 26 mm long × 26 mm wide, were used as substrate for the polymer films. Glass substrates were washed with ethanol and acetone three times, and dried with N_2 prior to use. To prepare the polymer film, 0.3 g polymer was dissolved in 1 ml DMF and 0.3 ml of the solution was added onto the cleaned glass substrate. The solution completely wet the glass surface, after which the polymer film was dried in a vacuum oven at 50 °C. For the crosslinking study, 0.3 g polymer and different amounts of oxidants $NaIO_4$ were added to 1 ml DMF. Then 0.3 ml of the solution was spread immediately onto a cleaned glass substrate, which was left to dry under well-ventilated conditions for 24 h. Subsequently, the substrate was dried in a vacuum oven.

Optical microscopy

Cross-sections of the polymer films on the glass substrates were imaged using an Olympus BX 60. Images were obtained using a 10× magnification.

Atomic force microscopy

The roughness of the polymer films was analyzed using a Nanoscope V in Scan Asyst imaging mode, using nonconductive silicon nitride probes (Veeco, NY, U.S.A.) with a spring constant of 0.35 N/m. Images were recorded between 0.2 and 0.99 Hz and further processed with Nanoscope Analysis 1.20 software (Veeco Instruments Inc. 2010, U.S.A.).

Adhesion test

In adhesion tests, a 9.525 mm diameter glass sphere was fixed on a glass slide using Norland optical 61 adhesive and attached to a fixed stage. A thin polymer film was coated on a second glass slide and mounted to the stem of a Futek load cell (model LSB 200, S/N 454653 mated with USB210, S/N 454846, capacity: 250 g). The coupled actuator (Thorlabs Z825B) was connected to a controller (Thorlabs TDC001) to control the motion of the polymer film (a picture of the setup is shown in Fig. 5.1). For all the measurements under both dry and wet conditions, the polymer film was indented at 0.01 mm/s until a predefined preload force was achieved. Subsequently, the polymer film and glass probe were allowed to be in contact for 300 s. The polymer film was then retracted at 0.01 mm/s and the adhesion force between the glass probe and polymer film was measured. Wet adhesion measurements were performed in aqueous hydrogen chloride solutions at pH 3. Before the measurement, the polymer film was immersed in the aqueous solution for at least one hour to completely swell the polymer films.

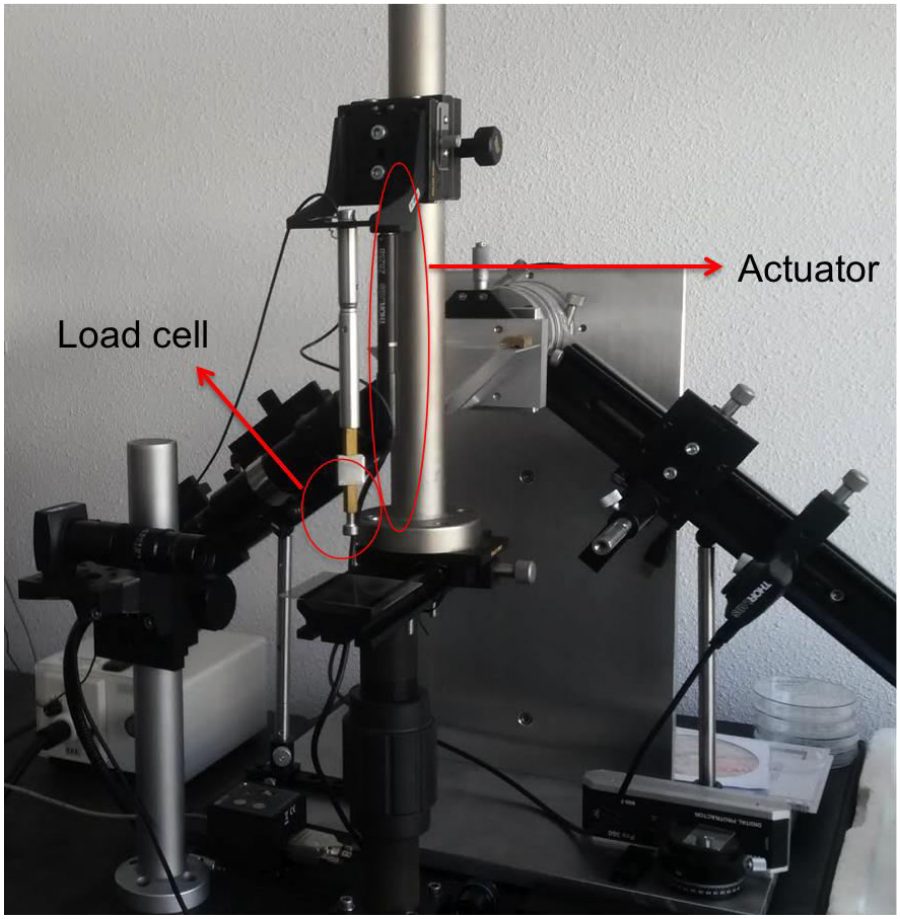

Figure 5.1. Picture of setup for indentation adhesion test

Dynamic mechanical analysis

Viscoelastic behavior of the polymers was studied with a TA instruments dynamic mechanical analyzer Q800. For polymer P($DMA_{0.25}$-co-$MEA_{0.75}$), a film tension clamp was used. The polymer was dissolved in chloroform, subsequently cast in a Teflon beaker and dried in a vacuum oven. The obtained polymer film was cut to rectangular specimens of 7.0 mm × 4 mm × 0.17 mm. For P($DMA_{0.05}$-co-$MEA_{0.95}$) and P($DMA_{0.10}$-co-$MEA_{0.90}$), a 8.65 mm diameter compression clamp was used. Polymer pieces were placed on the

clamp after which a few drops of chloroform were added, which enabled the polymer to form a homogeneous sample of the right dimensions (4 mm height × 8.65 diameter). The sample was left to dry overnight under ambient conditions before measurements were carried out. Frequency sweeps from 100 to 0.01 Hz were performed to measure the storage modulus (G') and loss modulus (G'') at 26-30 °C. Measurements were repeated after 8 hours and did not result in significant differences, indicating that most solvent had evaporated.

Rheometry

Rheological measurements were performed on the DHR3 Rheometer (TA instruments, US) equipped with a Peltier temperature control system. A plate of 8 mm diameter was used as top geometry while the Peltier serves as bottom geometry. We applied sinusoidal oscillations with a small constant deformation amplitude of 1% (which was tested to be in the linear regime) at an oscillation frequency of 1 Hz) and at a temperature specifically mentioned in the result part. To prepare the polymer samples, polymer PMEA was heated up to 90 °C in a vacuum oven and cooled down to room temperature. The resulting cylindrical sample with diameter of 8 mm was subsequently squeezed between the plates.

RESULTS AND DISCUSSION

1 Polymerization

We synthesized copolymers p(DMA-*co*-MEA) with different molar ratios of the two monomers DMA and MEA (Table 5.1) by free radical polymerization using DMF as solvent. DMF, which is polar, yet aprotic was chosen to reduce the ability of catechols to donate hydrogens to scavenge free radicals during polymerization. In a polar solvent such as DMF, catechols may interact with DMF by forming hydrogen bonds, thereby limiting, to some extent, the interaction between catechols with propagating radicals. It is important to avoid the use of protic polar solvents such as methanol, which can also form hydrogen bonds with surrounding methanol molecules. For these solvents, the hydrogen atom donating behavior of catechols to scavenge free radicals is not reduced.[16, 17]

The chemical compositions of the final polymers were identified by comparing the integrated area of the protons of the catechol and methoxy groups in DMA and MEA at chemical shifts (δ) 6.90-6.69 and 3.56, respectively (see Fig. 5.2). As shown in Table 5.1, the composition of DMA and MEA in the final polymer was somewhat different from the feed composition of the monomers, which may be due to the difference in monomer reactivity of DMA and MEA. The molecular weight M_n of the polymers became smaller when more DMA was added, which is possibly due to faster termination of the polymer chains by increased radical scavenging probabilities. The polydispersity index (PDI) of the polymers containing low amounts of DMA is around 2.0, which is typical for polymers synthesized using free radical polymerization. For P($DMA_{0.25}$-*co*-$MEA_{0.75}$), the PDI is

2.9, which is higher than those for polymers obtained from normal free radical polymerization. This higher PDI might be due to the still existing radical scavenging effect of catechols, which will be elucidated later.

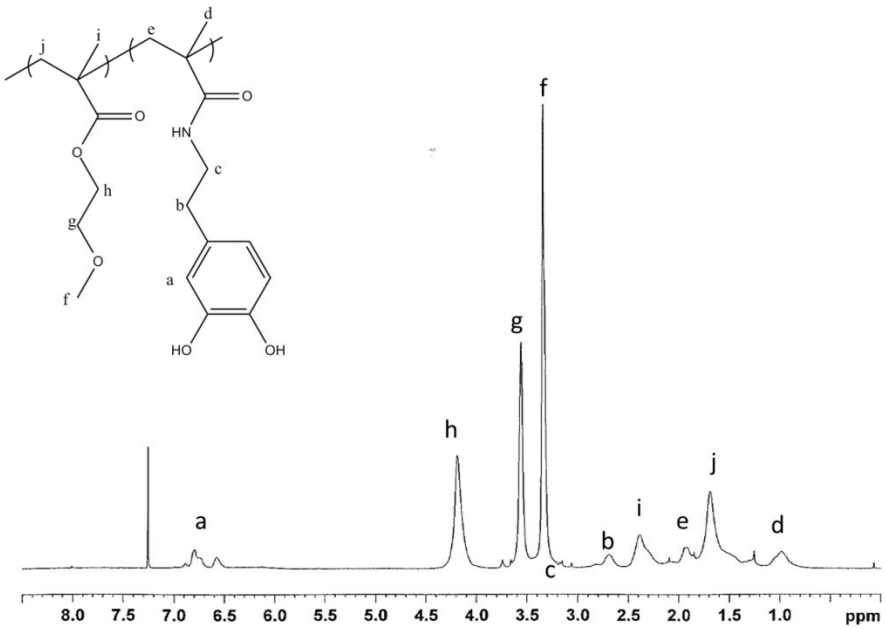

Figure 5.2. ^{1}H NMR spectra of poly($DMA_{0.10}$-*co*-$MEA_{0.90}$) in $CDCl_3$

During polymerization, the catechol groups in DMA were not protected. Although we tried to keep the scavenging ability to a minimum by using DMF, the propagating radicals in one polymer chain may still react with the catechol radicals in another polymer chain, so as to form a crosslinked structure.[29]

The possibility of crosslinking was tested using SEC-MALLS by determining the weight-average number of branch points per polymer chain in the final polymer (see Fig. 5.3). As shown in Table 5.1, with more incorporation of DMA, the number of branches in every polymer chain increased, although the number of branches in all the copolymers is small.

Moreover, it was observed that polymers with a higher DMA content were more difficult to dissolve in common organic solvents. Homopolymer PDMA was insoluble in most common organic solvents and only showed limited solubility in DMF. Due to the limited solubility, PDMA could not be measured using SEC-MALLS. Yet the poor solubility is a clear indication that a crosslinked architecture is formed in PDMA. The number and position of crosslinks that were obtained during the free radical polymerization process are poorly controlled. Despite this lack of control, crosslinking may affect the adhesion performance of the polymers.[19] This will be discussed below. Scheme 5.4 shows a proposed crosslinking mechanism during the radical polymerization.

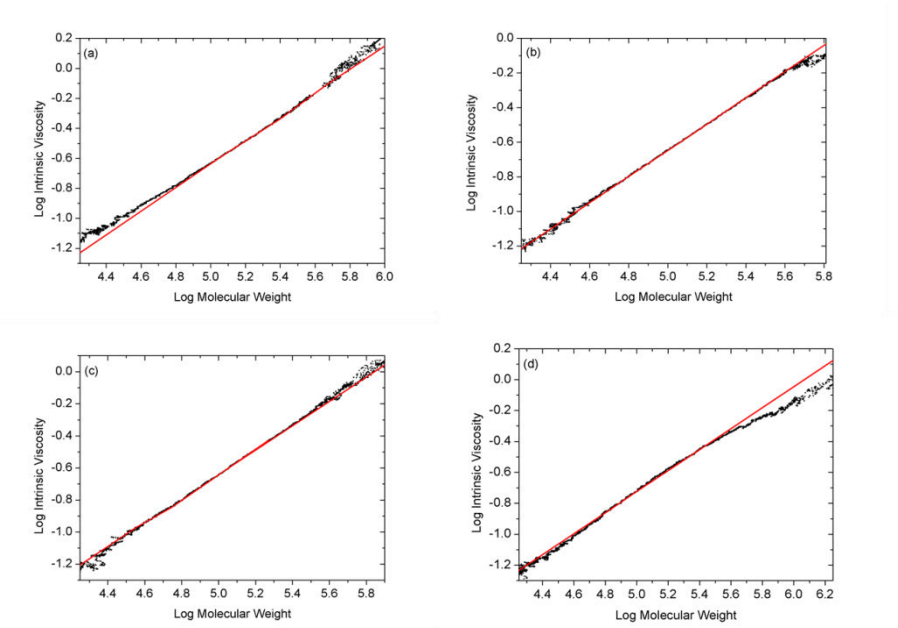

Figure 5.3. SEC-MALLS data of four polymers: intrinsic viscosity as a function of molecular weight on log-log scale. (a) PMEA; (b) poly($DMA_{0.05}$-*co*-$MEA_{0.95}$); (c) poly($DMA_{0.10}$-*co*-$MEA_{0.90}$); (d) poly($DMA_{0.25}$-*co*-$MEA_{0.75}$); (e) PDMA

Table 5.1. Specifications of the synthesized polymers

	Feed molar ratio		Polymer			
	DMA	MEA	M_n[a]	M_w[b]	PDI	B_n[d]
PMEA	0	1	54,946	95,440	1.7	0.041
P($DMA_{0.05}$-*co*-$MEA_{0.95}$)	1	19	64,397	121,867	1.9	0.12
P($DMA_{0.10}$-*co*-$MEA_{0.90}$)	1	5.7	61,634	124,589	2.0	0.18
P($DMA_{0.25}$-*co*-$MEA_{0.75}$)	1	2	37,331	106,784	2.9	0.31
PDMA	1	0	n.d.	n.d.	n.d.	n.d.

a: the number average molecular weight; b: the weight average molecular weight; c: polydispersity; d: weight-average number of branch points per molecule.

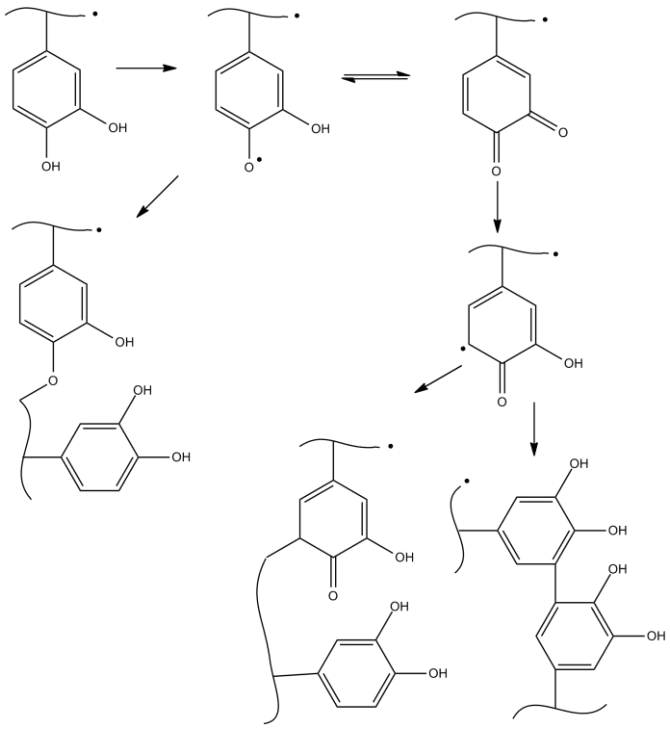

Scheme 5.4. Proposed crosslinking mechanism for the radical polymerization of vinyl monomers bearing unprotected catechols.[29]

More experiments need to be performed to verify this mechanism. However, it is challenging to perform mechanistic studies on these polymeric systems due to the small degree of crosslinking. A resulting architecture obtained from free radical polymerization of monomers MEA and DMA is proposed, as shown in Scheme 5.5.

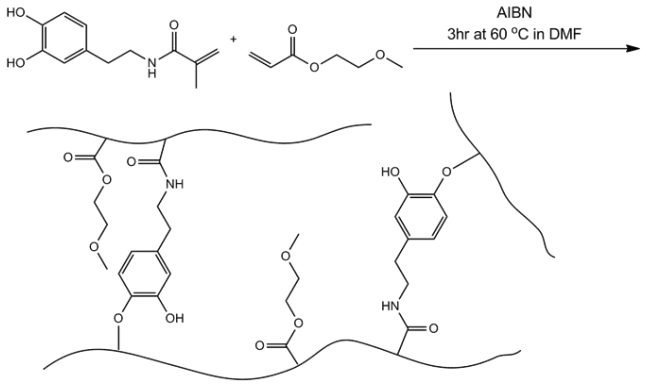

Scheme 5.5. Synthesis and a proposed resulting architecture of copolymer p(DMA-*co*-MEA)

To verify the crosslinked structure of PDMA, a second catechol-functionalized homopolymer was prepared by free radical polymerization of N-(3,4-dimethoxyphenethyl)acrylamide (NDMA) under the same polymerization conditions. In the new polymerization, methyl-protected catechols prohibit radical scavenging and linear polymer chains should be obtained.[13] The obtained polymer was demethylated using BBr_3 to free the catechol groups and linear PDMA (l-PDMA) was obtained. The synthesis and characterization details are given in Fig. 5.4.

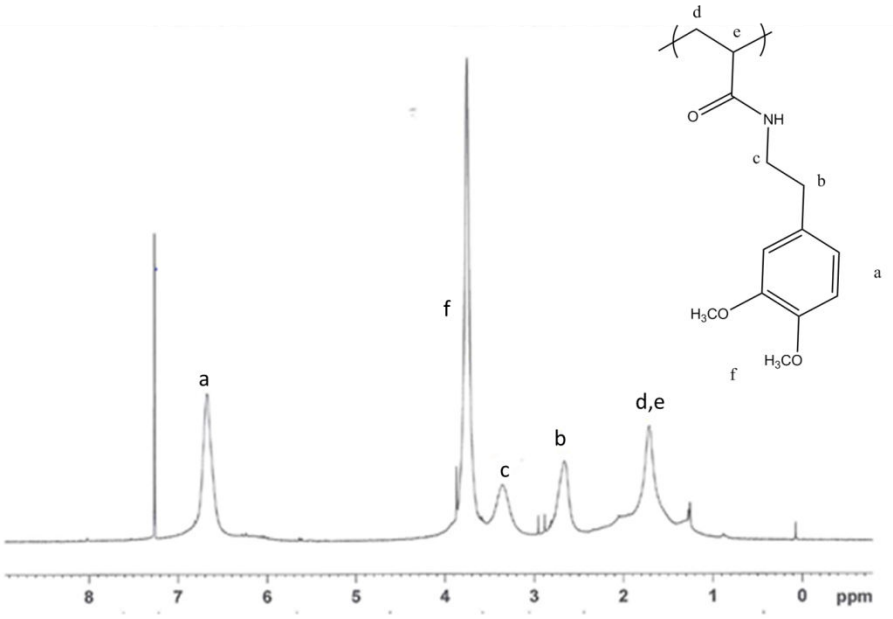

Figure 5.4. ^{1}H NMR spectra of poly(N-(3,4-dimethoxyphenethyl)acrylamide) in $CDCl_3$

Full characterization and property profiles of (co)polymers synthesized using protected catechol monomers will be the subject of a subsequent paper. PDMA and l-PDMA were dissolved in 0.1 mM NaOH solutions at pH = 10 under inert conditions. At this pH the catechols in the polymers should be partially deprotonated and the polymers charged and soluble in water. The solubility test showed that PDMA was insoluble while l-PDMA was soluble (Fig. 5.5). We note that full deprotection of l-PDMA was not confirmed. However, partial deprotection would lower the solubility of l-PDMA in 0.1 mM NaOH, due to the hydrophobicity of the residual methoxy groups. Therefore, the strongly increased solubility of l-PDMA in 0.1 mM NaOH in comparison to PDMA verified the crosslinked structure of PDMA.

Figure 5.5. Pictures of l-PDMA (top left) and PDMA (top right) and enlarged picture of PDMA (bottom) in 0.1 mM NaOH solution kept under the protection of nitrogen

2 Mechanical properties of polymers

The mechanical properties of the polymers were measured by dynamic mechanical analysis (DMechA) and rheometry. DMechA is used as an abbreviation for dynamic mechanical analysis to differentiate it from dopamine methacrylamide. Due to the large variation in material properties different techniques and different measuring geometries were used. As shown in Table 5.2, PMEA was measured with rheometry using a compression geometry, while the copolymers of DMA and MEA were measured with DMechA using a compression clamp for P($DMA_{0.05}$-*co*-$MEA_{0.95}$) and P($DMA_{0.10}$-*co*-$MEA_{0.90}$), and a film tension clamp for P($DMA_{0.25}$-*co*-$MEA_{0.75}$). The choice of geometry for each measurement depended on the processability of the polymer and the required sample dimensions. For example, whereas PMEA flows at room temperature which precludes the use of a film tension clamp, P($DMA_{0.25}$-*co*-$MEA_{0.75}$) has a T_g at 33 °C, rendering the film tension clamp more appropriate than the compression clamp. For PDMA, the incorporation of only DMA without MEA resulted in very high T_g (> 160°C) for the polymer, which may be due to the presence of a benzene ring in DMA. The high T_g and the poor solubility of PDMA make this polymer so difficult to process that no proper dynamic mechanical analysis data could be obtained. Since the measurements were performed with different methods, geometries and temperatures, the storage and loss moduli obtained here should be regarded as an estimate of the polymer mechanical properties. Mechanical properties of the different polymer compositions at a frequency of 1 Hz are shown in Table 5.2.

Table 5.2. Mechanical properties of the polymer compositions

	Method used	Storage Modulus (kPa)	Loss Modulus (kPa)	T (°C)	Tan δ
PMEA	Rheometry	25	27	20	1.08
P($DMA_{0.05}$-*co*-$MEA_{0.95}$)	DMechA, compression	229	84	29	0.37
P($DMA_{0.10}$-*co*-$MEA_{0.90}$)	DMechA, compression	230	130	30	0.56
P($DMA_{0.25}$-*co*-$MEA_{0.75}$)	DMechA, film tension	$4.8x10^4$	$3.7x10^3$	26	0.08
PDMA	n.d.	n.d.	n.d.	n.d.	n.d.

The overall polymer composition strongly influences the mechanical properties. The value of the storage modulus for a given temperature increased from tens to ten thousands of kPa by increasing the ratio of DMA to MEA from 0/100 to 25/75. Polymers with a glass transition temperature below room temperature (e.g. PMEA with T_g -36 °C) exhibit both a low storage modulus and a high damping factor (tan δ). In comparison, polymers with more DMA have a higher T_g (e.g. P($DMA_{0.25}$-*co*-$MEA_{0.75}$) with T_g 33 °C), exhibiting a higher storage modulus and a lower damping factor. Thus, PMEA shows significant viscoelastic behavior at room temperature, whereas P($DMA_{0.25}$-*co*-$MEA_{0.75}$) is stiff and elastic.

Small amounts of crosslinking can lead to drastic changes in the rheological behavior of polymer melts.[30] Typically, as the number of entanglements increases upon increasing the degree of crosslinking, the resistance to creep increases. However, for the set of polymers

described here, not only crosslinking, but also the T_g and molecular weight vary significantly between polymers. Therefore, creep studies on a larger set of polymers would be needed to study the effect of crosslinking on the frequency dependence of the mechanical properties of P(DMA-*co*-MEA) copolymers.

3 Adhesion properties

To study the adhesion properties of the polymers under dry and wet conditions, a polymer film on a cleaned glass substrate for each polymer was prepared. The thickness for the five polymer films was similar to avoid substrate-induced artifacts on the indentation measurement results. The film thickness of the five samples was measured and listed in Table 5.3; a representative sample is shown in Fig. 5.6.

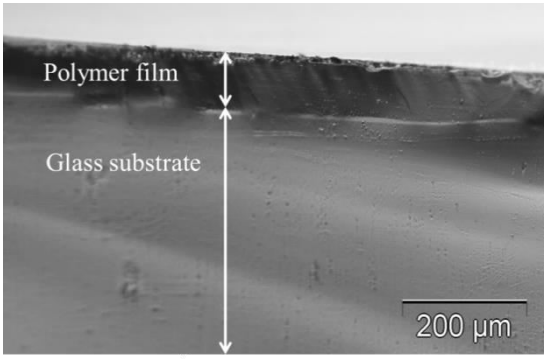

Figure 5.6. Optical microscopy image of (co)polymer on a pre-treated glass substrate. The thickness of the polymer layer was measured with optical microscopy (× 10 magnification).

Table 5.3. Thickness of polymer films as determined by optical microscopy. The standard deviation of the thickness of each sample is based on three measurements at different locations in the same film.

Polymer	Thickness (μm)
PMEA	121.3±1.7
P($DMA_{0.05}$-*co*$MEA_{0.95}$)	101.1±1.8
P($DMA_{0.10}$-*co*-$MEA_{0.90}$)	115.6±2.5
P($DMA_{0.25}$-*co*-$MEA_{0.75}$)	79.1±3.9
PDMA	128.4±1.4

The topography of the polymer films was imaged with AFM (Fig. 5.7). The mean square roughness of the polymer films R_q was around 1 nm, which means that relatively homogeneous films were formed on the substrate.

The adhesion of the polymers under dry and wet conditions was measured by indentation adhesion tests. Fig. 5.8 shows a typical force-time curve of P($DMA_{0.05}$-*co*-$MEA_{0.95}$) for dry adhesion. The pull-off force is obtained from the force-time curves and is defined as the maximum force required for debonding. The adhesion force as a function of preload force for dry adhesion is shown in Fig. 5.9.

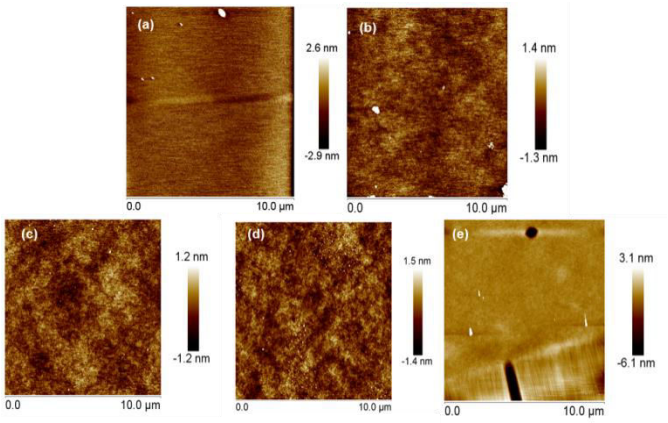

Figure 5.7. AFM topography images of a polymer film on a glass substrate. a) PMEA. Roughness average= 0.36 nm. b) P($DMA_{0.05}$-*co*-

$MEA_{0.95}$). Roughness average= 1.3 nm. c) P($DMA_{0.10}$-*co*-$MEA_{0.90}$). Roughness average= 0.37 nm. d) P($DMA_{0.25}$-*co*-$MEA_{0.75}$). Roughness average= 0.4 nm. e) PDMA. Roughness average= 0.96 nm.

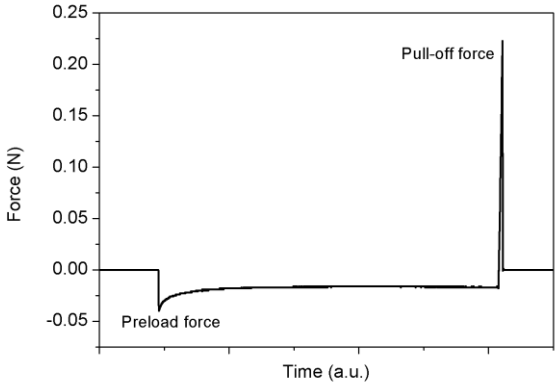

Figure 5.8. Typical curve of force as a function of time obtained from adhesion test. Positive loads are tensile and negative loads compressive.

Dry adhesion

In Fig. 5.9, we compare dry adhesion strength for the various catechol-functionalized polymers. PMEA shows moderate dry adhesion in the investigated preload range from 0 to 35 mN. During the retraction step, a bundle of fibrils were observed between the probe and the polymer film and polymer residue was left on the probe, suggesting that in this case debonding occurred as cohesive failure. By incorporating 5 mol% of DMA into the polymer, P($DMA_{0.05}$-*co*-$MEA_{0.95}$ exhibited higher dry adhesion, with pull-off forces in the range of 0.06-0.2 N. By incorporating 10 mol% of DMA into the polymer, P($DMA_{0.10}$-*co*-$MEA_{0.90}$) exhibited decreased adhesion, with pull-off forces in the range of 0.015-0.05 N. A further increase in the

DMA content, represented by P($DMA_{0.25}$-*co*-$MEA_{0.75}$) and PDMA, resulted in negligible adhesion. Therefore, in our set P($DMA_{0.05}$-*co*-$MEA_{0.95}$) is the optimal composition under dry conditions. DMA-containing polymers all show adhesive failure, without fibril-formation during the retracting step and without optically detectable residue left on the probe.

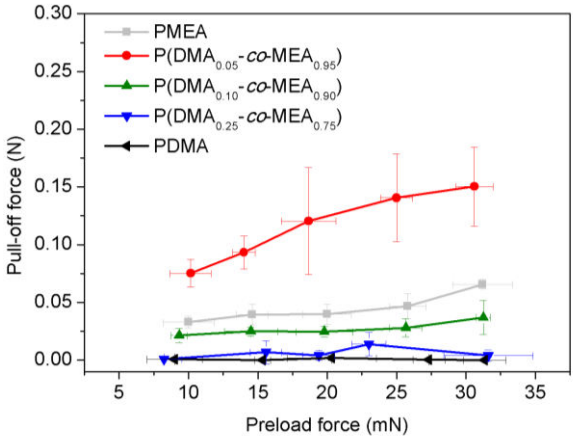

Figure 5.9. Pull-off forces under dry conditions as a function of preload force for (co)polymers with different DMA/MEA ratios. Probe speed was 0.01 mm/s for all measurements. Each data point resulted from an average of three to five measurements.

For most polymers, the adhesion force displayed a slight increase with increasing preload force. This trend is mainly due to the deeper indentation of the probe into the polymer film for higher preload force, resulting in a larger contact area and a higher strain. For a more viscoelastic material more energy will be dissipated leading to increased adhesion, thus the effect of preload is more pronounced for viscoelastic materials. However, in the current polymer system,

polymers that are more viscoelastic, PMEA in particular, have a lower storage modulus and fewer branches (see Table 5.1). Polymers with a lower storage modulus and fewer branches feature lower cohesive strengths, which may reduce the effect of preload on pull-off force. Therefore, no large differences in preload dependence are obtained between the different polymers. The adhesion strength was obtained by dividing the adhesion force by the calculated contact area. The contact area A is obtained by calculating by $A = 2\pi R\delta$, where R is the radius of the glass probe, and δ is the indentation depth. The contact area is different for each preload force and each polymer (at the same preload force). Fig. 5.10 presents the adhesion strength of the polymers at the same preload force of 13 mN and the calculated contact areas. It can be seen that the trend is the same as obtained in Fig. 5.9. P($DMA_{0.05}$-*co*-$MEA_{0.95}$) exhibits the highest dry adhesion strength, and a further increase in DMA content in the polymer results in a significant decrease in adhesion.

The bulk mechanical properties determine the adhesive performance to a large extent. Typically, at a deformation rate of 1 Hz, the storage modulus for a pressure sensitive adhesive (PSA) lies within the range 10 – 300 kPa. In this range polymers are compliant enough to form good contact within the contact time and the debonding process is then determined by the coupling of bulk and interfacial properties of the material.[31] PMEA, P($DMA_{0.05}$-*co*-$MEA_{0.95}$) and P($DMA_{0.10}$-*co*-$MEA_{0.90}$) fall in this range, while P($DMA_{0.25}$-*co*-$MEA_{0.75}$) has a storage modulus of 4.8 x 10^4 kPa. PDMA is very brittle, and most likely exhibits a storage modulus that is even higher than P($DMA_{0.25}$-*co*-$MEA_{0.75}$). Therefore, P($DMA_{0.25}$-*co*-$MEA_{0.75}$) and PDMA are too

stiff to be tacky. They will not be able to form a good contact with the probe and, thus, the interface can only support very limited deformation of the bulk. Tan δ/storage modulus is a measure for the strain the material can withstand before detachment will occur, this is indeed very low for P($DMA_{0.25}$-*co*-$MEA_{0.75}$).[32]

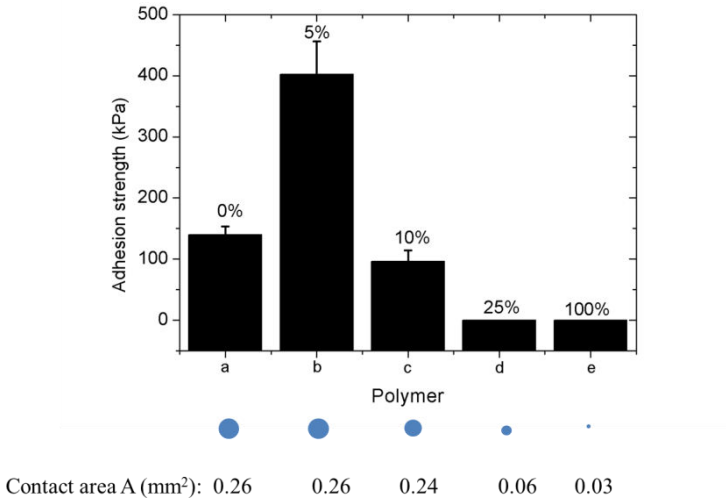

Figure 5.10. Adhesion strength of polymers at a preload force of 13 mN. The polymers are: a) PMEA, b) P($DMA_{0.05}$-*co*-$MEA_{0.95}$), c) P($DMA_{0.10}$-*co*-$MEA_{0.90}$), d) P($DMA_{0.25}$-*co*-$MEA_{0.75}$) and e) PDMA. The number on top of each bar is the molar percentage of DMA in the respective polymer. The standard errors were calculated based on three measurements for each sample.

In our study, the adhesion strength of P($DMA_{0.05}$-*co*-$MEA_{0.95}$) was 169% higher than that of PMEA. This increase can be explained by the property profile of the two polymers. First, although the storage modulus is low, PMEA is not cross-linked, leading to a low cohesive strength. This is also reflected in the fact that during the de-bonding process fibrils were formed between the PMEA film and the glass

probe. Second, it has been reported that catechol can displace water molecules from wet silica and adheres strongly by hydrogen bonding.[33, 34] Third, the more hydrophobic monomer MEA as compared to DMA, will decrease the surface energy of the polymer. On a surface of high surface free energy such as the glass probe used in our measurement, a more hydrophilic polymer will exhibit a better wettability.[35] It is unclear why P($DMA_{0.10}$-*co*-$MEA_{0.90}$) shows much lower adhesion than P($DMA_{0.05}$-*co*-$MEA_{0.95}$) even though the DMechA experiments indicated very similar mechanical properties. It may be that during the DMechA experiment residual solvent was left in the sample, resulting in a measured storage modulus that is lower than the actual storage modulus of the polymer.

Effect of crosslinking on the dry adhesion

As becomes clear from the discussion above, it is difficult to draw conclusions about the influence of crosslinking in the polymers on the adhesion properties, because not only crosslinking, but also the T_g and *Mw* vary significantly between polymers. Therefore, one polymer, i.e. P($DMA_{0.05}$-*co*-$MEA_{0.95}$) that showed the best dry adhesion performance, was selected to study the influence of crosslinking.

To study the effect of crosslinking on dry adhesion, a certain amount of oxidant $NaIO_4$ was added to the polymer film to induce catechol oxidation and subsequent crosslinking. As shown in Fig. 5.11, addition of small amounts of oxidant, i.e. $NaIO_4$/Catechol = 1/100 and $NaIO_4$/Catechol = 1/10, resulted in slightly reduced adhesion. A further increase in amount of oxidant, i.e. $NaIO_4$/Catechol = 1/3, resulted in negligible adhesion. These observations indicate that for

P(DMA$_{0.05}$-*co*- MEA$_{0.95}$) the addition of oxidant will always reduce adhesion. The reduction in adhesion may be due to changes at the interface and changes of the bulk properties: First, part of the catechols is oxidized to quinones, and quinones can lower the adhesion significantly.[8] Second, the oxidants will add crosslinks to the polymer systems which will lead to an increase in stiffness. Therefore, the crosslinked polymers are less tacky, resulting in reduced adhesion. Similar observations have been reported by Washburn et al. [20], who studied the dry adhesion of copolymer poly(DMA-*co*-MEA) containing 12 mol% DMA by adding a divinyl cross-linking agent.

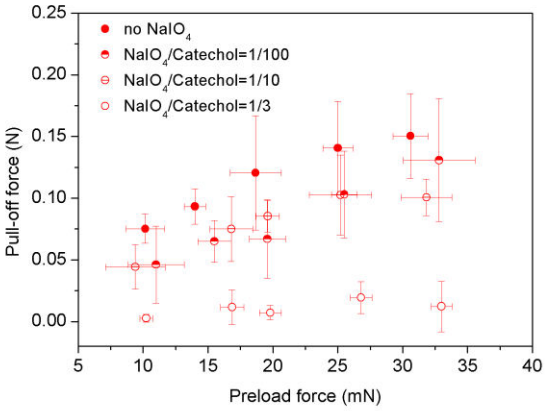

Figure 5.11. Dry adhesion of P(DMA$_{0.05}$-*co*-MEA$_{0.95}$) in the presence of an oxidant $NaIO_4$. Each data point resulted from an average of three to five measurements.

Wet adhesion

For the wet adhesion in aqueous conditions at pH 3, the polymer films were fully immersed in aqueous HCl at pH 3 for at least one hour to equilibrate the water uptake into the polymer. Measurements were performed at pH 3 due to the sensitivity of catechol to oxidation at

moderate to high pH. Oxidation of the catechols may influence the adhesion performance.[36]

As shown in Fig. 5.12, the adhesion force for PMEA, P($DMA_{0.05}$-*co*-$MEA_{0.95}$) and P($DMA_{0.10}$-*co*-$MEA_{0.90}$) under wet conditions is lower than for dry adhesion. It is interesting to note that P($DMA_{0.25}$-*co*-$MEA_{0.75}$) showed considerable wet adhesion, but almost no dry adhesion. PDMA showed negligible wet adhesion. The effect of DMA content on wet adhesion followed a similar trend as for dry adhesion: Incorporation of 5 mol% of DMA in the copolymer resulted in enhanced wet adhesion. A further increase in DMA content reduced the wet adhesion significantly. A different trend was observed by Butt and coworkers.[37] They investigated the single-molecular wet adhesion of poly(dopamine methacrylamide-*co*-butylamine methacrylamide), and observed an independence of catechol content on wet adhesion. However, single-molecule force measurements differ from macroscopic adhesion measurements and different properties are assessed.

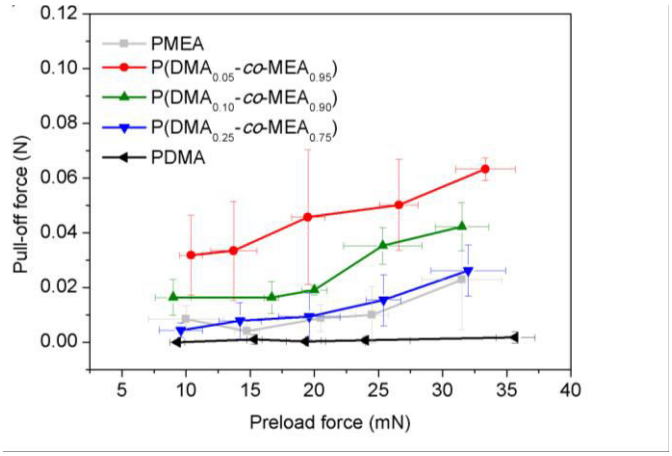

Figure 5.12. Pull-off forces under wet conditions as a function of preload force for (co)polymers with different DMA/MEA ratios. Probe speed was 0.01 mm/s for all measurements. Each data point resulted from an average of three to five measurements.

Compared to dry adhesion, the decreased adhesion under wet conditions may be due to weaker surface interactions. To investigate the difference in mechanical properties of the polymer films between dry and wet conditions, the compressive parts of the force-displacement curves, i.e. the linear part of the approaching step, were analyzed using the Hertz theory of elastic contact.[38] The Hertzian indentation model can be expressed as:

$$P = \frac{3}{4} E^* \sqrt{R\delta^3} \tag{2}$$

where P is the preload force, $E^* = E/(1-\upsilon^2)$ is the effective Young's modulus of the surface, υ is Possion's ratio, R is the radius of the indentation sphere, and δ is the indentation depth. Table 5.4 shows E^* for all polymers obtained from Hertz theory under both dry and wet conditions. Since some of the polymers display significant viscoelastic

effects, the model has limited applicability and the E^* values are only used to compare the differences in stiffness of polymers under dry and wet conditions.

Table 5.4. Changes in stiffness of the five polymers under wet and dry conditions

	Stiffness (N/mm^2)		
	Dry	Wet	Δ^a
PMEA	11	5.2	5.8
P($DMA_{0.05}$-*co*-$MEA_{0.95}$)	19.4	9.5	9.9
P($DMA_{0.10}$-*co*-$MEA_{0.90}$)	31.2	18	13.2
P($DMA_{0.25}$-*co*-$MEA_{0.75}$)	47	27	20
PDMA	48	38	10

Under dry conditions, an increase in stiffness was obtained with increasing DMA content in the polymer. Under wet conditions, all polymers showed a significantly lower stiffness than the stiffness under dry conditions. The decrease in stiffness (Δ) was more pronounced for polymers with a higher DMA content, except for PDMA. Whitening of the polymers was observed upon immersion indicating swelling with water. Water acts as a plasticizer, lowering the T_g and the stiffness of the polymer films. DMA is a more hydrophilic monomer than MEA. Therefore, when more DMA is incorporated, the polymer is swollen to a larger extent compared to polymers containing less DMA. In PDMA swelling may be limited due to the crosslinked nature of the polymer. For P($DMA_{0.10}$-*co*-$MEA_{0.90}$), and P($DMA_{0.25}$-*co*-$MEA_{0.75}$), the swollen films become

more compliant, which results in a better contact with the probe. Therefore, a relatively higher adhesion under wet conditions than under dry conditions is obtained as compared to the other compositions.

Conclusions

We synthesized poly(DMA-*co*-MEA) copolymers with different compositions and found an increase in the degree of crosslinking by increasing the catechol content in the polymer. The effect of catechol content on the adhesion properties was studied and an optimal composition for dry adhesion was achieved at a DMA concentration of 5 mol%. Polymers with a higher concentration of DMA showed little dry adhesion, which is attributed to the high stiffness of the material, resulting in poor contact with the probe. The adhesion properties of the polymer under dry conditions are a balance between catechol content to strengthen the interface, compliance to ensure good contact formation and a small degree of crosslinking to increase cohesion.

Under wet conditions, the copolymers showed a similar dependence on the DMA composition as compared to dry conditions. An optimal composition for the best wet adhesion was found at a DMA concentration of 5 mol%. Polymers with a higher DMA content are more hydrophilic and will take up more water. As water acts as a plasticizer and reduces the effective stiffness, polymers with a higher DMA content will show a larger decrease in stiffness, which improved their wet adhesion performance.

References:

1. J. H. Waite, *Biol. Rev.*, 1983, **58**, 209-231.
2. J. H. Waite, T. J. Housley and M. L. Tanzer, *Biochemistry*, 1985, **24**, 5010-5014.
3. H. Zhao, C. J. Sun, R. J. Stewart and J. H. Waite, *J. Biol. Chem.*, 2005, **280**, 42938-42944.
4. J. H. Waite, R. A. Jensen and D. E. Morse, *Biochemistry*, 1992, **31**, 5733-5738.
5. J. H. Waite, *Polym. Prepr.*, 1990, **30**, 181-182.
6. H. J. Meredith, C. L. Jenkins and J. J. Wilker, *Advanced functional materials*, 2014, **24**, 3259–3267.
7. H. Lee, N. F. Scherer and P. B. Messersmith, *Proceedings of the National Academy of Sciences of the United States of America*, 2006, **103**, 12999-13003.
8. J. Yu, W. Wei, E. Danner, J. N. Israelachvili and J. H. Waite, *Advanced materials*, 2011, **23**, 2362-2366.
9. Q. Ye, F. Zhou and W. M. Liu, *Chem. Soc. Rev.*, 2011, **40**, 4244-4258.
10. C. L. Frye, *J. Am. Chem. Soc.*, 1964, **86**, 3170-3171.
11. Q. Lin, D. Gourdon, C. J. Sun, N. Holten-Andersen, T. H. Andersen, J. H. Waite and J. N. Israelachvili, *Proceedings of the National Academy of Sciences of the United States of America*, 2007, **104**, 3782.
12. J. L. Dalsin, L. J. Lin, S. Tosatti, J. Voros, M. Textor and P. B. Messersmith, *Langmuir*, 2005, **21**, 640-646.
13. E. Faure, C. Falentin-Daudré, C. Jérôme, J. Lyskawa, D. Fournier, P. Woisel and C. Detrembleur, *Progress in Polymer Science*, 2013, **38**, 236-270.
14. C. R. Matos-Perez, J. D. White and J. J. Wilker, *Journal of the American Chemical Society*, 2012, **134**, 9498-9505.
15. M. Guvendiren, D. A. Brass, P. B. Messersmith and K. R. Shull, *The Journal of Adhesion*, 2009, **85**, 631-645.

16. N. Schweigert, A. J. B. Zehnder and R. I. L. Eggen, *Environmental Microbiology*, 2001, **3**, 81-91.

17. V. Thavasi, R. P. A. Bettens and L. P. Leong, *J Phys Chem A*, 2009, **113**, 3068-3077.

18. H. Lee, B. P. Lee and P. B. Messersmith, *Nature*, 2007, **448**, 338-341.

19. P. Glass, H. Chung, N. R. Washburn and M. Sitti, *Langmuir*, 2009, **25**, 6607-6612.

20. H. Chung, P. Glass, J. M. Pothen, M. Sitti and N. R. Washburn, *Biomacromolecules*, 2011, **12**, 342-347.

21. H. Shao and R. J. Stewart, *Advanced materials*, 2010, **22**, 729-733.

22. H. Shao, K. N. Bachus and R. J. Stewart, *Macromolecular Bioscience*, 2009, **9**, 464-471.

23. H. Shao, G. M. Weerasekare and R. J. Stewart, *J. Biomed. Mater. Res., Part A*, 2011, **97**, 46-51.

24. B. P. Lee, K. Huang, F. N. Nunalee, K. R. Shull and P. B. Messersmith, *J Biomat Sci-Polym E*, 2004, **15**, 449-464.

25. C. Creton, G. J. Hu, F. Deplace, L. Morgret and K. R. Shull, *Macromolecules*, 2009, **42**, 7605-7615.

26. J. Yang, M. A. Cohen Stuart and M. Kamperman, *Chem. Soc. Rev.*, 2014, **43**, 8271-8298.

27. J. Cazes, ed., *Encyclopedia of Chromatography*, Marcel Dekker Inc 2005.

28. G. Hohne, W. F. Hemminger and H. J. Flammersheim, *Differential Scanning Calorimetry*, Springer, 2003.

29. L. A. Burzio and J. H. Waite, *Biochemistry*, 2000, **39**, 11147-11153.

30. C. Gabriel, E. Kokko, B. Lofgren, J. Seppala and H. Miinstedt, *Polymer*, 2002, **43**, 6383.

31. A. V. Pocius, *Adhesion and adhesives technology: an introduction*, Carl Hanser Verlag, München, 2012.

32. C. Creton, F. J. Hu and F. Deplace, *Macromolecules*, 2009, **42**, 7605-7615.

33. S. A. Mian, X. F. Gao, S. Nagase and J. Jang, *Theor Chem Acc*, 2011, **130**, 333-339.

34. S. A. Mian, L. C. Saha, J. Jang, L. Wang, X. F. Gao and S. Nagase, *J. Phys. Chem. C*, 2010, **114**, 20793-20800.

35. H. Yamamoto, Y. Sakai and K. Ohkawa, *Biomacromolecules*, 2000, **1**, 543-551.

36. B. P. Lee, C. Y. Chao, F. N. Nunalee, E. Motan, K. R. Shull and P. B. Messersmith, *Macromolecules*, 2006, **39**, 1740.

37. J. Wang, M. N. Tahir, M. Kappl, W. Tremel, N. Metz, M. Barz, P. Theato and H.-J. Butt, *Advanced materials*, 2008, **20**, 3872-3876.

38. H. Hertz, *J. Reine Angew. Math.*, 1882, **92**, 156-171.

Chapter 6

General discussion

Abstract

In this chapter of "general discussion", we revisit the motivation of this PhD project, and build up connections among various subjects discussed in the previous chapters. We highlight some of the important findings in the context of whole thesis, and category them into three main aspects: i) importance of pH, ii) mechanistic understanding of catechol chemistry; and iii) design and synthesis of catechol-containing polymer. We also find new questions and challenges related to the catechol chemistry and catechol-containing polymers. We discuss these open questions here, and speculate on possible solutions to answer these questions.

Introduction

The central question we asked at the beginning of this thesis is: can we design a catechol-containing polymer that can be used as water-soluble binder for waterborne paints? The associated questions are focused on two points: i) is the polymer soluble in water at low pH during storage and application? ii) can the polymer switch to a water-repelling film at high pH during drying and curing? After three years and six months of work on this project, we conclude that we have successfully designed a polymer that can switch its aqueous solubility upon pH adjustment. The polymer switches from being water-soluble at low pH to insoluble at high pH owing to the crosslinking chemistry of catechols with amines. We have also gained more understanding on the reaction mechanisms of catechol-amine crosslinking, and the role of catechol on the adhesion properties. There are, however, remaining questions unanswered, and potentially interesting research paths unexplored. In this section, we will touch upon some remaining questions that can be interesting for a continuation of this research line. The discussion is divided into three aspects: i) section 6.1, importance of pH ii) 6.2 mechanistic understanding of catechol chemistry; iii) section 6.3, the design and synthesis of catechol-containing polymer.

6.1 Importance of pH

As stated before, the aim of this thesis is to design a pH-responsive catechol-containing polymer that can be used as binder for water-borne paints. The principle of the polymer design is mainly guided by the dependence of catechol chemistry on pH, and the pH route has changed significantly along with the investigations proceeded. Current dispersion-based waterborne paint systems follow a “pH down” route. To be more specific, the paint system is stable at high pH during storage; by exposing

the paint to air and applying it on a surface, the volatile base, e.g. ammonia, or alkanolamine[1], evaporates, and the pH drops. Simultaneously, the coagulation of the polymeric binder, and water evaporation take place. After a certain period, a water-resistant film is formed. Initially, we tried to also follow a "pH down" route. We hypothesized that at high pH, the catechols in the polymer would be deprotonated, and charged, making the polymer soluble. At low pH, when the pH drops below the pKa of two hydroxyls groups in the catechols, the catechols would be protonated, and become neutral. This loss of charge would reduce the hydrophilicity and solubility of the polymer, and hopefully lead to the formation of a hydrophobic film. However, we found that it is tricky to design such a system using catechol-containing polymers mainly due to two reasons. Firstly, catechols have a pKa value around 9. To keep catechols in the deprotonated form, the pH should be at least more than 10. At such high pH, catechols are very susceptible to oxidation and further crosslinking, making the storage of a stable paint system difficult. Secondly, during curing and drying, the pH drops. The rate of catechol oxidation and crosslinking would therefore decrease significantly with lower pH. Therefore, it is not favorable to have a low pH if we intend to make use of catechol crosslinking as the curing tool. In summary, the "pH down" route is working against the catechol chemistry, and therefore, this route is not feasible.

To make full use of the catechol chemistry, we switched to a "pH up" route, namely, the polymer is soluble at low pH when catechols are stable, and become insoluble at high pH when catechol crosslinking accelerates significantly. With this in mind, we designed a polymer containing both catechol and amine groups. At low pH, the polymer is soluble, the catechols

are stable, and the amines are charged. At high pH, i.e., pH 11.5, catechol oxidation takes place rapidly, forming *o*-quinones. The *o*-quinone reacts with the deprotonated amines to form a water-insoluble polymer. However, by testing this polymer with current water-borne paint systems, i.e. producing a suspension including additives, pigments, etc., the polymer formed flocs immediately. Two reasons might account for the formation of this flocculation. Firstly, titanium dioxide added as the additive might bind strongly with catechols in the copolymer. Secondly, the current paints systems are mainly anionic; the negatively charged additives interact with the positively charged amines in our polymer through electrostatics interactions, leading to the formation of flocs.

A third possible route can be "pH constant". There are two possible options. Firstly, since the flocculation may result from the positive charges of the amines at low pH, it is desirable if the amines are neutral so as to avoid the electrostatic interactions. One possible way is to protect amines using protection reagent di-*tert*-butyl dicarbonate to give *N*-*tert*-butoxycarbonyl or so-called Boc derivatives (Scheme 6.1). During storage, the polymer should stay soluble and no flocs should be formed. By deprotecting the amines upon application, the catechols can be oxidized and react with the free amines.

Secondly, instead of using only amine functionalized monomers, we may use a tri-copolymer containing carboxylic acid, catechol groups and protected amines. The amines are protected using reagent di-*tert*-butyl dicarbonate to give the *N*-*tert*-butoxycarbonyl or so-called Boc derivatives. At slightly basic pH during storage, the carboxylic acid bears a negative charge and the polymer is soluble. To avoid the catechol oxidation, we may

add a volatile reducing agent e.g. diethylhydroxylamine, carbohydrazide, and methylethylketoxime[2], to the system. Upon application and exposure to air, the reducing agent disappears either by evaporation or by reaction with oxygen. By deprotecting the amines, catechol oxidation and crosslinking takes place gradually to form crosslinked and water-resistant films.

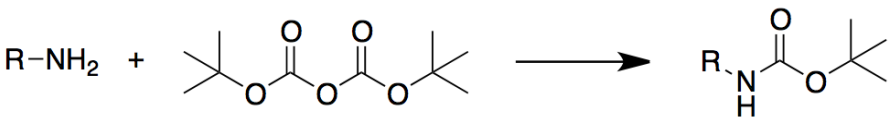

Scheme 6.1 Synthesis of BOC-protected amines.

6.2 Mechanistic understanding of catechol chemistry

Catechol oxidation and crosslinking is affected by a variety of parameters. Among these parameters, pH is an essential one that we should particularly pay attention to. For instance, in Chapter 3, we tried to unveil the crosslinking mechanism of catechol and amine by using the model compounds 4-methyl catechol (4MC) and propylamine (PA). The choice of pH in this study is tricky. On one hand, it is known that the primary amines need to be deprotonated to be reactive towards the *o*-quinones.[3] For an aliphatic amine, the pKa is usually around 9. Therefore, the pH of the reaction medium should be above 10. On the other hand, the catechol oxidation accelerates significantly upon increasing pH. Too fast catechol oxidation leads to the formation of too much *o*-quinones, which may significantly complicate the crosslinking chemistry.. Therefore, it is favorable to keep the pH at a proper level, i.e., pH should be high enough to keep aliphatic amines free; but not too high to generate too much *o*-quinones. In our case, in Chapter 3, the pH of the reaction medium was chosen as ~11 since PA has a pKa of 10.71. We observed that a lot of

products had already been formed in the first five minutes. To achieve a better understanding of the mechanisms, we suggest two possible further investigations. First, from DLS measurements, we found that during the reaction, clusters with different sizes were formed, which indicated that very big particles might be formed from the polymeric products. The polymeric products themselves could not be detected with the techniques we used, i.e., LC-MS. Therefore, one could use solid state nuclear magnetic resonance (ssNMR) to check the molecular structure of the clusters. Secondly, in order to use NMR techniques to identify the structures of each fraction as detected in LC-MS, we tried to collect fractions as they eluted. However, the fractions are very unstable, and each fraction reacted further to form other products. Therefore, we tried to focus on one of the simplest products, namely 4-*n*-propylamino-5-methyl-1,2-benzoquinone (PMB) (Scheme 6.2), the structure of which was determined from LC-MS. We tried to synthesize PMB using a different route based on a report in the literature[4], i.e., the reaction of 4MC and PA in acetic acid. It is expected that, by lowering the pH, the majority of the product is PMB. However, during purification, the product was again very unstable, making the separation very difficult. Therefore, it is difficult to get pure PMB for further NMR analysis. Therefore, we propose to synthesize PMB from protected catechols. The synthesis protocol is shown in Scheme 6.3. The obtained PMB can then be further analyzed with NMR techniques to identify the structure. HPLC of PMB can be used under the same elution conditions to match the elution profile we obtained in Chapter 3. In this way, the structure of PMB in our study can be double checked.

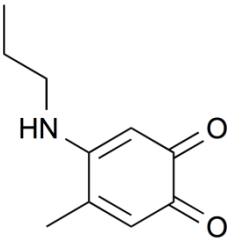

Scheme 6.2 Molecular structure of identified intermediate 4-*n*-propylamino-5-methyl-1,2-benzoquinone (PMB)

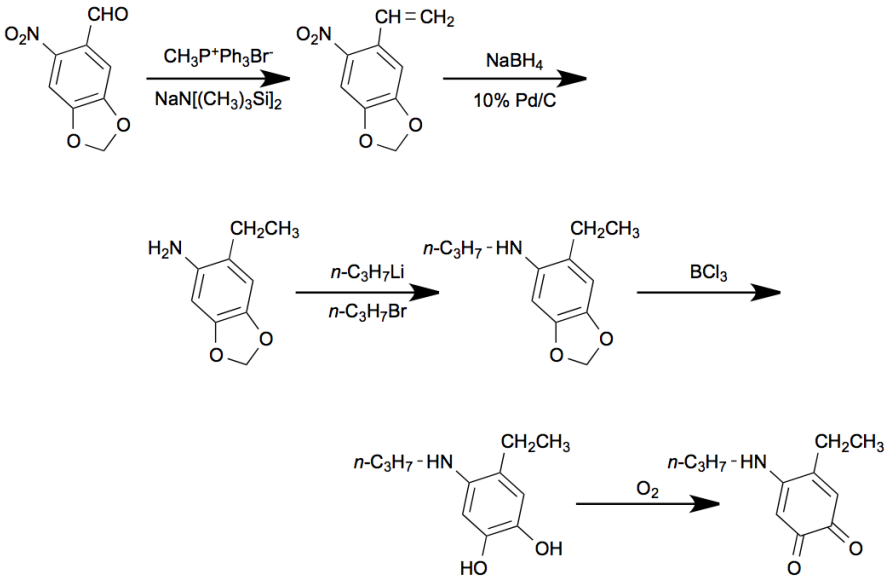

Scheme 6.3. Synthesis procedure of 4-*n*-propylamino-5-ethyl-1,2-benzoquinone[5] from a protected catechol precursor.

From the HPLC elution profiles of the reactions, in Chapter 3, we found that all the peaks of different fractions only decreased with time; there was no peak showing an increasing trend. This trend means that the reaction is so fast that we cannot capture the intermediates. In a reaction proceeding at an appropriate speed, we expect the formation of certain intermediates, which, with time, transform to other intermediates or products. In other words, in the HPLC elution profiles, some peaks would increase with time, while some other peaks would decrease. Therefore, it would be helpful if

we could slow down the reaction. One possible way is to add a reducing agent such as sodium borohydride $NaBH_4$. $NaBH_4$ can reverse the oxidation of catechols, and reduce the formation of *o*-quinones. Consequently, the reaction between *o*-quinones and amines can be slowed down, which may facilitate capturing the reaction kinetics. A second method is to reduce the pH of the reaction medium. For instance, instead of performing the reaction at basic conditions, it is possible to use acidic or neutral aqueous solvent. In this way, we can exclude the accelerating effect of basic pH on the catechol oxidation and crosslinking. The catechol oxidation rate is controlled by adjusting the amount of oxidizing agent (e.g. $NaIO_4$ or $NaIO_3$). In this way, the reactions might be slowed down. However, in acidic conditions, amines are charged and protonated, which limits the reactivity towards *o*-quinones. Nevertheless, in literature, the production of amine-catechol adducts in acidic conditions has been reported, so that this is a viable option to further explore the reaction mechanisms of charged amines and *o*-quinones.

Besides covalent bonds are catechols able to form non-covalent bonds. In Chapter 4, we designed the polymer p(DAA-AEMA). We found that, pure PAEMA is very water-soluble. Incorporation of only 6 mol% of DAA reduced the solubility significantly. In fact, the copolymer p(DAA-AEMA) (6 mol% DAA) in acidic conditions forms a gel. We therefore propose that catechols might form hydrophobic interactions in the solution, making the polymer solution behave like a gel. To verify this hypothesis, it would be interesting to study the effect of catechol on the mechanical properties of the polymer gels, and check whether or not the polymer gel self-heals. The gel behavior of this polymer might be an advantage for coating applications, since during application a gel would suppress the unwanted “sagging” on vertical surfaces.

6.3 Design and synthesis of catechol-containing polymer

To synthesize linear polymers containing catechol groups, special attention is required due to the radical scavenging ability of catechols. For instance, in Chapter 5, we synthesized a polymer by free radical copolymerization of dopamine methacrylamide (DMA) monomers carrying unprotected catechols and 2-methoxyehtyl methacrylate (MEA) monomers. By performing SEC-MALLS measurements on the copolymers, we found that a crosslinked polymer had been formed. The crosslinked structure may be formed due to the side reaction of catechols with the propagating radicals during polymerization.

To avoid the radical scavenging effect of catechols during polymerization, one can protect the catechols by various groups before polymerization. In this thesis, we have employed two methods. The first method, as suggested in Chapter 5, is protecting the catechols by methyl groups. The advantage of this method is the high stability of methyl-protected catechol (Me-Catechol) under common conditions such as high temperature, basic pH, etc. However, Me-Catechol is so stable that the deprotection step requires very harsh acidic conditions, i.e., using BBr_3. Under these extreme conditions, common comonomers such as acrylates are hydrolyzed. Therefore, the use of methyl protection limits the possibility of using acrylates as monomers. Moreover, the deprotection of Me-Catechol was performed in organic solvent, which is not compatible with our goal in this thesis- the production of environmentally friendly polymers. Therefore, it is more favorable to prepare the polymers under "friendly" aqueous conditions. The second method, as suggested in Chapter 4, is to protect the catechols by borax groups. In contrast to Me-Catechol, borax protected catechols are easy to

deprotect. The borax esters can be simply removed by lowering the pH to around 2 using aqueous HCl solution. The usage of borax protection has been proved to be effective and efficient in Chapter 4. In this way, the deprotection can be performed without the presence of organic solvent, and therefore, it is more environmentally friendly.

An alternative method for obtaining the polymer from unprotected catechol precursors is the post-modification of an existing polymer, using 1-Ethyl-3-(3-dimethylaminopropyl)carbodiimide (EDC) as the coupling agent.[6] An example is shown in Scheme 6.4. One could start from a commercially available polymer that contains functional groups such as carboxylic acid, and modify it by catechol-containing derivatives.

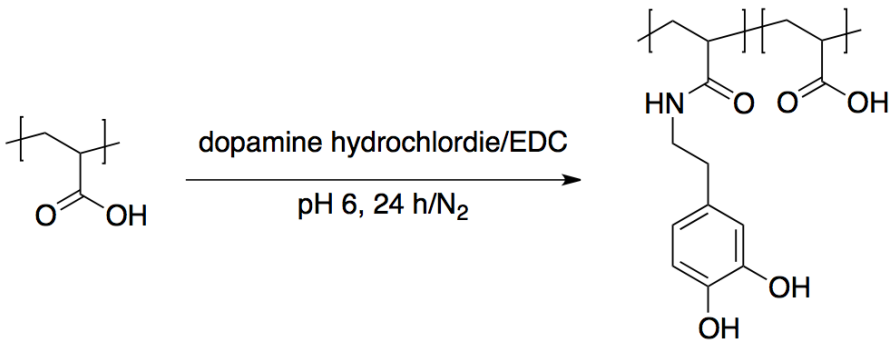

Scheme 6.4 Synthesis of catechol-containing polymer by modifying poly(acrylic acid) using dopamine hydrochloride and EDC coupling

References:

(1) Michael, D. G.; Conor, M. D. In *Paint & Coating Industry* Philadelphia, PA, 2006.

(2) Buecker, B. Power plant water chemistry: a practical guide; PennWell Books, 1997.

(3) Faure, E.; Falentin-Daudré, C.; Lanero, T. S.; Vreuls, C.; Zocchi, G.; Van De Weerdt, C.; Martial, J.; Jérôme, C.; Duwez, A.-S.; Detrembleur, C. *Advanced Functional Materials* **2012**, *22*, 5271.

(4) Akagawa, M.; Suyama, K. Biochemical and Biophysical Research Communications **2001**, 281, 193.

(5) Mure, M.; Wang, S. X.; Klinman, J. P. *Journal of the American Chemical Society* **2003**, *125*, 6113.

(6) Wu, J. J.; Zhang, L.; Wang, Y. X.; Long, Y. H.; Gao, H.; Zhang, X. L.; Zhao, N.; Cai, Y. L.; Xu, J. *Langmuir* **2011**, *27*, 13684.

Summary

Mussels adhere strongly to various types of underwater surfaces, ranging from soft polymer tissues to hard rocks, via a byssus. The formation of a byssus is a key step towards the sedentary life of mussels. When a mussel approaches a surface, it produces fluidic proteins inside its body at pH 5. Instantly, when the proteins are secreted into the seawater at pH 8, the proteins undergo a fast curing process, resulting in the formation of the byssus. The proteins in the byssus contain significant amounts of catecholic compounds, e.g., DOPA. It has been claimed that the excellent adhesion properties and fast curing of mussel proteins are related to the versatile chemistry of catechols.

The formation of mussel byssus is similar to the working principle of industrial water-borne paints. In industry, the paint is usually applied to a surface as a fluid suspension. After evaporation of the solvent and curing a water-repelling film is formed. The current waterborne paint system can fulfill the requirement of forming a hydrophobic film during drying, but they are colloidal polymer dispersions rather than solutions, and as a consequence, the rheological properties are not as good as those of solvent-based paints, in which the resin is dissolved. Therefore, the aim of this thesis is to take a bio-inspired approach, to develop a polymer that can be used as binder for waterborne paints, based on catecholic crosslinking chemistry. In other words, the polymer is expected to be water-soluble during application; during drying/curing, by triggering the crosslinking chemistry of catechol, the polymer is crosslinked to form a water-resistant film (Chapter 4). A clear understanding of the catecholic chemistry is crucial to obtain a well-designed polymer, so we investigated the reaction mechanisms of catechols (Chapter 2 and 3). Moreover, good adhesion properties are important for paints, so we also studied the adhesion

properties of catechol-containing polymers (Chapter 5). Therefore, in this thesis, several aspects are covered: the mechanistic understanding of catecholic chemistry, the production of catecholic polymers, and industrial application of the polymers.

In Chapter 2, a comprehensive overview of the possible crosslinking mechanisms of catechols that have been proposed in the last few decades is given. The chemistry of catechols is very versatile. A schematic description of the possible pathways is shown in Fig. 1.

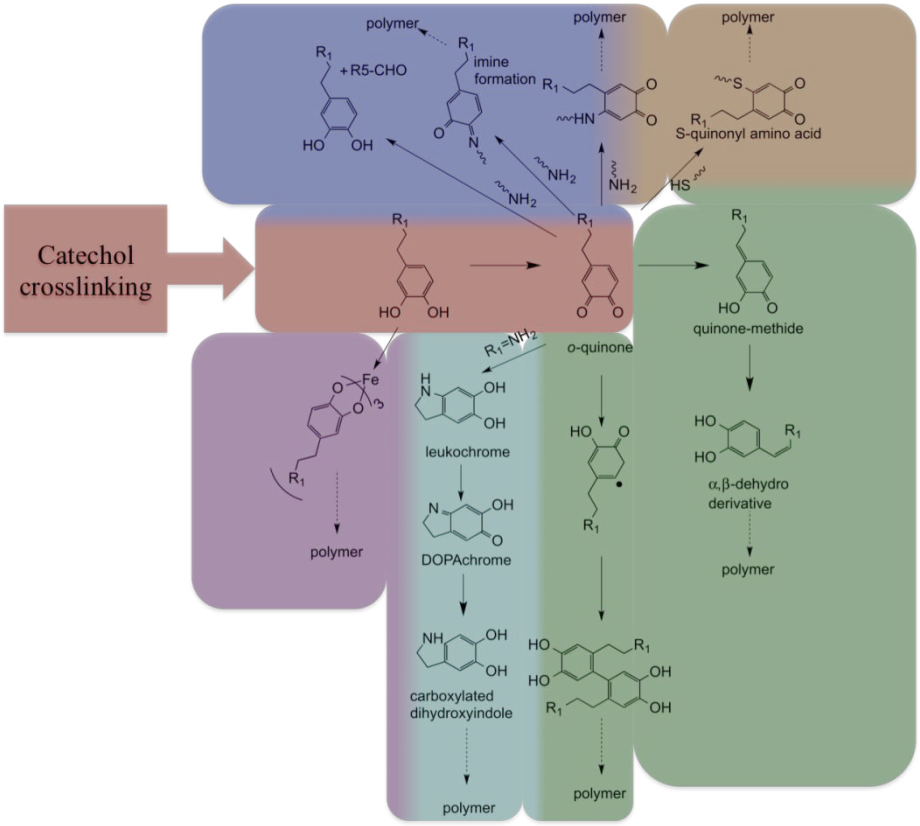

Figure 1 An overview of crosslinking pathways of catechol-derivatives

Catechols can react with a variety of functionalities, e.g., amines, thiols, and interact with metal ions (e.g. Fe^{3+}). The catechol-containing polymers or proteins are crosslinked by forming either covalent or non-covalent bonds.

In general, the covalent crosslinking pathways start from the oxidation of catechol either by oxygen, by enzymes or by chemical oxidants, to form *o*-quinone. The formed *o*-quinone is highly reactive and electrophilic and, therefore, susceptible to reaction with nucleophiles such as thiols and amines. The reaction with amine either proceeds via a Michael addition or a Schiff base reaction. In addition, *o*-quinone can undergo dismutation reactions with catechol to form *o*-semiquinone, which then forms di-catechol crosslinks via phenol radical coupling. In these reactions, the *o*-quinone formation has been well studied; and the presence of di-catechol crosslinks, thiol-catechol and amine-catechol adducts has been detected in either natural organisms or synthetic polymers. The reaction kinetics of these reactions are dependent on a variety of parameters such as pH, type of oxidant (e.g. enzymes or chemical oxidant), type of ring substituents on the aromatic ring of the catechols, and nucleophilic strength of the thiols/amines. By tuning these parameters, the reaction kinetics can be optimized. DOPA-analogues containing both catechol and free amines in one molecule, e.g. dopamine, can undergo oxidative self-polymerization under mild conditions via intramolecular cyclization. Several mechanisms have been proposed. This process is affected by pH, dopamine concentration, type of oxidant used, etc. In addition, catechols can also complex metal ions (e.g., Fe^{3+}) by forming coordination bonds. The modes of complexation are highly dependent on the pH. At high pH (pH 10), tris DOPA-Fe^{3+} is formed. At moderate pH (e.g., 6 to 8), bis DOPA-Fe^{2+} is formed; and at pH 5, mono DOPA-Fe^{3+} is formed. Fe^{3+} can also oxidize catechols to form *o*-quinones, which then can form crosslinks via covalent

bonding. Parameters that can be tuned to optimize the (non-covalent) crosslinking are pH, concentration of metal ions, the type of metal ions, etc.

Based on the overview in Chapter 2, we found that a clear understanding on the secondary reactions of *o*-quinones with amines is still lacking. However, the reaction has been vastly employed as a tool to crosslink catechol-containing polymers, which can be used in various applications. Therefore, there is a gap between the in-depth understanding of the reaction mechanism and optimal usage of the crosslinking chemistry in applications. To bridge this gap, we performed in Chapter 3 a mechanistic study on the reaction of the model compounds 4-methyl catechol (4MC) and propylamine (PA) in aqueous conditions. We identified the type of the reaction, i.e., Schiff-base reaction or Michael-type addition, the possible products, and the reaction rate. By employing various experimental techniques, including LC-MS, HPLC, UV-vis, DLS, NMR, we found that the reaction of 4MC with PA is surprisingly fast. In the first five minutes, more than 30 products have already been formed. These products are mainly formed via three pathways, i.e., Michael-type addition, Schiff-base reaction, and phenol-phenol coupling. Among these products, the majority are amine-catechol adducts formed by Michael-type addition.

In Chapter 4, we designed a “green” synthesis of a catechol-containing pH-responsive polymer that can be used as binder for water-borne paints. The polymer is expected to switch from being water-soluble to water-insoluble when the pH is changed from low/acidic to high/basic. To achieve this, without using organic solvents, we synthesized a polymer containing both catechols and amines, by means of free radical polymerization of borax-protected dopamine acrylamide (DAA-*p*) and 2-aminoethyl methacrylamide hydrochloride (AEMA) in aqueous medium. We found that the polymer

was indeed water-soluble at low pH (pH 2). At high pH (pH 11.5), catechol was oxidized to *o*-quinones, which reacted with free amines from the deprotonation of AEMA to form crosslinks. In this way, the polymer became water-insoluble. Adding a chemical oxidizing agent, $NaIO_4$, enhanced the rate of crosslinking of the polymer.

It is commonly believed that paint should have proper adhesion properties to work effectively. Therefore, the adhesion performance of a polymer is important to function as a binder in paints. In Chapter 5, we investigated the effect of catechol on the adhesion properties of catechol-containing polymers under both dry and wet conditions. We synthesized five copolymers by free radical polymerizations of dopamine methacrylamide (DMA) and 2-methoxyethyl methacrylate (MEA) with different compositions. We found that, under dry conditions, an optimal composition for the best dry adhesion is achieved at 5 mol% DMA. Polymers with a higher concentration of DMA showed little adhesion, which is attributed to the high stiffness of the material, resulting in poor contact with the probe. Under wet conditions, the copolymers showed a similar dependence on the DMA composition as compared to dry conditions. An optimal composition for the best wet adhesion was found at a DMA concentration of 5 mol%. Polymers with a higher DMA content are more hydrophilic and will take up more water. As water acts as a plasticizer and reduces the effective stiffness, polymers with a higher DMA content will show a larger decrease in stiffness, which improved their wet adhesion performance.

List of publications

This Thesis

- Juan Yang, Vittorio Saggiomo, Aldrik Velders, Martien A. Cohen Stuart, Marleen Kamperman; *Reaction pathways in catechol/primary amine mixtures: a window on crosslinking chemistry*. (In preparation) (Chapter 3)
- Juan Yang, Inge Bos, Wim Pranger, Anthonie Stuiver, Aldrik Velders, Martien A. Cohen Stuart, Marleen Kamperman; *A clear coat from a water soluble precursor: a biomimetic paint concept*. (Submitted) (Chapter 4)
- Juan Yang, Jaap Keijsers, Maarten van Heek, Anthonie Stuiver, Martien A. Cohen Stuart, Marleen Kamperman; *Effect of molecular composition and crosslinking on adhesion of a bio-inspired adhesive*. **Polym. Chem.,** 2015, 6(16), 3121-3130. (Chapter 5)
- Juan Yang, Martien A. Cohen Stuart, Marleen Kamperman; Jack of all trades: versatile catechol crosslinking mechanisms. **Chem. Soc. Rev.**, 2014, in press, DOI: 10.1039/C4CS00185K. (Chapter 2)

Other work

- A. M. Frey, J. Yang, J. H. Bitter, and K. P. de Jong, C. Feche, N. Essayem, and F. Figueras; *Influence of base strength on the catalytic performance of nano-sized alkaline earth metal oxides on CNF*. **J. Catal.**, 2013, 305, 1-6.
- Juan Yang, Dapeng Cao; *Counterion Valence-induced Tunnel Formation in a System of Polyelectrolyte Brushes Grafted on Two Apposing Walls*. **J. Phys. Chem. B**, 2009, 113(34), 11625-11631.
- Juan Yang, Ran Ni, Dapeng Cao and Wenchuan Wang; *Polyelectrolyte--Macroion Complexation in 1:1 and 3:1 Salt Content: A Brownian Dynamics Study*. **J. Phys. Chem. B**, 2008, 112(51), 16505-16516.

Acknowledgement

In 2012, I joined Fysko for my four-year PhD adventure. This adventure started with a New-Year breakfast, which has impressed me with a stimulating, lively and harmonious atmosphere and given me a lot of hope. At the end of this journey, I would like to extend my thanks to all the people who have helped bring this thesis into being, and made this journey interesting, fun and satisfying.

First of all, I would like to thank my supervisors- Martien and Marleen for offering me the opportunity to pursue my PhD in Fysko. Martien, I am always impressed by your intimate knowledge, open mind and wisdom. I am grateful for the great atmosphere in Fysko you have created for us and all the constructive suggestions and guidance regarding my research, manuscripts and thesis. My sincere gratitude goes to my co-promoter, Marleen. Marleen, you are a very positive-thinking, stimulating and considerate supervisor. I still clearly remember the situation after I got the first NMR spectrum of my first-synthesized DMA. I was pretty upset at the wild NMR spectrum although later it turned out to be a successful synthesis. Your comforting and encouraging words really helped me relieved. I have received a lot of this encouragement/relief from you during the past four years, and your optimistic/assuring attitude has definitely made my adventure more stedfast. Besides, your insight of research and your attitude of balance between research and life have set a great example of female scientist for me. I have learnt a lot from you, both professionally and personally. Marleen, many thanks for all the things you have done for me. I hope to keep collaborations with you in my future research.

Moreover, I would like to thank Jasper for the helpful suggestions on the project of catechol-containing self-healing gel formation. Joshua, thank you for all the workshops, e.g. Matlab, etc, you have organized, and the advice/help you have offered regarding rheology/Raman measurements. Aldrik, you have impressed me with the power of NMR technique, and thank you for the collaboration and NMR measurements in two chapters of this thesis. I would also like to thank Frank, Elbert, Pepijn and Barend from ORC for all the help on various characterization/testing techniques.

Special thanks go to Anthonie, Wim and Mark for all the helpful discussions we had on the project. Anthonie, thank you for arranging all the meetings in Sassenheim, organizing the trip to Slough, and showing us the beautiful city. I am impressed by your broad knowledge on coating/paints. I also want to thank Andreas and Guillaume for helping me on the paint formulation experiments. I also would like to thank the students who worked with me on the project: Jaap and Inge B. You are talented, hard-working students, and I enjoyed working together with you.

Additionally, I would like to thank all the staff members in Fysko. Josie, thank you for being always very supportive, kind, considerate and positive. Mara, thank you for taking care of all the chemical ordering, thesis printing for me in a very efficient way. Bert, thank you for making thesis pre-reading book for me, and arranging the financial issues for conferences. Anita, thank you for arranging optare, reimbursement declaration, etc. Remco, thank you for the help on light scattering measurements. I would also like to thank: Frans, Mieke, Herman, Renco, Anton, Ronald, Diane, Hannie, Rene and Dirk for all the help and support.

I want to thank my lovely officemates in room 1010, Gosia B., Hande, Natalia, Monica and Cecilia. It is very nice of sharing the same office with you and I really enjoyed our many discussions on both research and life. I want to thank the collaborators in the group. Merve, we both work tremendously on polymer synthesis, and we have shared our experience and feelings in the joy-and-pain moments in synthesis/purification/characterization. Although we have discussed a lot, we only have the opportunity to collaborate on my last project. I hope we can have more collaboration in the future. I have really enjoyed our discussion on both research and life. Vittorio, thank you for our collaborations on catechol crosslinking chemistry. Your knowledge on LC-MS impressed me a lot. Maarten, thank you for your help on the indentation adhesion setup. In addition, I want to thank the small Chinese sub-division of Fysko, Huanhuan, Tingting and Junyou. We have shared a lot of discussions on current Chinese research status and personal life as well. Without you, this overseas study would bring me much more homesick. I am grateful to have your accompany. I also want to thank all the present and former members of Fysko for the past beautiful four years we shared together: Antsje, Celine, Christian, Gosia W., Hanne, Harke, Ilse, Inge S., Evan, Kamuran, Jacob, Jan Bart, Jan Maarten, Jeroen, Johan, Sabine, Katarzyna, Lennart, Soumi, Liyakat, Marcel, Wolf, Maria, Nadia, Lione, Ruben, Rui, Surender, Ties, Thao, Yunus and Helene.

I would also like to thank my thesis committee Prof. WJH van Berkel, Prof. C. Detrembleur, Prof. F. Picchioni and Prof. H. Birkedal for reading and accepting my thesis.

In addition, I would like to thank people outside Wageningen for the help and helpful discussions in the past years. Prof. John Kelly, thank you for enrolling me as a master student in Utrecht. I am grateful for all the help you have offered in the past years. Wei Qiang, thank you for our discussions in the mussel field as well as many other interesting topics. Sinedu, thank you for the great time we had together and the one-day graduation-trip in Botanic garden. Zhixiang Sun, thank you for your hospitality during our visit to Stuttgart. I also want to thank Anjan and his wife for the hospitality during our visit in Utrecht. Yehua Li and Kewei Huang, thank you for all the wonderful time we had together, and hopefully we will have more get-togethers in Nanjing/Singapore. I would also like to thank all the Chinese friends in and outside Wageningen: Meng Chen, Xiaofeng Sui, Yuying Gao, Xiaoman Liu, Xinlin Zhang, Ya Wang, Jiao Long, Wenjuan Mou, Xuezhen Guo, Junyou Wang, Junli Guo, Kun Liu, Ginny Gu, Qie Ke, Ye Tian, Wenjie Yang, Yuping Zhang, Jie Chen, Jinfeng Peng, Tingting Zheng, Huanhuan Feng, Yuan Li.

我还要感谢我的父母，杨长锦先生及邓克花女士，感谢您们多年来的悉心教导和养育。爸爸，在我的生命里，您身兼多职：在我迷茫时指引着我的方向，在我失意时给与我鼓励，在我志得意满时告诉我要淡然，您教会了我要坚强和慎独。妈妈，您数年如一日的关爱给与了在外漂泊的我很多温暖和力量，您身体力行地教给了我柔韧，温婉的品质。我还要感谢我的公婆倪受仓先生和徐娅女士，感谢您们对我一直以来的关心和支持。我也要感谢我的妹妹杨艳女士，妹夫朱军先生以及朱钰涵小朋友，感谢你们对我的关心，支持以及给与我家庭里的温暖和欢笑。最后，我要感谢我的先生倪冉，我们风雨同舟的一路走来，你给与了我很多包容，支持和期盼。遇你之前，我从未想过结婚。嫁你之后，我从未后悔。此生有你相伴，真好！

About the author

Juan Yang was born on 26 August 1985 in Jiangsu, China. In 2002, she entered a selective class in Nanjing Tech University, majoring macromolecular materials science and engineering. After four years, she obtained her bachelor degree in 2006. Afterwards, she continued her master study in chemical engineering in Beijing University of Chemical Technology. In 2009, She moved to Utrecht University, the Netherlands to continue her master program in nanomaterials: physics and chemistry with Debye Graduate Scholarship, and got the master degree in 2011. She started her Ph.D research sponsored by AkzoNoble at the Laboratory of Physical Chemistry and Soft Matter of Wageningen University, under the supervision of prof. Martien A. Cohen Stuart and dr. Marleen Kamperman. This thesis is the result of that research project.

Overview of completed training activities (VLAG)

General courses

How to supervise master thesis	Wageningen	2012
Career perspective	Wageningen	2014
Scientific writing	Wageningen	2014
Presentation skills	Wageningen	2014
Information Literacy PhD including EndNote Introduction	Wageningen	2015
Journal club	Wageningen	2015-2016

Conferences and meetings

Dutch polymer day ∗†	Lunteren	2012-2015
Dutch soft matter meeting †	Wageningen	2012
S-PolyMat	Kerkrade	2012
Frontiers in polymer science †	Stiges (Spain)	2013
Soft-matter symposium ‡	Wageningen	2013
Gordon research conference: bio-inspired materials †	Newry (USA)	2014
Macromolecular colloquium †‡	Freiburg (Germany)	2014
MRS fall meeting ∗†	Boston (USA)	2015

Discipline-specific courses

RPK-A polymer chemistry	Utrecht	2012
EUcost training fundamental & principles of technical adhesives	Bremen (Germany)	2012
AFM training in Bruker	Karlsruhe (Germany)	2013
European school on rheology	Leuven (Belgium)	2015

Optional

PhD trip∗	USA	2013
Advanced soft matter course	Wageningen	2013
Group meetings	Wageningen	2012-2015
Journal club	Wageningen	2014-2015
Quarterly meeting with Akzo Nobel	Netherlands/UK	2012-2015

∗ Oral presentation, † Poster presentation, ‡ Soundbite